DYNAMIC MODULATION OF EXOCYST INTERACTION NETWORKS INTEGRATES HIPPO AND mTOR PATHWAY RESPONSE TO PATHOGEN DETECTION

APPROVED BY SUPERVISORY COMMITTEE

Michael White, Ph.D.

Sandra Schmid, Ph.D.

Rolf Brekken, Ph.D.

Hamid Mirzaei, Ph.D.

ACKNOWLEDGMENTS

Life, to me, is a puzzling gift from my parents. As a child, I remember, spending hours in brooding, rather ineffectively, about the meaning of life and happiness. Little had I any idea how universal and inexplicable the nature of these questions was. My parents did not instill any particular religious faith into me; I grew up knowing Mother Nature and my parents as the only true deities. And I was convinced that the tree of life, as magical as it might seem, is governed by definable physical laws. Hence, I decided to embark on a journey to understand these laws for pursuit of happiness in my life; life which otherwise seemed 'meaningless'.

Continuing on that journey, during my PhD training, I called 'NL7.120F' in Dr. Michael White's laboratory my home for the last four years. Like any other educational experiences, this too was a mosaic of surprises, agonies, excitements and learning curves. I can hardly thank Mike enough for his guidance, clear-headed vision and insightful opinions throughout my training period. And I was extremely fortunate to work alongside some great minds in the White lab. Rarely do you find such dynamic, hardworking and bright circle. I am grateful for all the camaraderie, thought provoking discussions, pranks and random lab outings I shared with this brilliant group of people.

I am also grateful to my thesis committee- Dr. Sandra Schmid, Dr. Rolf Brekken and Dr. Hamid Mirzaei for mentoring and guiding me through this journey, for relaying sense of assurance under testing times and for admonishing or complimenting when necessary. The nurturing environment of UT Southwestern is ideal for learning through collaboration and discussion and I am truly proud to be part of this great institution.

I am also eternally thankful to all my friends and well-wishers for putting up with my ‘nerdy sarcasms’ or ‘deep thoughts’, for keeping me company in midnight foodie ventures or for backpacking with me as explorers.

Last but not the least, I am thankful to countless favorite authors and movie directors; musicians and comedians; scientists and engineers; entrepreneurs and explorers who in the time of disheartening pessimism set shining example of courage and optimism. I believe art and science are the most effective tools for building a fact and knowledge based society; relentless heart and soul efforts put forth by fellow artists and scientists worldwide is what make living my life worthwhile. And this is why I would like to dedicate this work to all these inquisitive beautiful souls trying to push for a humanity and future worth living for.

DYNAMIC MODULATION OF EXOCYST INTERACTION NETWORKS INTEGRATES HIPPO AND mTOR PATHWAY RESPONSE TO PATHOGEN DETECTION

by

Aubhishek Zaman, Ph.D.

DISSERTATION

Presented to the Faculty of the Graduate School of Biomedical Sciences

The University of Texas Southwestern Medical Center at Dallas

In partial Fulfillment of the Requirements For the Degree of

DOCTOR OF PHILOSHOPHY

The University of Texas Southwestern Medical Center

Dallas, Texas

December 2017

DYNAMIC MODULATION OF EXOCYST INTERACTION NETWORKS INTEGRATES HIPPO AND mTOR PATHWAY RESPONSE TO PATHOGEN DETECTION

Publication No._____

Aubhishek Zaman, Ph.D.

The University of Texas Southwestern Medical Center at Dallas, 2017

Michael A White, Ph.D.

Monomeric RALGTPases, via direct binding to the exocyst (a.k.a Sec6/8 complex), help mount productive cell autonomous responses to trophic and immunogenic signals. However, RAL-exocyst downstream effectors register in a bewildering array of signaling events— suggesting the presence of mechanisms that confer context dependent coordination amongst them. Here, we employed quantitative proteomics-based characterization of dynamic signal-dependent modulation of the exocyst interactome as an approach to detect such mechanisms. We identified sentinel innate immune kinases- PKR and TBK1 as host defense stimulus induced effectors of distinct exocyst subcomplexes specified by the presence of Exo84 versus Sec5 subunits. We find that, under virally compromised conditions, the Exo84 subcomplex accommodates Hippo signaling kinase MST1 together with PKR whereas a Sec5 subcomplex assists assembly of anabolic growth regulatory kinase mTOR together with TBK1. Detailed functional and biochemical analysis indicated that PKR directly phosphorylates MST1 for activation of Hippo signaling and consequent YAP1 inactivation. In parallel, TBK1 was found to be a positive regulator for mTOR and a negative

regulator of YAP1 activity. Furthermore, RALB, which is activated by the host defense response, was found to be required and sufficient for induction of both Hippo and mTOR signaling through dual exocyst subcomplex engagement. RALB-dependent activation of these pathways can help cells deflect viral challenge and can be corrupted by oncogenes to help deflect apoptotic checkpoint activation. Thus, RAL-exocyst signaling complexes can be recognized as context-dependent mechanisms for integrated engagement of Hippo and mTOR signaling pathways.

TABLE OF CONTENTS

PRIOR PUBLICATIONS

Cooper J, Ou Y, McMillan E, Vaden R, Zaman A, Bodemann B, Makkar G, Posner B, and White M† (2017). “Context-Selective Support of AKT/mTOR Pathway Activation in Mesenchymal KRAS-mutant Lung Cancer Cells by TBK1.” Cancer Res. 15;77(18):5077-5094.

Eskiocak B, McMillan E, Kollipara R, Zhang H, Humphries G., Mendiratta S, Wang C, Zaman A, Garcia-Rodriguez, J, Rosales T, Eskiocak U, Komoruv K, Davies M, Wargo J, De Brabander J, Williams N, Chin L, Kittler R, and White M (2017). “Biomarker accessible and chemically addressable mechanistic subtypes of BRAF melanoma.” Cancer Discov. 7(8):832-851

Torres M, Pandita R, Kulak O, Kumar R, Formstecher E, Horikoshi N, Mujooc K, Hunt K, Zhaoe Y, Lum L, Zaman A, Yeaman C, White M and Pandita T (2015) " Role of the exocyst complex component Sec6/8 in genomic stability" Mol Cell Biol.; 35(21):3633-45

Najnin R, Shafrin F, Polash A, Zaman A, Hossain A, Taha T, Ahmed R, Tuli J, Barua R, Sajib A, Khan S (2015) ‘A diverse community of jute (Corchorus spp.) endophytes reveals mutualistic host–microbe interactions’ Annals of Microbiology; 65 (3): 1615–1626

Zaman A, Razzaque S, Rahman H (2013) ‘Kaposi's sarcoma: a computational approach through protein-protein interaction and gene regulatory networks analysis’ Virus Genes; 46(2):242-54

Islam R, Zaman A, Jahan I, Chakravorty R, Chakraborty S (2013) ‘In silico QSAR analysis of quercetin reveals its potential as therapeutic drug for Alzheimer's disease.’ J Young Pharm.; 5(4): 173–179

Islam R, Sakib M, and Zaman A (2012) ‘A Computational assay to design an epitope-based peptide vaccine against Chikungunya Virus.’ Future virology; 7(10) 1029-1042

Zaman A, Fancy N (2012) ‘A computational prediction of structure and function of novel homologue of Arabidopsis thaliana Vps51/Vps67 subunit in Corchorus olitorius’ Interdiscip Sci.; 4(4):256-67

LIST OF FIGURES

LIST OF TABLES

LIST OF ABBREVIATIONS

Ab	Antibody
AKT	RAC-alpha serine/threonine protein kinase
AMOT	Angiomotin
AMPK	AMP-activated protein kinase
ATP	Adenosine-5'-triphosphate
AZI2	5-azacytidine-induced protein 2
Beclin	Coiled-coil myosin-like BCL2-interacting protein
CCNH	Cyclin-H
CDK7	Cyclin-dependent kinase 7
DMEM	Dulbecco's Modified Eagle's medium
ds	Double stranded
EBSS	Earle's Balanced Salt Solution
ED50	Median effective dose
EIF	Eukaryotic Translation Initiation Factor
EXOC1	Exocyst complex component 1/ Sec3
EXOC2	Exocyst complex component 2/ Sec5
EXOC3	Exocyst complex component 3/ Sec6
EXOC4	Exocyst complex component 4/ Sec8
EXOC5	Exocyst complex component 5/ Sec10
EXOC6	Exocyst complex component 6/ Sec15
EXOC7	Exocyst complex component 7/ Exo70
EXOC8	Exocyst complex component 8/ Exo84
GAPDH	Glyceraldehyde-3-Phosphate Dehydrogenase
GTP	Guanosine-5'-triphosphate
HA/ml	Hemagglutinin unit per milliliter
HSV	Herpes simplex virus
i	Inhibitor
IFN	Interferon
IKKε	IKK-related kinase epsilon
IRF	interferon regulatory factor
IVNS1ABP	influenza virus NS1A-binding protein
LAMTOR1/2/3	Late Endosomal/Lysosomal Adaptor, MAPK And MTOR Activator 1/2/3
LATS1/2	Large Tumor Suppressor Kinase 1/2

MEF	Mouse embryonic fibroblasts
MNAT1	CDK-activating kinase assembly factor MAT1
MOI	Multiplicity of infection
MST1/2	Mammalian STE20-Like Protein Kinase 1/2
mTORC1/2	Mammalian target of rapamycin complex 1/2
NF2	Neurofibromin 2, Merlin
ns	Non-significant
PI3K	Phosphatidyl insoitol 3 kinase
pI:C	Polyinosinic-polycytidylic acid
PKR	Protein Kinase R
PPI	Protein protein interaction
PRPS1/2	Ribose-phosphate pyrophosphokinase 1/2
PRPSAP1	Isoform 2 of Phosphoribosyl pyrophosphate synthase-associated protein 1
RNAi	Small RNA-mediated gene interference
RAF	Raf Proto-Oncogene, Serine/Threonine Kinase
Rag A/B/C/D	Ras-related GTP-binding A/B/C/D
Ral A/B	Ras-like GTPase A/B
RalGAP	Ral-specifc GTPase activating protein
RalGEF	Ral-specific Guanyl nucleotide exchange factor
RAS	RAS Proto-Oncogene, GTPase
RBD	Ral binding domain
S6K	Ribosomal S6 kinase
SC	Spectral count
Sec	Secretory mutant
SeV	Sendai virus
siRNA	Short interfering Ribonucleic acid
TEAD	TEA Domain Transcription Factor
TBK1	Tank binding kinase 1
TP53BP1	Isoform 2 of Tumor suppressor p53-binding protein 1
ULK1	Unc-51-like kinase 1
v-SNARE	Vesicular soluble NSF attachment protein receptor
VPS34	Vacuolar protein sorting 34
WDR73	WD repeat-containing protein 73
YAP1	Yes Associated Protein 1

CHAPTER ONE

INTRODUCTION

Ras GTPases function as important nodes in signal transduction networks regulating cell proliferation and differentiation by integrating extracellular mitogenic and hormonal cues. Three direct effector pathways of RAS GTPases are: Raf/mitogen-activated protein kinase (MAPK) pathway, ii) (PI3K)-dependent second messenger pathway and iii) Ral guanine exchange factor (RalGEF)/Ral GTPases pathway. Out of these three arms, the RAL arm regulates diverse biological functions depending on the context, which, if corrupted, lead to pathogenic development. Preclinical data indicated concordant dependency of RAS GTPase on the RAL arm (Cooper, Bodemann et al. 2013). Previous work from our lab has established a critical role of the protein complex exocyst, a major direct effector of RAL-GTPases, in harboring important protein protein interactions (PPI) during growth homeostasis and innate immune program driven cancer cell survival signaling. However, the coordination and crosstalk between these signaling effectors are not well understood. This work annotates the dynamic PPI constituency of the exocyst entities and outlines the functional significance of the interactions under host defense signaling.

Exocyst: canonical and non-canonical functions

The mammalian membrane trafficking system involves a complex web of distinct organelles, transient membrane structures and multi-component protein complexes. The coordinated and dynamic communication between these components are responsible for intracellular trafficking, cytoskeletal remodeling for cell migration, tethering, fusion and eventual secretion of intracellular contents- a cellular process defined as exocytosis. Pre-fusion tethering of secretory

vesicle to the plasma membrane is facilitated by the evolutionarily conserved octameric protein complex called the exocyst (a.k.a Sec6/8 complex).

The exocyst was first identified in a genetic screen for temperature-sensitive secretory (sec) mutants of the yeast *Saccharomyces cerevisiae* (Novick and Schekman, 1979; Novick et al., 1980). Out of 23 complementation groups of sec mutants, six of the exocyst subunits namely Sec3, Sec5, Sec6, Sec8, Sec10, and Sec15 were implicated in late-acting Golgi-to-cell surface transport. Exo70 and Exo84, the two remaining exocyst components, were identified biochemically from the purified yeast complex or the homologous mammalian complex, respectively. Subsequently, the mammalian homologs of the heterooctameric exocyst complex were assigned aliases designated from EXOC1 through 8.

The crystal structures of larger domains of four exocyst subunits have been solved. Each has repeated helical-bundle units that pack together into elongated rod-like structures. Mapping of the binding sites along with electron micrographs of exocyst complexes support a model where the subunits pack together in an elongated side-to-side manner. Exo84 has a Plecstrin Homology (PH) domain through which it is capable of binding phosphoinositides for plasma membrane recruitment (Moskalenko, Henry et al. 2002). Moreover, using yeast two hybrid and *in-vitro* transcription and translation assays, multiple pair-wise interactions between exocyst subunits have been established. Because each subunit can form multiple interactions, a large number of distinct compositions may be possible for different subcomplexes (Table1.1). Although selective contribution of a given subunit to a specific biological function can be investigated using antisense interfering RNA technology or specific loss of function point mutations; the pleiotropic and essential nature of the subunits often complicate such analyses. Recent work on exocyst stoichiometry questioned presence of subcomplexes in *Saccharomyces cerevisiae,* but not in mammalian cells. These remarkable differences in the

composition of the exocyst entities were conceptually credited to the presence of RAL GTPases in mammalian cells (Heider, Gu et al. 2016).

Table 1.1: Pair-wise (direct and indirect) interactions between exocyst subunits.

Subunit	***Interacting subunits***
Sec3/EXOC1	*Sec5*, Sec8**
Sec5/EXOC2	*Sec3*, Sec6*, Exo84#*
Sec6/EXOC3	*Sec5*, Sec8*†, Sec10†, Exo70**
Sec8/EXOC4	*Sec3, Sec6*†, Sec10*†, Exo70†*
Sec10/EXOC5	*Sec6†, Sec8*†, Sec15**
Sec15/EXOC6	*Sec10*, Exo70*, Exo84**
Exo70/EXOC7	*Sec6*, Sec8†, Sec10†, Sec15*, Exo84**
Exo84/EXOC8	*Sec5#, Sec15*, Exo70**

* Matern, Yeaman et al. 2001
# Moskalenko,Tong et al. 2003
† Vega, Hsu et al. 2001

RAL-GTPases dependent exocyst signaling events

Ras-like GTPase A and B (RALA and B), close relatives of the founding member of the RAS GTPase superfamily, are 82% identical to each other and specific to metazoans. Compared to RAS, RAL is present not only on the plasma membrane, but also on intracellular vesicles (Moskalenko, Henry et al. 2002). RAL GTPases gained prominence after their discovery as direct downstream effectors of oncogenic Ras. Importantly, activation of Ral GTPases as a consequence of Ras expression in 2D cell culture and preclinical model systems suggested potential tumorigenic roles for RAL GTPases (Rangarajan, Hong et al. 2004). Further mechanistic analysis implicated these G-proteins in seemingly diverse processes including cell

proliferation, motility, maintenance of cellular architecture, growth homeostasis and host defense signaling.

There are at least two direct downstream effectors of the RAL GTPases: RAL Binding Protein1 (RALBP1) and the exocyst. RALs regulate participation of the heterooctameric complex, the exocyst, by direct physical interaction with two distinct subunits Exo84 and Sec5. RAL-exocyst effectors register in a bewildering range of cellular processes including, but not limited to, targeting and tethering of secretory vesicle. Moreover, distinct from intracellular chauffeuring functions, RAL-exocyst signaling has been implicated in stimulus dependent regulation of growth homeostasis and host defense signaling through molecular scaffolding. The RALB-Exo84 subcomplex promotes productive interaction between the UNC-51-like kinase 1 (ULK1) and the Beclin1-Vps34 complex to induce autophagy (Bodemann, Orvedahl et al. 2011). In addition, a separate RalB-Sec5 subcomplex favors activation of the innate immune kinase, TANK binding kinase 1 (TBK1) to promote cancer cell survival (Ou, Torres et al. 2011). Thus, during trophic and immunogenic signaling, distinct exocyst subcomplexes function as a context dependent molecular scaffold by accentuating local concentration of the effectors. These signal dependent spatial platforming of signaling effectors possibly restrict otherwise autoreactive and concomitant engagement of mutually exclusive pathways. Pathogenic and neoplastic developments often manifest a collapse in these regulatory restrictions to overcome cell-death checkpoints and to promote aberrant growth signaling. For example, preclinical data suggest that oncogenes such as RAS-GTPases can often corrupt RAL signaling for abnormal growth advantages (Rangarajan, Hong et al. 2004).

Figure 1.1

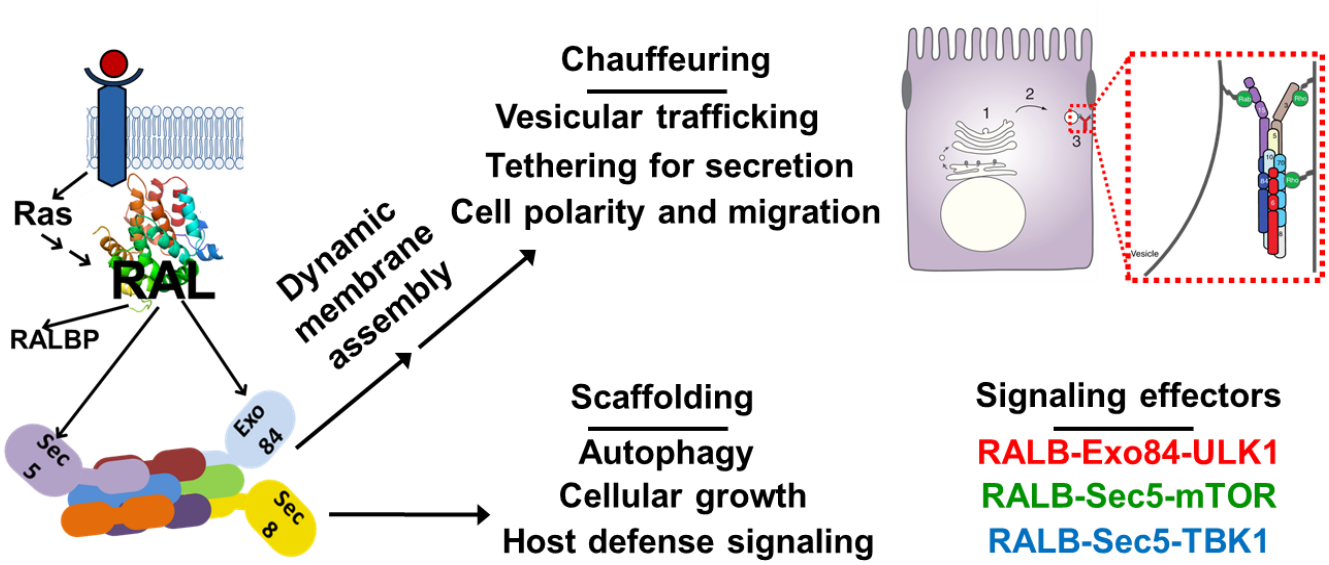

Figure 1.1: RALB dependent 'chauffeuring' and 'scaffolding' functions of the exocyst. RAS activation can integrate extracellular signaling to RAL GTPase activation. RAL GTPases can interact with its effectors- RALBP1 and the exocyst. RAL-exocyst interactions give rise to functions such as vesicular trafficking related 'chauffeuring' or stimulus dependent 'scaffolding' for signaling pathways.

RAL-exocyst signaling in disease

The exocyst is remarkably conserved across eukaryotes in sequence and structure. Remarkably, both polarized growth of fungi hyphae and dendritic growth of mammalian neurons require critical participation of the exocyst (Martin-Urdiroz, Deeks et al. 2016). However, in complex metazoans, the exocyst has acquired novel upstream instructor and downstream effectors to diversify its functions. For example, presence of distinct exocyst subcomplexes in multicellular organisms, but not in unicellular yeast cells, has been credited to presence of RAL GTPases in the former, but not in the later. Therefore, the exocyst, in more complex organisms, appears to be engaged in both constitutive and stimulus dependent regulatory circuits. Hence, differentiating functions from exocyst subcomplexes and the holocomplex, although daunting, might enable us to annotate cell biological circuits that have evolved for coping with stimulus dependent regulations.

Consistent with its multifunctional nature, exocyst subunits have been shown to localize in multiple compartments distinct from its initially identified localization on tight junctions. For instance, the exocyst localizes in the apical junctional complex, plasma membranes, trans-Golgi network, recycling endosomes and primary cilia. Primary cilia are chemo and mechanosensory organelles that regulate signal transduction for key developmental and secretory signaling pathways (Seixas, Choi et al. 2016). The exocyst subunit, Sec10, directly interacts with the ciliary proteins IFT20, IFT88, and polycystin-2, and knock down of Sec10 in Madin Darby Canine Kidney (MDCK) cell line and Sec15 in a human retinal pigment epithelial cell line caused a marked reduction in the length of cilia ultimately leading to ciliopathy (Feng, Knodler et al. 2012, Fogelgren, Zuo et al. 2014). The detailed mechanism of exocyst mediated support of cilium has not been worked out yet, but exocyst has been hypothesized to be a scaffold for ciliary basal body positioning and intracellular trafficking of exosome-like vesicle (ELV) (Chacon-Heszele, Choi et al. 2014).

In accordance with exocyst's critical role in ciliogenesis, development and growth homeostasis, full knockout of the exocyst members in mice show early embryonic lethality at the blastocyst stage. *Sec3*−/− embryos are defective in inner cell mass proliferation whereas *Sec8-/-* mice are defective in mesoderm formation (Mizuno, Takami et al. 2015). A wide range of developmental defects have been reported in other conditional, partial, or heterozygous mutant mice of the exocyst members. For example, conditional Sec10 KO mice exhibit defects in the organogenesis of its genito-urinary track leading to complete anuria in newborns followed by death within a day after birth (Fogelgren, Zuo et al. 2014). These combined observations place the exocyst subunits as so-called 'essential genes' making loss of function genetic epistasis experiments, to measure exocyst's contribution on cell biological processes of interest, somewhat challenging. Furthermore, in the course of higher plant speciation, through whole genome duplications, plants have acquired multiple paralogs and splice forms of the exocyst subunits in the genome. In *Arabidopsis thaliana* there are at least two isoforms present for Sec3, Sec5, Sec10 and Sec15. This might partially explain why CRISPR/Cas9 mediated gene targeting of exocyst components in *Arabidopsis* was challenging (Hyun, Kim et al. 2015).

Accumulating evidence indicates that multiple classes of phytopathogens have developed immune evasion strategies to suppress and manipulate the host exocyst complexes and their paralogs. For example, the rice pathogen *M.oryzae* has an array of secreted proteins, including avirulence protein AVR-Pii, to suppress activation of host defense protein (Fujisaki, Abe et al. 2015). AVR eventually triggers effector triggered immunity (ETI) response to activate anti-pathogen host R proteins. Recent, publications indicated that AVR-Pii interacts with Exo70 isoforms Exo70F2 and Exo70F3 to form a decoy complex for evading ETI (Fujisaki, Abe et al. 2015).

In mammalian cells, however, exocyst mediated the innate immune response is regulated through Tank binding kinase (TBK1) activation on the Sec5 subcomplex. TBK1 activation was

shown to be a direct consequence of RAL binding to Sec5 and subsequent conformational change on its interaction interface (Chien, Kim et al. 2006). Moreover, TBK1 mediated host defense pathway activation was identified as a targetable vulnerability in KRAS induced lung cancers (Barbie, Tamayo et al. 2009). These results suggested that RAS addicted cancers can hijack the RAL downstream regulatory network for survival advantage.

The first direct connection between cancer and exocyst was suggested, when exocyst was identified as a RAL effector (Moskalenko, Henry et al. 2002). RAS GTPases are one of most widely studied oncogenes, mutation or amplification of which is often causative of neoplastic progression leading to transformation of normal signaling states to states favorable for tumorigenic growth. RAL GTPases belong to one of the three direct effector pathways of oncogenic RAS: the Raf/mitogen-activated protein kinase (MAPK) cascade, the (PI3K)-dependent second messenger pathway, and the Ral guanine nucleotide exchange factor (RalGEF)/Ral GTPases cascade. Raf/MAPK and PI3K pathways have been established as bona fide targets in cancer and are associated with successful development of antineoplastic drugs. However, weak response of these inhibitors in RAS driven tumors, rapid development of resistance and context-specific limitations in the spectrum of PI3K and Raf inhibitor sensitive tumors have forced consideration of additional intervention points within the oncogenic Ras regulatory network. In this regard, a RalGEF/Ral pathway remains a road less explored.

During oncogenic progression, macroautophagy, as a cellular process, is thought to undergo a major switch in its role- from anti-tumor to pro-tumor in nature. Autophagy is considered to be a ‘double edged sword’ because of its pro-survival and pro-apoptosis roles (White and DiPaola 2009). In normal conditions, autophagy is a process that assists ageing cells in initiating apoptotic cellular program. However, once cancerous, autophagy can be exploited by cells to deal with the oncogenic stress. Since RAL-exocyst has been established as a major genetic

requirement for autophagy, pro survival signaling through macroautophagy might be another regulatory axis that connects exocyst to cancer (Bodemann, Orvedahl et al. 2011).

RAL exocyst signaling has also been implicated in secretion of matrix metalloproteases (MMPs), formation of invadopodia and promoting epithelial to mesenchymal (EMT) related cell migratory phenotype of cancer cells (Chen, Inoue et al. 2006). In hepatocellular carcinoma cells, the exocyst has been reported to position G-coupled chemokine receptors CXCR4 at the plasma membrane to promote tumor growth and metastasis (Cepeda, Dediulia et al. 2015). Thus a growing body of literature establishes the exocyst as a clinically relevant hub due to its constitutive trafficking and stimuli dependent signaling functions.

mTOR, autophagy and Hippo signaling

In response to appropriate trophic stimuli, unicellular and multicellular organisms restore perturbed homeostasis. This integrates coordinated adjustment of mass accumulation, proliferation and survival to upstream instructive signals to kinetic, spatial and dosage regulation of effector signaling pathways (Levine and Kroemer 2008, Zoncu, Efeyan et al. 2011, Yu, Zhao et al. 2015). In higher metazoans Mammalian Target of Rapamycin (mTOR) and Yes Associated Protein 1 (YAP1) have been credited as two sentinel signaling effectors responsive to acute perturbation of cellular nutrient status (Ma and Blenis 2009, Laplante and Sabatini 2012, Yu, Zhao et al. 2012). However, context dependent coordination between mTOR and YAP1 is yet to be fully understood. mTOR, when induced by the nutrient sensing machinery, phosphorylates Ribosomal Protein S6 Kinase (S6K) leading to activation of Ribosomal Protein S6 (S6) and initiation of cellular anabolic metabolism for growth and survival (Ma and Blenis 2009). Cellular growth signaling-mediated anabolic programs are complex and often nutrient type specific. A relatively simplified basic schema is presented in Figure 1.2. Recognition of nutrients by growth factor receptors results in activation of master growth kinase AKT (a.k.a

Protein kinase B) through Class I phosphatidylinositol 3-phosphate kinases (PI3Ks). AKT causes derepression of mTOR on the lysosomal surface causing eventual activation of S6K, leading to protein synthesis and growth (Ma and Blenis 2009). mTOR activation has been studied in great details and Ragulator complex (a.k.a LAMTOR complex) in the lysosomal surface has been demonstrated as one of the major bona fide scaffolds of mTOR (Sancak, Bar-Peled et al. 2010).

There is an intimate link between regulation of cellular growth and starvation signaling. Although the key regulators of energy stress and autophagy have been studied in great details, it was not well understood until a few years back, when coordinated crosstalk amongst these regulators was worked out. As demonstrated (Figure 1.2), the energy stress sensor AMP activated Protein Kinase (AMPK) directly phosphorylates ULK1 for initiation of autophagy (Egan, Shackelford et al. 2011, Russell, Tian et al. 2013) and inactivates mTOR for suppression of the cellular growth program. Interestingly, ULK1 activation, under nutrient rich conditions, is kept in check by mTOR, the same kinase responsible for cellular growth response (Kim, Kundu et al. 2011). Thus AMPK, mTOR and ULK1 form a fine-tuned catalytic triangle detailed spatial, temporal and contextual regulatory circuit of which is yet to be fully understood (Figure 1.2).

Autophagy, cellular catabolic response to nutrient deprivation, is a multi-step process involving distinct steps of vesicle nucleation, elongation, lysosome fusion and autolysis. Activated ULK1-VPS34-Beclin ClassIII PI3K complex formation is one of the initial events preceding vesicle nucleation for autophagosome. This is followed by a sequence of Atg proteins localization for vesicle elongation. Finally, docking and fusion of the lysosome with the autophagosome results in delivery of lysosomal hydrolases for degradation of encapsulated materials in autophagosome. Activation of autophagy has also been reported to lead to a feed forward signaling loop for biogenesis of new lysosomes through the transcription factor TFEB (Settembre, Di Malta et al. 2011, Perera, Stoykova et al. 2015). LAMP1 and LAMP2 are

glycoproteins that have been used widely for localizing lysosome structures within the cells, and phosphatidylethanolamine conjugated higher molecular weight LC3 (often called LC3-I) cleavage onto lower molecular weight LC3 (often called LC3-II) is a reliable marker for autophagy initiation (Levine and Kroemer 2008).

In contrast, nutrient rich environment induces nuclear translocation of transcription coactivator YAP1 to form an 'enhancosome' with target transcription factor TEA Domain Transcription Factors (TEADs). This results in activation of a YAP1/TEAD responsive transcription program, termination of which is initiated by a feedback activation of Hippo signaling (Yu, Zhao et al. 2012). Hippo signaling negatively regulates its downstream target- YAP1, affecting both its stability and activity (Zhao, Li et al. 2010). The Hippo signaling is summarized in Figure 1.3.

The responsiveness of Hippo signaling to diverse upstream mechanical, mitogenic, trophic and immunogenic stimuli suggest that sequential activation of the invariable Hippo core cascade is regulated by a broad variety of contextual upstream regulators that specify localization, duration and kinetics (Varelas, Samavarchi-Tehrani et al. 2010, Aragona, Panciera et al. 2013, Liu, Zheng et al. 2016). The core Hippo components consist of two kinases Macrophage Stimulating 1/2 (MST1/2) and Large Tumor Suppressor Kinase 1/2 (LATS1/2) along with transcription co-activators YAP1 and TAZ (Moroishi, Hansen et al. 2015). Hippo pathway induction is marked by MST1 mediated activating phosphorylation on LATS1. Activated LATS1/2 directly phosphorylates YAP1, flagging it for proteasomal degradation. Conversely, YAP1, when active, is translocated to nucleus and coactivates TEAD regulated genes (Figure 1.3)

Although, the presence of additional kinases such as MAP4Ks has recently been proposed to act in parallel with MST1/2, LATS1/2-mediated inhibitory phosphorylation of YAP1 is a reliable marker for Hippo induction (Meng, Moroishi et al. 2015). The upstream regulators of MST1/2 are even more diverse and their contextual coordination is not well-defined. Interestingly, recent

publications suggested an uncanny relationship between the downstream Hippo signaling component, YAP1 and anti-viral immunity related proteins IKK-Related Kinase ε (IKKε) as well as its homolog TBK1 (Wang, Xie et al. 2017, Zhang, Meng et al. 2017). However, upstream events for Hippo responsiveness during immunogenic signals remain elusive. Further studies are needed to establish the dynamic coordination between host defense response and Hippo signaling.

Host defense signaling

The cell autonomous host defense machinery for sensing and responding to pathogens involves intricate crosstalk between upstream pattern recognition receptors (PRR), such as Toll-like receptors (TLR), RIG-I-like receptor (RLR) or NOD-like receptors (NLR), and downstream cellular homeostasis pathways that result in anti-viral signaling cascades and activation of the interferon transcription program. Stimulus dependent activation of these signaling cascades involves precise organization of signaling scaffolds on endo-membrane and less characterized cytosolic compartments. A confluence of observations indicates direct participation of RAL-exocyst signaling for organization and maintenance of TLR signaling on endosomes. For instances, RAL GTPases contribute to relaying TLR3-mediated recognition of dsRNA through TBK1 for eventual induction of IFN-β response. (Chien, Kim et al. 2006). Distinct from its contribution to interferon signaling, TBK1 also participates in a wide array of cellular processes including regulation of growth homeostasis (Cooper, Ou et al. 2017). Indeed, accumulating evidence indicates that TBK1 and PKR function as a signaling hub that connects immune and growth homeostasis pathways (Cooper, Ou et al. 2017, Hasan, Gonugunta et al. 2017, Wang, Xie et al. 2017, Zhang, Meng et al. 2017). In parallel, the combined role of RAL-exocyst complexes' in engagement of anti-viral signaling and regulation of growth homeostasis also indicated that their potential role for dynamic orchestration of cellular responses to trophic and immunogenic stimuli.

Figure 1.2

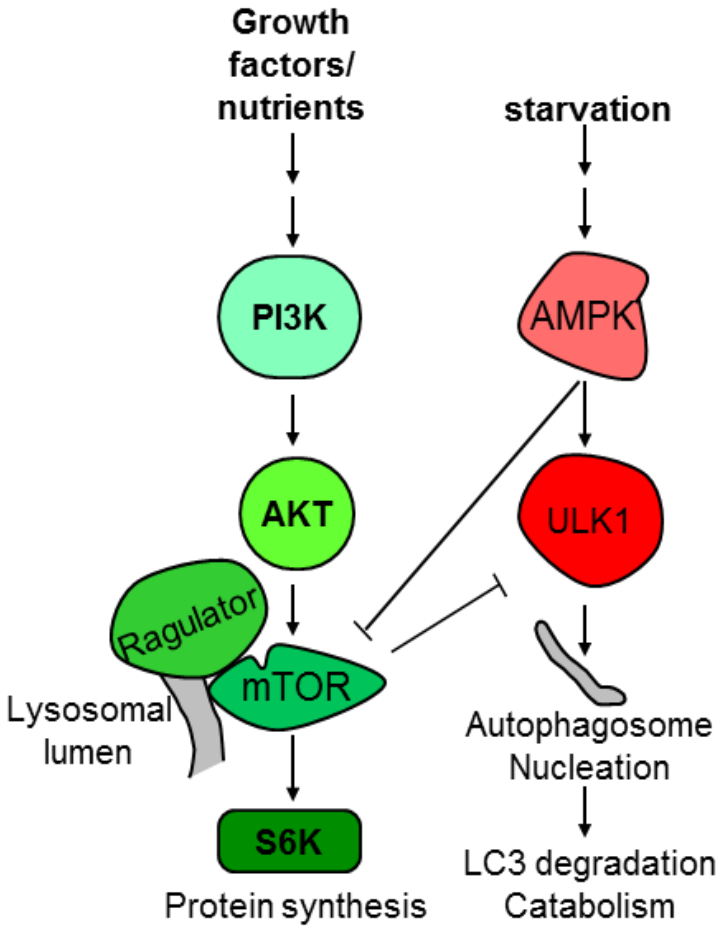

Figure 1.2: Nutrient dependent cellular growth homeostasis signaling network. Nutrient and growth factors can be sensed by cells either through extracellular receptors or intracellular sensor molecules. Replete or depleted nutrient status dictates activation of anabolic growth or catabolic starvation programs. Growth signals activate PI3K/AKT poathway for eventual activation of mTOR leading to activation of ribosomal S6K. Lysosomal surface contains mTOR activation scaffolds including the Ragulator complex. Nutrient deprived cells activate AMPK, which inactivates mTOR and activates master autophagy kinase ULK1 leading to activation of catabolic autophagic program. LC3 cleavage is a reliable marker for autophagy activation.

Figure 1.3

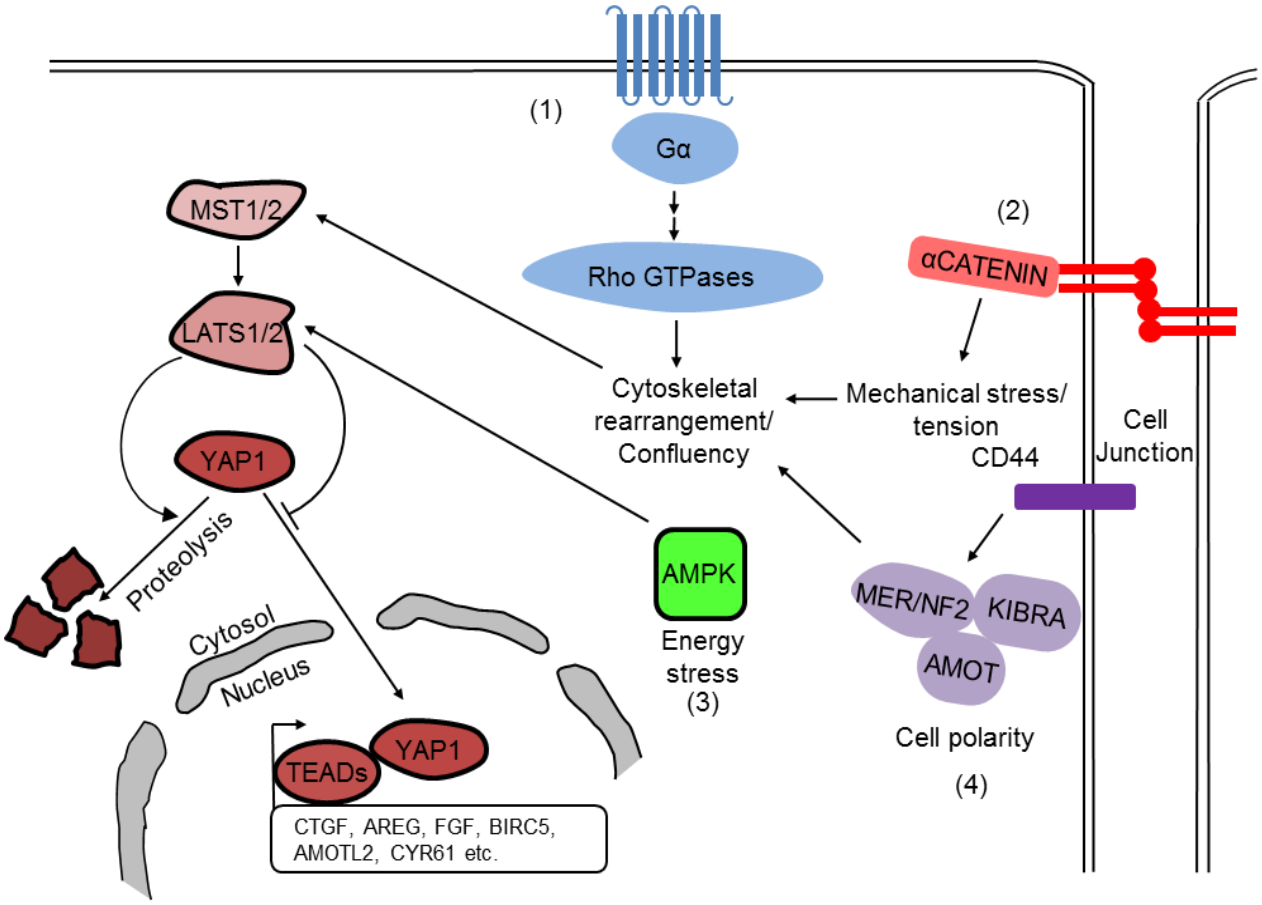

Figure 1.3: Hippo signaling network. Upstream signals such as (1) GPCR mediated cytoskeletal rearrangement (2) adheren junction mediated mechanical stress (3) energy stress and (4) cell polarity signaling activate the Hippo core cascade. Hippo core cascade includes MST1 mediated activating phsohorylation on LATS1 and LATS1 mediated inactivating phosphorylation on YAP1. YAP1 inactivation results in cytotsolic retention and degradation. Active YAP1 translocates onto nucleus as a coactivator for TEADs for activation of YAP1 repsonsive genes.

To induce immunogenic signaling *in vitro*, we chose dsRNA Sendai virus (SeV) and dsDNA Herpes Simplex Virus Type1 (HSV1) for prototypic virus infection. Both of these viruses are pleomorphic enveloped particles with average diameters of around 100-200 nm and are known to activate antiviral host proteins TBK1 and PKR (Sun, Sun et al. 2006, Talloczy, Virgin et al. 2006). HSV1 encodes ICP 34.5 to suppress PKR activation and thus HSV1Δ34.5 mutant demonstrates more robust activation of PKR (Orvedahl, Alexander et al. 2007). Therefore, to induce cytotoxicity we used HSV1 wild type virus and for studying antiviral signaling pathways we used HSV1Δ34.5.

SeV belongs to the family *Paramyxoviridae* with negative sense single stranded RNA. SeV entry is initiated by the binding of the HN, H, or G protein on the virion envelope to sialic acid on the cell surface glycolipids. Intact viral RNA polymerase proteins carry out transcription of the positive messenger RNA strand. Protein synthesis and replication of the genome occur using host cell machinery in the cytoplasm. Mature virions then bud from the host cell plasma membrane to carry out second round of infections (Vainionpaa and Hyypia 1994). HSV1 on the other hand, as a dsDNA virus, directly use the host machinery to initiate transcription of three classes of viral genes- immediate early, early and late. The HSV-1 entry is a multistage complex process that requires involvement of both host surface receptors such as glycoproteins and heparin sulfates and glycoproteins in the virus envelope. HSV1 encoded proteins are classified in two major classes: structural proteins (Virus Particle or VP) and proteins required for transcription, replication and protein synthesis (Infected cell proteins or ICPs) (Everett 2014).

PKR and TBK1: two sentinel immune kinases of multifunctional nature

Although, the canonical function of PKR and TBK1 are to mediate cellular innate immune responses, a growing body of literature supports their participation in a wide array of other cellular functions. Both of them are major sensors and responders of viral virulence factor or

pattern recognition nucleic acids such as dsRNA. PKR can directly bind dsRNA or gets recruited by receptor mediated recognition of virus, whereas TBK1, an atypical IkB kinase, recognizes these signals through upstream receptors such as TLR3 or through adapters such as STING/MAVS or Sec5 (Figure 1.4 and 1.5).

PKR's canonical substrate is EIF2α which shuts off cellular transcription during cellular stress response. However, upon activation PKR has also been implicated in regulation of cellular interferon and NFKβ immune response, JNK pathway activation, DNA damage response and JAK-STAT pathway activation (Figure 1.4). On the other hand, TBK1's canonical substrate is IRF3, which regulate IFN-β Transcription program to defend viral infection. TBK1 also has been demonstrated to regulate a wide range of cellular processes such as cancer cell survival, self-renewal and pathogen clearance. A number of studies have also demonstrate that TBK1 plays role in developmental disorders, inflammatory disease, and cancer (Figure 1.5).

In this body of work, we demonstrate that immunogenic stimuli mediated activation of RALB promotes formation of distinct RALB-Exo84 and RALB-Sec5 subcomplexes for activation of Hippo and mTOR signaling during antiviral and pro-tumor survival responses. The mechanism of action is through PKR mediated MST1 phosphorylation on the Exo84 subcomplex and TBK1 mediated mTOR activation on Sec5 subcomplex. Thus, RALB-exocyst effector complexes define two proximal regulatory signaling pathways during cellular host defense response.

Figure 1.4

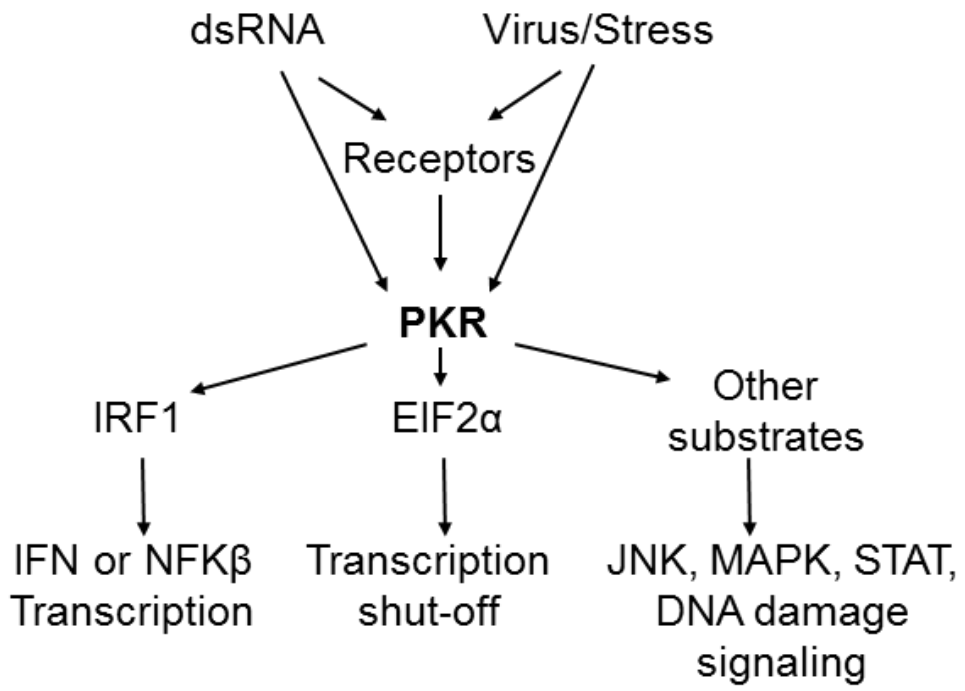

Figure 1.4: Multifunctional nature of PKR. PKR integrates cellular stress response and dsRNA mediated pattern recognition receptors to multiple downstream signaling functions such as inhibition of transcription initiation factors EIF2α and activation of interferon response or other signaling shown in the flowchart above.

Figure 1.5

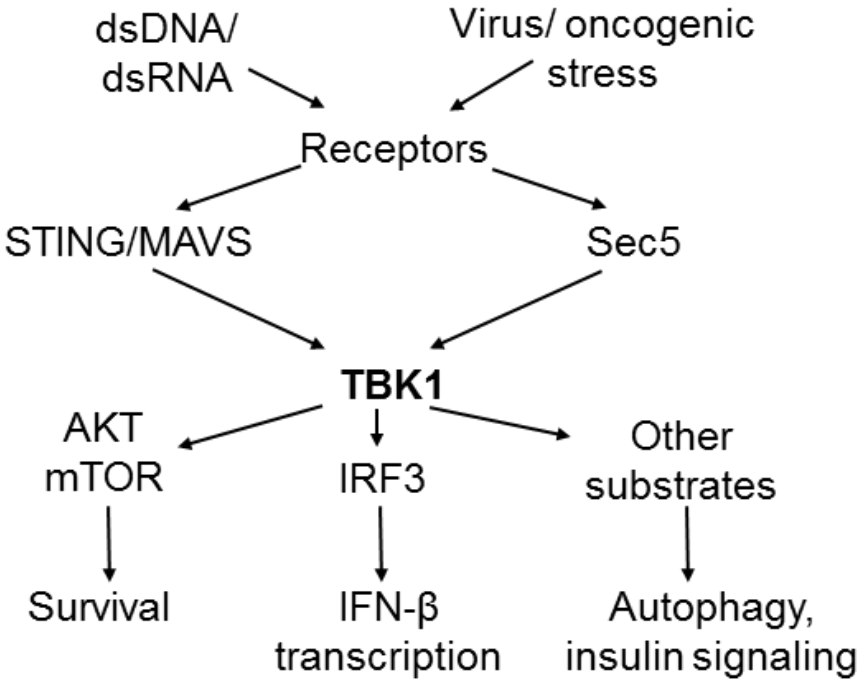

Figure 1.5: Multifunctional nature of TBK1. Viral pattern recognition molecules such as dsDNA or dsRNA is recognized by endosomal or cytosolic receptors (e.g. TLR3, RIG-I, MDA5). The recognition process favors formation of distinct immune signaling protein complexes that activates TBK1. Receptor mediated TBK1 activation have multiple functional output such as cancer cell survival, interferon response etc.

CHAPTER TWO

PART ONE: RAL-Exocyst-effector interactions mediate concomitant activation of Hippo and mTOR signaling for survival against viral cytotoxicity and antitumor apoptotic checkpoint.

Immune stimuli induce distinct exocyst subcomplex interaction with PKR and TBK1

Accumulating evidence links direct participation of the exocyst (a.k.a Sec6/8) in multiple biological functions such as adaptive response to pathogen infection and autophagy (Chien, Kim et al. 2006, Bhuvanakantham, Li et al. 2010, Bodemann, Orvedahl et al. 2011, Ou, Torres et al. 2011). The multi-functional nature of this protein complex stems, in part, from is its ability to form sub-stoichiometric complexes and signaling scaffolds in a context specific manner, coordination of which is yet to be fully understood. To identify molecular leads that may participate in the exocyst mediated regulation of growth homeostasis and host defense signaling, we initially affinity purified and analyzed partners of exocyst using Sec8 (EXOC4) as a bait under optimized trophic and immunogenic stimuli (Figure 2.1 A). The choice of the bait was underpinned in the previous observation that Sec8, a core exocyst subunit, recovered all characterized exocyst entities indicating its suitability as a good ‘handle’ (Grindstaff, Yeaman et al. 1998).

For trophic stimuli, we incubated cells in regular growth media devoid of any serum (DMEM) or in Earle’s balanced saline solution (EBSS) lacking serum and amino acids (Figure 2.1 B). As demonstrated, amino acid starvation induced endogenous LC3 protein re-localization from a diffused cytosolic pattern to a condensed punctate pattern (Figure 2.1 C). This phenotype is characteristic to initiation of autophagy when phosphatidylethanolamine conjugated higher molecular weight LC3 (often called LC3-I) is cleaved through lysosomal proteolysis (Figure 2.1 B). Amino acid deprivation also initiated a global cellular starvation response marked by

increase in activating phosphorylation on AMPK and decrease in activating phosphorylation of mTOR substrate S6K (Figure 2.1 B). For immunogenic stimuli, we used synthetic dsRNA poly I:C (pI:C), which is a potent Toll-like receptor 3 (TLR3) and Rig-I like receptor (RLR) ligand (Chiu, Macmillan et al. 2009, Kawai and Akira 2010). We used uncoated pI:C, because as a treatment protocol it was robust, reproducible and readily scalable for mass spectrometry. The dose of pI:C was optimized in cell lines by measuring TBK1 activation (Figure 2.1 D). To identify whether TBK1 activation resulted in upregulation of host defense transcription program, we stimulated HeLa cells for 4 hour with pI:C and 6 hours with Sendai virus and measured enrichment of the commonly upregulated top 20 genes using RNAseq. As demonstrated, the cells treated as such showed a transcript level enrichment for genes that function in antiviral IFN-β response (Figure 2.1 E). Consistent with this, expression of MX1, a direct IFN-β target, was upregulated in response to pI:C stimulus (Figure 2.1 F).

Sec5 and Exo84 subunits have previously been implicated in distinct regulatory programs of pathogen and nutrient sensing pathways by forming two distinct subcomplexes (Chien, Kim et al. 2006, Bodemann, Orvedahl et al. 2011). To examine this, we isolated high molecular weight complexes from proliferating human epithelial cells with or without trophic and immunogenic stimuli. As shown, the bulk of endogenous Exo84 and Sec5 eluted in separate fractions of ~500 and ~700 KDa respectively (Figure 2.2 A, Figure 2.3 B). Interestingly, the RALB partition profile indicated co-elution of a ~34KDa modified RALB form with Sec5. This data appears to be consistent with previous reports that an ubiquitinated form of RALB preferentially associates with Sec5, but not with Exo84 (Simicek, Lievens et al. 2013). Taken together, these data indicated the presence of Exo84 and Sec5 exocyst sub-complexes.

To identify Sec8 partners we immunoprecipitated endogenous Sec8 and performed a multiplexed quantitative mass spectrometry assay using Tandem Mass Tag (TMT) affinity purification mass spectrometry (AP-MS) technology. Sec8 was immunoprecipitated in two

human epithelial cell lines using three epitope specific antibodies in the presence and absence of nutrient and immune stimuli totaling a set of twenty specific and twelve control datasets. Datasets were subjected to two layers of comparisons- ‘static comparison’ to identify a set of specific candidates followed by ‘dynamic comparison’ to compare enrichment of the specific candidates in presence and absence of stimuli (Figure 2.1 G). Using iterative clustering of normalized protein estimate profiles and dataset intersection strategy we identified a set of 14 partners that consistently co-immunoprecipitated with Sec8 (See methods for details). This group of proteins was defined as the constitutive core interactome of Sec8 (Figure 2.4 A).

Interestingly, this core Sec8 interactome constituted a subset of four exocyst subunits, which included Sec5 but not Exo84. Although, semi-quantitative and spectral count based proteomics, which usually provides a deeper coverage of affinity purified samples, identified all exocyst subunits in AP-MS of Sec8, a higher relative abundance of the same subset of subunits was observed (Figure 2.2 B and Figure 2.3 D). These data indicated that Exo84 and possibly its partners were under represented in the Sec8 interactome. This observation was consistent with previous studies where preferential co-immunoprecipitation of Sec5 in Sec8 AP-MS has been reported recently (Boldt, van Reeuwijk et al. 2016). In addition, Sec5 co-immunoprecipitated the same subset of exocyst subunits as Sec8, whereas Exo84 co-immunoprecipitated the remaining four exocyst subunits with high abundance (Fig 2.2 C). The core Sec8 interactome also identified known, TBK1-Azi2, and novel, CAK (CDK7, MNAT1, CCNH) and PRPS (PRPS1, PRPS2, PRPSAP1), physical complexes as partners (Figure 2.4 A and B). Interestingly, when we examined the effect of stimuli on these interactions, we found that trophic stimulus did not significantly alter relative abundance of any Sec8 partners (Figure 2.3 A). However, the immunogenic stimulus promoted statistically significant accumulation of TBK1-Sec8 complexes that was not due to an increase in TBK1 gene expression or protein stability (Figure 2.4 C and E). The relatively subtle nature of this dynamic alteration of exocyst constituency was also

reflected in relatively unchanged high molecular weight partition profile of exocyst subunits (Figure 2.3 B). None of the other Sec8 partners, such as CAK complex component CDK7, showed significant immune stimulus dependent enrichment or depletion (Figure 2.3 C).

To examine the effect of immunogenic stimulus on the Exo84 subcomplex, we analyzed stimulus specific Exo84 coIP from cells with stable ectopic overexpression of Exo84. Using this approach, we identified PKR as a novel Exo84 partner as it engages with Exo84 when cells are exposed to immunogenic stimulus (Figure 2.4 D and F). Because Sec8 was present, albeit in differing spectral count abundances, in both Sec5 and Exo84 immunoprecipitations, we reasoned that both TBK1 and PKR may interact with Sec8. Accordingly, we found TBK1 and PKR co-immunoprecipitated with Sec8; but when incubated with pI:C, PKR dissociated from Sec8 whereas TBK1 associated (Figure 2.4 E). Interestingly, PKR dissociation from Sec8 accompanied dissociation of Exo84 from Sec8. These observations resulted in the hypothesis that immunogenic stimulus favors steady state conversion of the exocyst holocomplex into Exo84-PKR and Sec5-TBK1 containing two subcomplexes. To examine this, we analyzed Exo84 and Sec5 immunoprecipitates for coimmunoprecipitation of PKR and TBK1 and found that the immune stimulus favored accumulation of Exo84-PKR and Sec5-TBK1 complexes and eliminated Sec5-PKR interaction (Figure 2.4 F and G).

Therefore, our quantitative proteomics based screen and subsequent biochemical validation indicates that TBK1 and PKR are bona fide immune context responsive Sec5 and Exo84 subcomplex interactors (Figure 2.4 H).

Figure 2.1

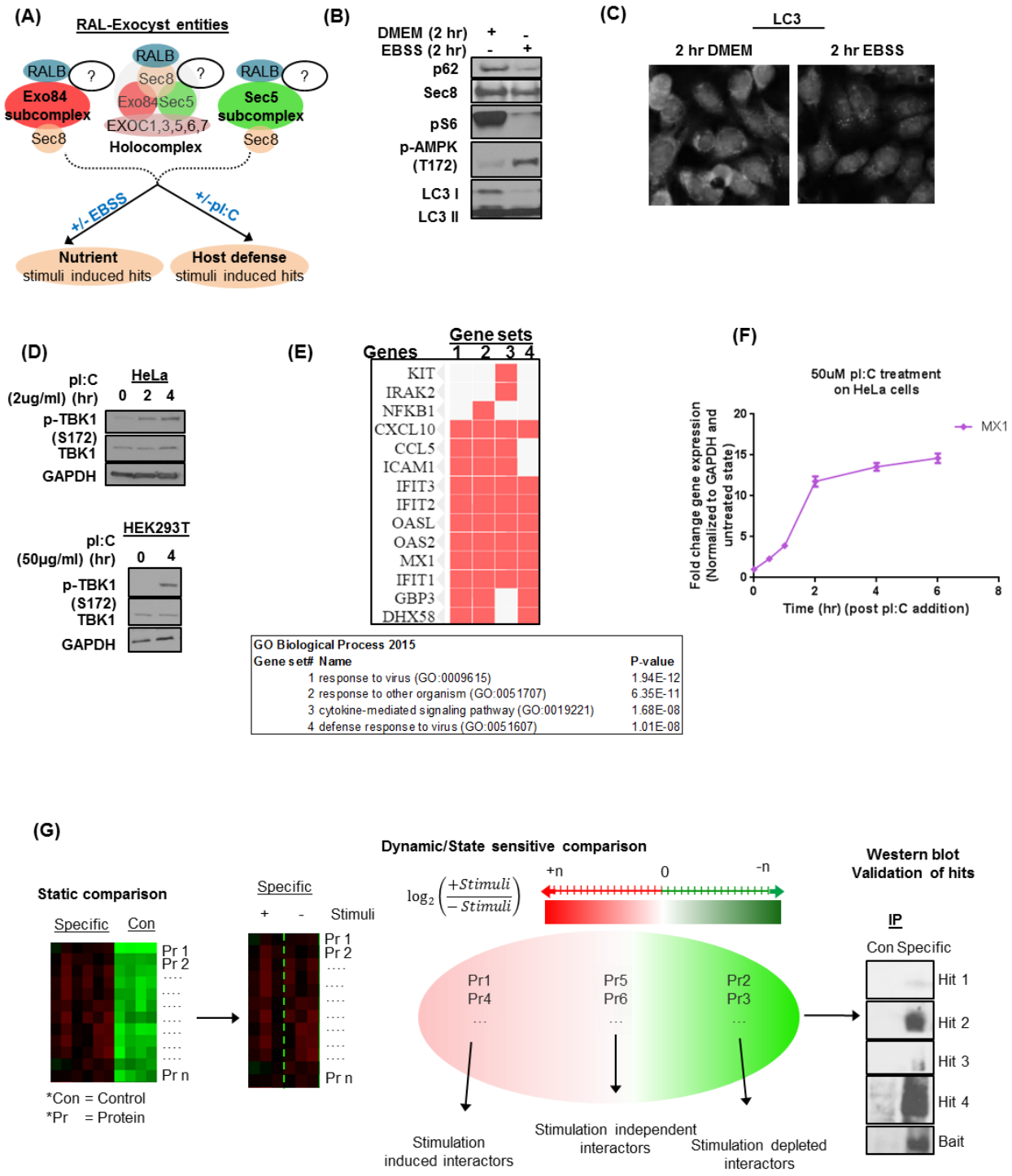
(A)
RAL-Exocyst entities
RALB
Sec8
Exo84
Sec5
EXOC1,3,5,6,7
Holocomplex
Exo84 subcomplex
Sec5 subcomplex
Sec8
+/- EBSS
+/-pI:C
Nutrient stimuli induced hits
Host defense stimuli induced hits
(B)
DMEM (2 hr)
EBSS (2 hr)
p62
Sec8
pS6
p-AMPK (T172)
LC3 I
LC3 II
(C)
LC3
2 hr DMEM
2 hr EBSS
(D)
pI:C (2ug/ml) (hr)
HeLa
0 2 4
p-TBK1 (S172)
TBK1
GAPDH
pI:C (50µg/ml) (hr)
HEK293T
0 4
p-TBK1 (S172)
TBK1
GAPDH
(E)
Genes
Gene sets
1 2 3 4
KIT
IRAK2
NFKB1
CXCL10
CCL5
ICAM1
IFIT3
IFIT2
OASL
OAS2
MX1
IFIT1
GBP3
DHX58
GO Biological Process 2015
Gene set# Name P-value
1 response to virus (GO:0009615) 1.94E-12
2 response to other organism (GO:0051707) 6.35E-11
3 cytokine-mediated signaling pathway (GO:0019221) 1.68E-08
4 defense response to virus (GO:0051607) 1.01E-08
(F)
50uM pI:C treatment on HeLa cells
MX1
Fold change gene expression (Normalized to GAPDH and untreated state)
Time (hr) (post pI:C addition)
(G)
Static comparison
Specific
Con
Pr 1
Pr 2
Pr n
*Con = Control
*Pr = Protein
Specific
+ -
Stimuli
Dynamic/State sensitive comparison
log2 (+Stimuli / −Stimuli)
+n
0
-n
Pr1 Pr4
Pr5 Pr6
Pr2 Pr3
Stimulation induced interactors
Stimulation independent interactors
Stimulation depleted interactors
Western blot Validation of hits
IP
Con Specific
Hit 1
Hit 2
Hit 3
Hit 4
Bait

Figure 2.1: Optimization of stimulation protocols and data analysis strategy

(A) Schematic illustration of the Ral-exocyst entities and the strategy for AP-MS discovery platform to identify novel context specific exocyst hits.

(B and C) Nutrient starvation protocol initiates cellular starvation response. HEK293T cells were incubated with growth media without serum or Earle's basic saline solution (EBSS). Collected cell lysates were analyzed for indicated proteins using SDS-PAGE **(A)** or fixed cells were probed for LC3 Immunofluorescence using anti-LC3 antibody **(B)**.

(D, E and F) Cellular host defense response protocol with dsRNA analog polyI:C or Sendai virus induces IFN-β response. (D) HeLa and HEK293T cells incubated with pI:C for indicated time periods were collected and analyzed for indicated proteins using SDS-PAGE. **(E)** Whole transcriptome level of the HeLa cells treated with polyI:C or SeV were analyzed for genes commonly upregulated when compared to an untreated sample using RNAseq and enrichments of gene ontologies under these stimuli were performed using a standard hypergeometric test. Induction of gene sets known to be induced as antiviral defense response such as ''GO: 0009615 response to virus'' were identified as enriched. **(F)** In HeLa cells, MX1 a known IFN-β response gene transcript level change with increasing hours of pI:C incubation was measured by RT-qPCR. Data is displayed as a line plot, represented as mean ± SEM. Cell lysates collected from.

(G) Strategy for analyzing the AP-MS datasets. Specific and non-specific control Immunoprecipitates from both treated or untreated conditions were analyzed using LC-MS/MS. The datasets generated as such, were noise controlled for specificity by comparing for enrichment over the non-specific controls. Generated specificity controlled datasets were divided into treated and untreated cohorts and compared for enrichment over one condition versus the other. Hits identified were subsequently validated by western blot.

Figure 2.2

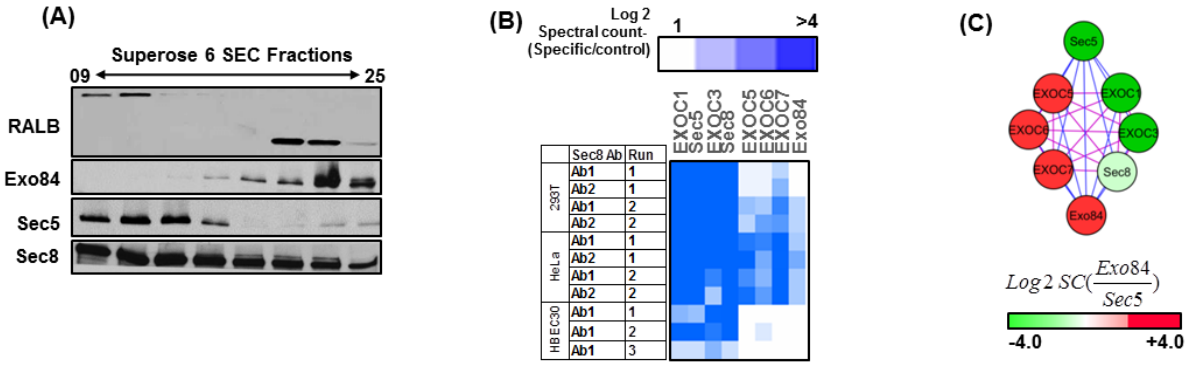

Figure 2.2: The exocyst forms subcomplexes

(A) Exocyst forms subcomplexes. Size exclusion column chromatography fractions of high molecular weight complexes in HEK293T cells were analyzed for partition profile of indicated proteins using SDS-PAGE.

(B) Sec8 immunoprecipitation protocol recovers all known subunits of the exocyst holocomplex. Sec8 was immunoprecipitated using multiple epitope specific antibodies and analyzed for spectral count abundance of the exocyst subunits using MS/MS.

(C) Exo84 and Sec5 have differential affinity for the exocyst subunits. Exo84 and Sec5 was immunoprecipitated from HEK293T cells overexpressing tagged Exo84 and Sec5 separately and analyzed for coimmunoprecipitation of exocyst subunits using LC-MS/MS. Data from separately generated Exo84 and Sec5 interactome was merged and represented as a network. Color bar indicates node color scheme whereas blue edges represent experimental and pink edges represent reported interactions.

Figure 2.3

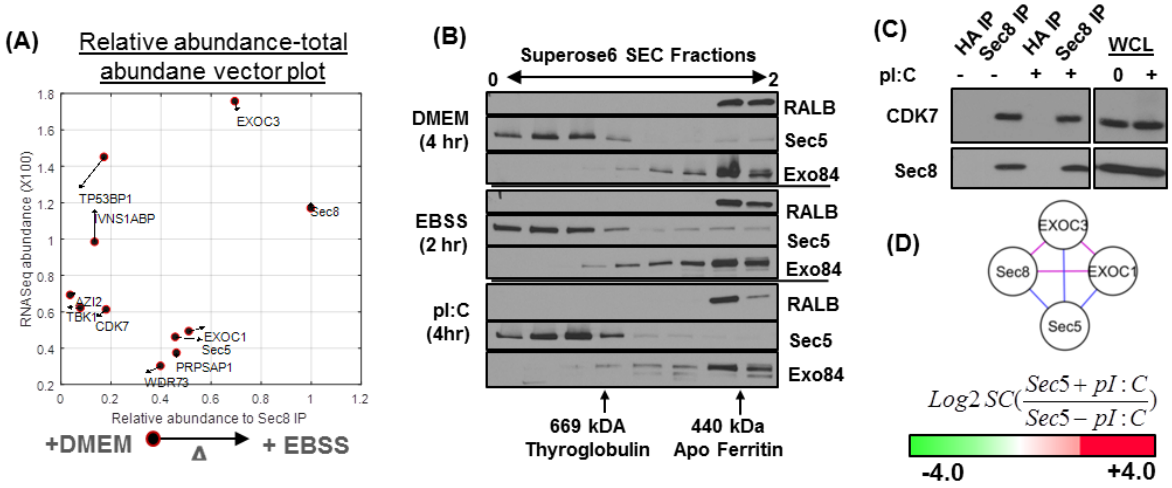

Figure 2.3: Relatively static nature of the exocyst interactome

(A) Total abundance versus relative abundance vector plot of the exocyst core complex components under nutrient stimulus. In HeLa cells relative abundance of core complex interactors versus total RNAseq abundance was plotted as vectors in presence or absence of nutrient stimulus. The X and Y variables were defined as follows- Relative abundance of any Protein to IP (i.e.= Average reporter ion intensity (Protein/Sec8); Total abundance (i.e.= Normalized transcript level quantified by RNAseq data. Filled) circles indicate pre-stimulus values whereas empty arrow-tip represents post-stimulus values.

(B) Exocyst subcomplex partition profile under nutrient and immune stimulus. High molecular weight complexes from HEK293T cell incubated with indicated reagents were isolated using Supersoe6 size exclusion column chromatography and the partition profiles for indicated proteins were analyzed using SDS-PAGE.

(C) CDK7-Sec8 interaction was insensitive to immune context. (L) CDK7-Sec8 interaction was insensitive to immune context. HEK293T cells were incubated with growth media or

polyI:C and endogenous Sec8 was immunoprecipitated and analyzed for coimmunoprecipitation of CDK7.

(D) Proteome interaction map of Sec5 interactors under host defense stimuli. HEK293T cells overexpressing tagged Sec5 were incubated in the presence or absence of pI:C and Sec5 was immunoprecipitated and analyzed for coimmunoprecipitation of proteins using mass spectrometry. Color bar indicates node color scheme whereas edges are color coded as indicated in **Figure 2.2C**.

Figure 2.4

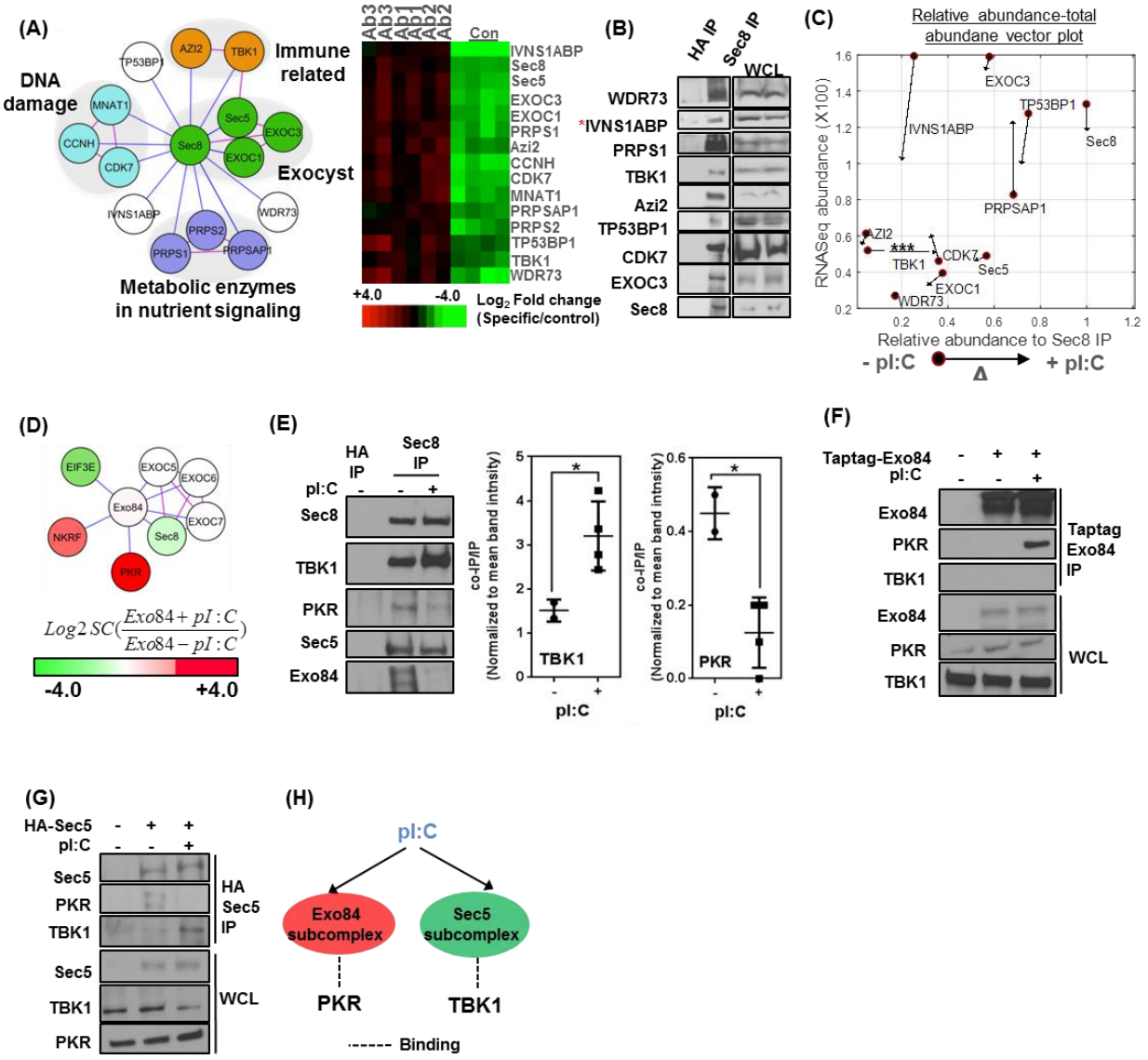

Figure 2.4: Constituency and dynamicity of the exocyst entities

(A) The network view of the Sec8 interactome. Sec8 was immunopreipitated from HEK293T or HeLa cells using three epitope specific antibodies under presence or absence of nutrient or immune stimuli. IP was analyzed for coimmunoprecipitation of partners using nano-HPLC electronspray ion trap tandem mass tag mass spectrometry. Nodes represent proteins, blue

edges represent experimentally observed interactions and pink edges represent known interaction imported from curated BIOGRID database. The complex encompasses components from different biological gene functions marked in grey ellipse manually annotated based on their gene function reported on STRING and GO databases. The inclusion criteria for the core complex were as such as Top (Ab1 ∩ Ab2 ∩ Ab3); Top(Run1 ∩ Run2); Top (HEK293T ∩ HeLa), where, Top= Proteins with reporter ion intensity (specific/control) ≥2, (Right) Heatmaps represent intensity profile of the core complex components in 6 samples and corresponding 4 controls in HeLa cells**.**

(B) Western blot validation of Sec8 interactome. Sec8 was immunoprecipitated and analyzed for coimmunoprecipitation for indicated core complex components defined in **(A)**. IVNS1ABP protein is marked with a red asterisk as it did not pass through a specificity threshold on CRAPOME database (see methods for details)

(C) Total abundance versus relative abundance vector plot of the exocyst core complex components under host defense response. In HeLa cells relative abundance of core complex interactors versus total RNAseq abundance was plotted as vectors in presence or absence of immune stimulus (n=8). The X and Y variables were defined as follows- Relative abundance of Protein X to IP (i.e= Average reporter ion intensity (Protein X/ Sec8); Abundance (i.e= Normalized transcript level quantified by RNAseq data). Filled circles indicate pre-stimulus values whereas arrow-tip represents post-stimulus values. Statistical significance for TBK1 enrichment were measured using student's t test ($p<0.01$)

(D) Proteome interaction map of Exo84 interactors under host defense stimuli. HEK293T cells overexpressing tagged Exo84 were incubated in the presence or absence of polyI:C and Exo84 was immunoprecipitated and analyzed for coimmunoprecipitation of proteins using mass spectrometry. Edges and nodes are color coded as in **(A).**

(E) Sec8 interacts with immune signaling kinases PKR and TBK1 in a stimulus dependent manner. HEK293T cells were incubated with or without pI:C for 4 hour and endogenous Sec8

was immunoprecipitated. Coimmunoprecipitation of the indicated proteins were analyzed using SDS-PAGE. Band intensities were quantified and statistical significance for co-IP/IP level between with or without pI:C cohorts were measured using unpaired student's t-test ($p<0.01$).

(F and G) Exo84 and Sec5 forms complex with PKR and TBK1 in a stimulus specific manner. Transiently expressed Taptag-Exo84 and HA-Sec5 HEK293T cells were grown to confluence and incubated with pI:C for 4 hours. Then Exo84 and Sec5 were immunoprecipitated with antibodies directed to the specified tags. Immunoprecipitates were analyzed for coimmunoprecipitation of the specified proteins.

(H) Cartoon representation summarizing immune stimuli dependent distinct exocyst subcomplexes and their partners.

Virus infection induces assembly of Exo84-PKR-MST1 and Sec5-TBK1-mTOR complexes

PKR and TBK1 are multifunctional proteins with substrates and effectors participating in a wide array of cellular functions (Williams 1999, Barbie, Tamayo et al. 2009, Kim, Welsh et al. 2013). Depending on upstream signals, TBK1 and PKR partner with a diverse downstream scaffolds and partners, in kinase dependent and independent manners (Shen, Niso-Santano et al. 2012, Cooper, Ou et al. 2017). We reasoned that an overlap between these immune kinases and the exocyst interactome might indicate potential shared biological functions carried out by them in tandem.

Hence, we generated PKR and TBK1 interactomes in the presence or absence of immunogenic stimulus and in the presence or absence of overexpressed kinase active or inactive cDNA. These datasets were generated separately and compared for a set of common and distinct partners. Final analysis indicated reciprocal isolation of Exo84, Sec5 from PKR and Sec5, Sec8 from TBK1 immunoprecipitation. And more importantly, pI:C stimulus resulted in accumulation of TBK1-Sec5/Se8 and PKR-Exo84 complexes (Figure 2.5 A).

The TBK1 interactome also identified S6K, RPTOR and YAP1 as partners, proteins that are known regulators of mTOR and Hippo signaling pathways (Figure 2.5 A). Interestingly, kinase-dead TBK1 did not associate with S6K and RPTOR, but was sufficient to associate with YAP1 (Figure 2.5 A and Figure 2.6 C). These data hinted that TBK1-RPTOR/S6K and TBK1-YAP1 interactions might depend on the activation status of TBK1.

The PKR interactome also identified Exo84 and multiple upstream regulators of Hippo signaling such as MST1, NF2, KIBRA as potential novel partners (Figure 2.5 A).

Interestingly, both two hybrid screening approach and focused affinity purification immunoblots from previous works indicated that upstream Hippo regulator KIBRA (WWC1) interacts with the exocyst (Rosse, Formstecher et al. 2009, Bodemann, Orvedahl et al. 2011, Yoshihama, Sasaki

et al. 2011). Moreover, careful investigation of our AP-MS datasets suggested two out of three epitope specific antibodies against Sec8 immunoprecipitated KIBRA as a validated partner for Sec8 (data not shown). Of these, MST1 and KIBRA interaction with PKR was validated using western blot (Figure 2.6 A and B).

Also, the confluence of mTOR signaling proteins in TBK1 and PKR interactome were compelling, since mTOR have previously been shown to be partners of the exocyst using two hybrid screen and affinity-purification immunoblot based analysis (Rosse, Formstecher et al. 2009, Martin, Chen et al. 2014). Moreover, because RPTOR is an immediate proximal partner of mTOR, we examined whether mTOR was also present in the TBK1 containing complex. As indicated, using immunoblot, mTOR was recovered from active TBK1 immunoprecipitation, but not from kinase defective TBK1 immunoprecipitation (Figure 2.6 C).

PKR and TBK1 are major kinases that recognize, respond and regulate cellular antiviral response. Therefore, we hypothesized that if mTOR and Hippo signaling are functionally regulated by TBK1 and PKR, virus infection mediated TBK1 and PKR activation would result in alteration of these pathways. To test that, in human embryonic kidney cell line, we generated a time-course read-out of phosphorylations on core Hippo signaling proteins MST1, LATS1, YAP1 and mTOR signaling substrate S6K upon Sendai virus (SeV) and Herpes Simplex Virus (HSV1) infection (Chien, Kim et al. 2006, Talloczy, Virgin et al. 2006, Chien and White 2008, Bodemann, Orvedahl et al. 2011, Simicek, Lievens et al. 2013, Tracy, Velentzas et al. 2016, Uhm, Bazuine et al. 2017, Wang, Xie et al. 2017, Zhang, Meng et al. 2017). Viral infections activated TBK1 and PKR. Interestingly, within 6 hours of infection with either virus, there was an induction of mTOR and Hippo singling as demonstrated by phosphorylation of S6K, downstream of mTOR and LATS and YAP1, downstream of MST1 (Figure 2.5 B and Figure 2.7 B). Notably, virus infection caused a molecular weight shift in MST1, but did not increase canonical MST1

phosphorylation (Figure 2.5 B and Figure 2.7 B). These indicated a possibility of virus infection mediated phosphorylation at an unknown site on MST1.

We also performed analysis of other exocyst relevant pathways such as autophagy and JNK pathway under identical stimuli (Balakireva, Rosse et al. 2006, Bodemann, Orvedahl et al. 2011). JNK pathway activity, measured by activating phosphorylation of p38 MAPK was not affected. As for autophagy, HSV1 (dsDNA virus), but not SeV (dsRNA virus) infection induced LC3-I degradation (Figure 2.7 A and B). These observations suggest that antiviral xenophagy response is not universal across different virus classes and does not coincide with SeV induced TBK1 and PKR activation. HSV1, but not SeV, infection was also associated with mild toxicity (Figure 2.7 C) and marked by a modest increase in cleaved caspase 3 accumulation (Figure 2.7 A and B). Also unlike HSV1, SeV protein expression was fairly uniform with a peak around 6 hours (Figure 2.7 D). Thus we used SeV, instead of HSV1, as a reagent for further functional studies.

Given that MST1 interacts with PKR and PKR is an Exo84 interactor after immunogenic stimulus, we next investigated whether Exo84-PKR-MST1 forms a complex upon viral exposure. We found that, within 6 hours of SeV exposure, Exo84-mTOR complexes disassembled (Figure 2.5 C, E) and gave rise to an Exo84-PKR-MST1 complex (Figure 2.5 D, E). In contrast, the same stimuli induced formation of Sec5-TBK1-mTOR complex and disassembly of the TBK1-YAP1 complex (Figure 2.5 F, G, H). In summary, we found novel evidence for virus-induced dynamic assembly of Exo84-PKR-MST1 and Sec5-TBK1-mTOR complexes that correlate with cellular Hippo and mTOR induction. Furthermore, our data indicate that TBK1 switches from interacting with YAP1 to associating with mTOR after viral challenge (Figure 2.5 I).

Figure 2.5

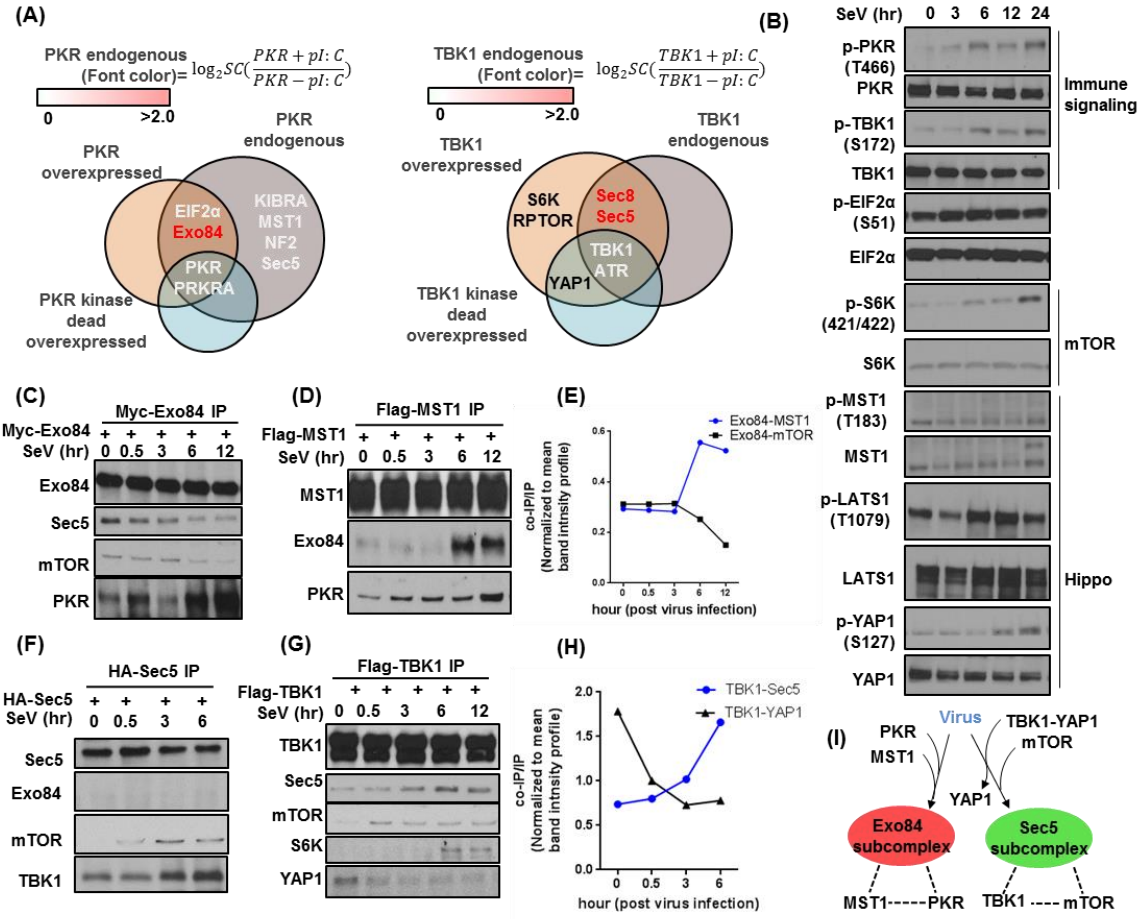

Figure 2.5: Interaction landscape of PKR and TBK1 containing Exocyst subcomplexes under viral infection

(A) PKR and TBK1 interactome identifies MST1 and mTOR as interactors. Endogenous and overexpressed PKR and TBK1 (both active and kinase dead) was immunoprecipitated using anti-protein or anti-tag antibody from HEK293T cells and were analyzed using LC-MS/MS for potential interactors. Endogenous IPs were done in the presence or absence of pI:C. Comparison between the separate datasets are represented as an euler plot where red font color indicates enrichment of relative abundance of the corresponding protein upon pI:C treatment.

(B) Sendai virus infection activates PKR, TBK1, Hippo and mTOR signaling. Non-confluent HEK293T cells were infected with 50 HA/ml Sendai virus for indicated time periods. Cells lysates were analyzed for levels of the indicated proteins using SDS-PAGE.

(C, D and E) Under SeV infection Exo84 forms a stable complex with PKR and MST1. HEK293T cells transiently expressing **(C)** Myc Exo84 and **(D)** Flag-MST1 were incubated with Sendai virus for indicated hours. Exo84 and MST1 were immunoprecipitated using antibodies directed to the specified fusion tags. Immunoprecipitates were analyzed for coimmunoprecipitation of the indicated proteins. **(E)** Kinetics of Exo84-MST1/mTOR and interaction was analyzed by quantifying band intensities of **(C)** and **(D)**.

(F, G and H) Under SeV infection Sec5 forms a stable complex with TBK1 and mTOR. HEK293T cells transiently expressing Flag-TBK1 **(F)** or HA-Sec5 **(G)** were incubated with Sendai virus for indicated hours. Then TBK1 or Sec5 were immunoprecipitated with antibodies directed to the specified fusion tags. Immunoprecipitates were analyzed for coimmunoprecipitation of the indicated proteins. **(H)** Kinetics of TBK1-Sec5/YAP1 and interaction was analyzed by quantifying band intensities of **(F)** and **(G)**.

(I) Schematic representation of Exo84-MST1-PKR and Sec5-mTOR-TBK1 complex formation under virus infection

Figure 2.6

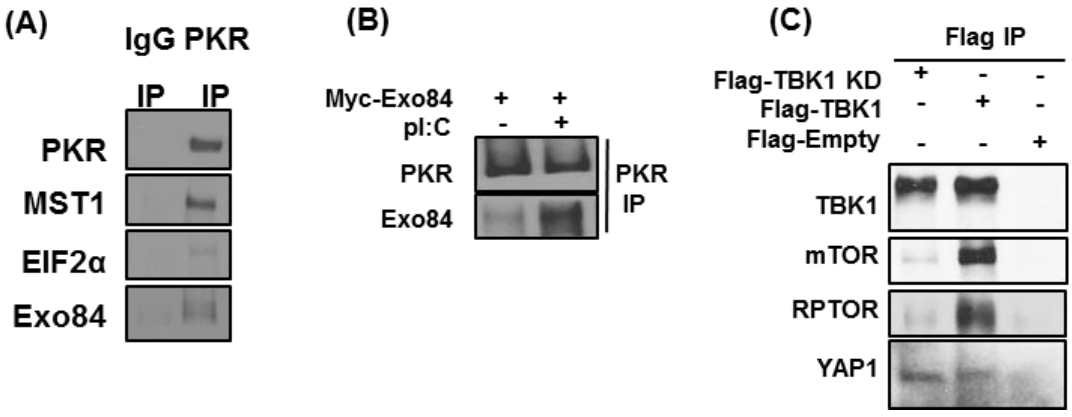

Figure 2.6: Validation of the PKR and TBK1 interactome

(A) PKR interacts with MST1 and Exo84. Endogenous PKR immunoprecipitate sample were analyzed by SDS-PAGE for coimmunoprecipitation of indicated proteins.

(B) PKR immunoprecipitation of Exo84 is stimulus sensitive. HEK293T cells ectopically expressing Myc-Exo84 were treated with pI:C for indicated hours and endogenous PKR was immunoprecipitated from confluent cells. Indicated proteins were analyzed for coimmunoprecipitation using SDS-PAGE.

(C) TBK1 interacts with mTOR and YAP1. Overexpressed Flag tagged active TBK1 or kinase dead (KD) TBK1 or empty vector was expressed in HEK293T cells and immunprecipitation was done using an anti-Flag antibody. Immunoprecipitates were analyzed for coimmunoprecipitation of indicated proteins.

Figure 2.7

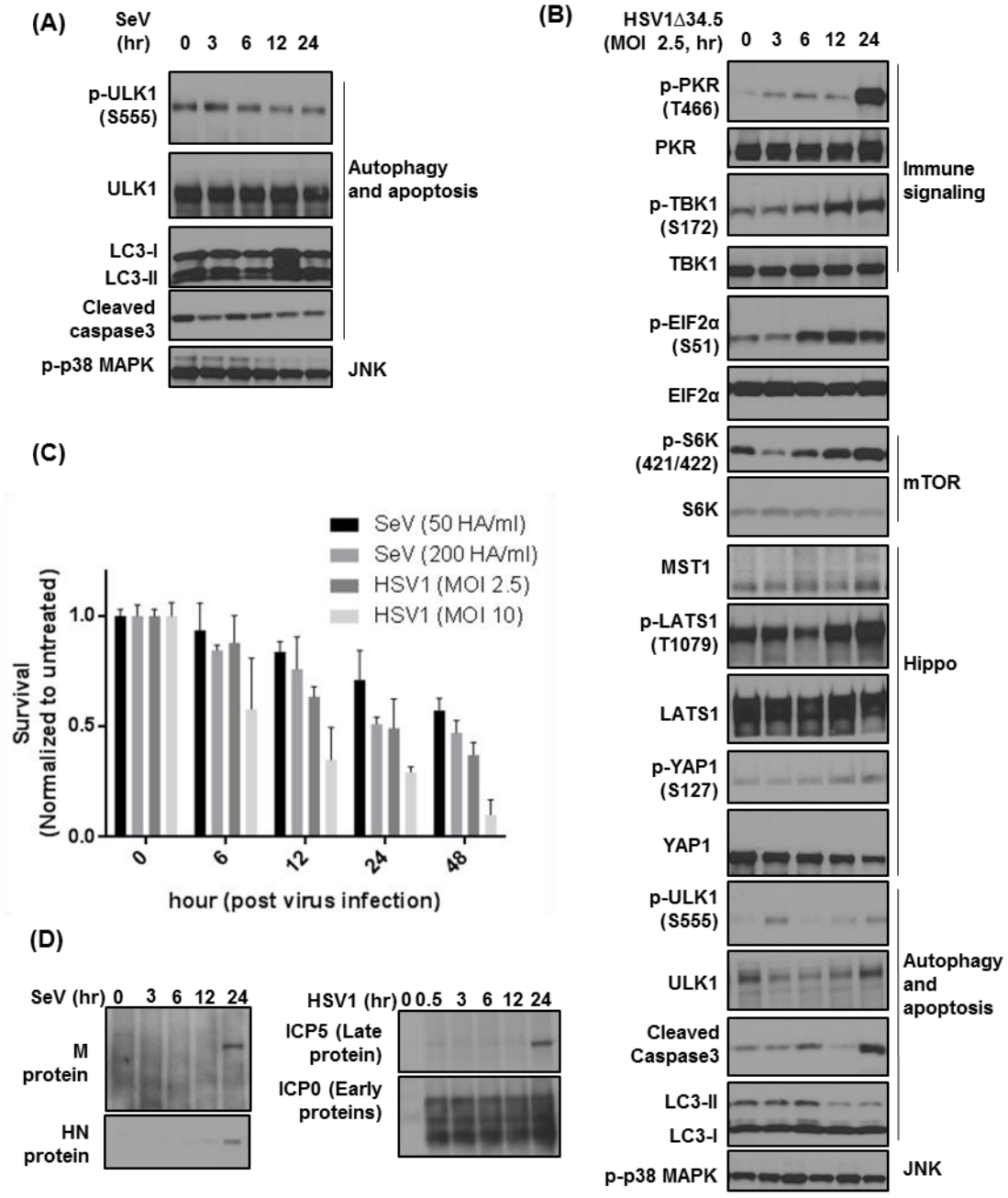
(A)
SeV (hr) 0 3 6 12 24
p-ULK1 (S555)
ULK1
LC3-I
LC3-II
Cleaved caspase3
p-p38 MAPK
Autophagy and apoptosis
JNK
(B)
HSV1Δ34.5 (MOI 2.5, hr) 0 3 6 12 24
p-PKR (T466)
PKR
p-TBK1 (S172)
TBK1
Immune signaling
p-EIF2α (S51)
EIF2α
p-S6K (421/422)
S6K
mTOR
MST1
p-LATS1 (T1079)
LATS1
p-YAP1 (S127)
YAP1
Hippo
p-ULK1 (S555)
ULK1
Cleaved Caspase3
LC3-II
LC3-I
p-p38 MAPK
Autophagy and apoptosis
JNK
(C)
SeV (50 HA/ml)
SeV (200 HA/ml)
HSV1 (MOI 2.5)
HSV1 (MOI 10)
Survival (Normalized to untreated)
1.0
0.5
0.0
0
6
12
24
48
hour (post virus infection)
(D)
SeV (hr) 0 3 6 12 24
M protein
HN protein
HSV1 (hr) 0 0.5 3 6 12 24
ICP5 (Late protein)
ICP0 (Early proteins)

Figure 2.7: Extended SeV and HSV1 kinetics

(A) Sendai virus infection does not activate autophagy. HEK293T cells infected with Sendai virus for indicated time periods. Cells lysates were analyzed for levels of the indicated proteins using SDS-PAGE.

(B) Kinetics of HSV1 infection on cellular pathways. HEK293T cells infected with HSV1 Δ34.5 (MOI 2.5) for indicated time periods. Cells were collected to analyze for levels of the indicated proteins using SDS-PAGE.

(C) Toxicity kinetics of SeV and HSV1. HEK293T cells were infected with two different doses of SeV and HSV1 viruses for indicated time periods and surviving fractions were measured using a standard cell titer glo assay.

(D) SeV and HSV1 viral protein expression kinetics. HEK293T cells infected with SeV (50 HA/ml) and HSV1 (MOI 2.5) for indicated time periods. Cells were collected to analyze for levels of the indicated proteins using SDS-PAGE.

PKR directly phosphorylates MST1 to regulate Hippo signaling

Having established that virus exposure induces Exo84-PKR-MST1 complex formation, we examined the functional implication of PKR and MST1 interaction with Exo84 is. PKR and MST1 have kinase activity. Hence, we acknowledged the possibility of a kinase-substrate relationship between them. Since PKR can directly sense viral RNA to activate itself and phosphorylate downstream substrates (Taylor, Haste et al. 2005), we reasoned that MST1 might be a substrate for PKR.

Because virus infection also activates Hippo signaling (Figure 2.5 B) (Hansen, Moroishi et al. 2015) and MST1 is a core component of Hippo signaling (Figure 2.8 A) (Zhou, Conrad et al. 2009), we hypothesized that PKR might regulate Hippo signaling under virus infection directly or indirectly. To examine this hypothesis, we investigated the effect of PKR loss on virus infection mediated Hippo induction. Interestingly, PKR-deficient mouse embryonic fibroblasts (MEFs) showed attenuated induction of Hippo signaling when infected with SeV indicating that PKR is required for maximal Hippo induction in that context (Figure 2.8 B). We next tested whether PKR kinase function was necessary for Hippo activation using validated PKR inhibitor C16 (Williams 1999, Ingrand, Barrier et al. 2007, Tronel, Page et al. 2014, Xiao, Tan et al. 2016). Human epithelial cell lines pre-treated with a non-toxic dose of C16 ablates SeV induced Hippo activation, indicated by ablation of LATS1 phosphorylation. C16 lowered LATS1 activity even in the absence of SeV stimulus (Figure 2.8 C). From this, we hypothesized that PKR might regulate Hippo signaling constitutively. Consistent with this, inhibition of PKR caused activation of YAP1 as indicated by nuclear translocation (Figure 2.8 D). Moreover, PKR overexpression decreased YAP1 stability and induced LATS1 phosphorylation (Figure 2.8 E). In agreement with this, ectopic PKR expression also inactivated YAP1 activity. On the contrary, PKR inhibition promoted YAP1 activity and that activation was ablated by ectopic expression of PKR (Figure 2.8 F). We then asked whether PKR regulates MST1 directly or indirectly through canonical PKR substrate EIF2α. To do so, we used an ED_{50} dose of PKR inhibitor C16 (1 μM) and known

EIF2α inhibitor Salubrinal (5 μM) in HEK293T cells and found C16, but not Salubrinal caused a significant increase in YAP1 activity (Figure 2.8 G). This data suggests that PKR-Hippo regulation is independent of EIF2α.

Because SeV exposure caused a molecular weight change in MST1, but did not increase known MST1 phosphorylation (Figure 2.5 B and Figure 2.7 B), we wondered whether PKR directly phosphorylated MST1 in a previously uncharacterized site. To test this, we used an *in vitro* co-transfection followed by 1D gel chromatography coupled LC-MS/MS approach. We transfected cells with MST1 along with either active or kinase dead PKR constructs. MST1 was immunoprecipitated and PKR specific post translational modifications were queried. The experiments were done in the presence of the endogenous PKR. And since endogenous PKR constitutively signals through the Hippo pathway (Figure 2.8 C), instead of a simple presence-absence call we took a ratio of the probability of modifications. Thus, if PKR phosphorylated MST1, we expected a ratiometric increase of that phosphorylation in the active versus kinase-dead samples (Figure 2.8 H). We identified that MST1 serine 18 had 49 times higher phosphorylation probability in PKR kinase active versus kinase dead sample according to ModLS score (David C. Trudgian 2012). Moreover, we identified the 9 amino acid long peptide sequence matched the putative PKR recognition sequence built from 52 known PKR substrates except for in -3 and +4 sites (Figure 2.8 I). Thus we suggest that S18 on MST1 is phosphorylated by PKR after viral infection.

To examine whether PKR directly phosphorylated the peptide sequence, we incubated a synthetic peptide with the same sequence and a mutated peptide, where serine was replaced by alanine, with recombinant active PKR and found that the native peptide, but not the mutated one, was phosphorylated (Figure 2.8 J). These data strongly support that the sequence identified on MST1 was a bona fide PKR recognition motif and central serine as an obligate requirement for phosphorylation.

Next, using site specific mutagenesis technology, we mutated S18 on MST1 cDNA to an otherwise non-phosphorylatable 18A and found this mutation was sufficient to attenuate MST1 mediated dose-dependent phosphorylation of its canonical substrate, LATS1 (Figure 2.8 K). These data suggest that S18 phosphorylation is essential for MST1 mediated LATS1 activation. Thus, we identified a novel regulatory interaction between PKR and MST1.

Figure 2.8

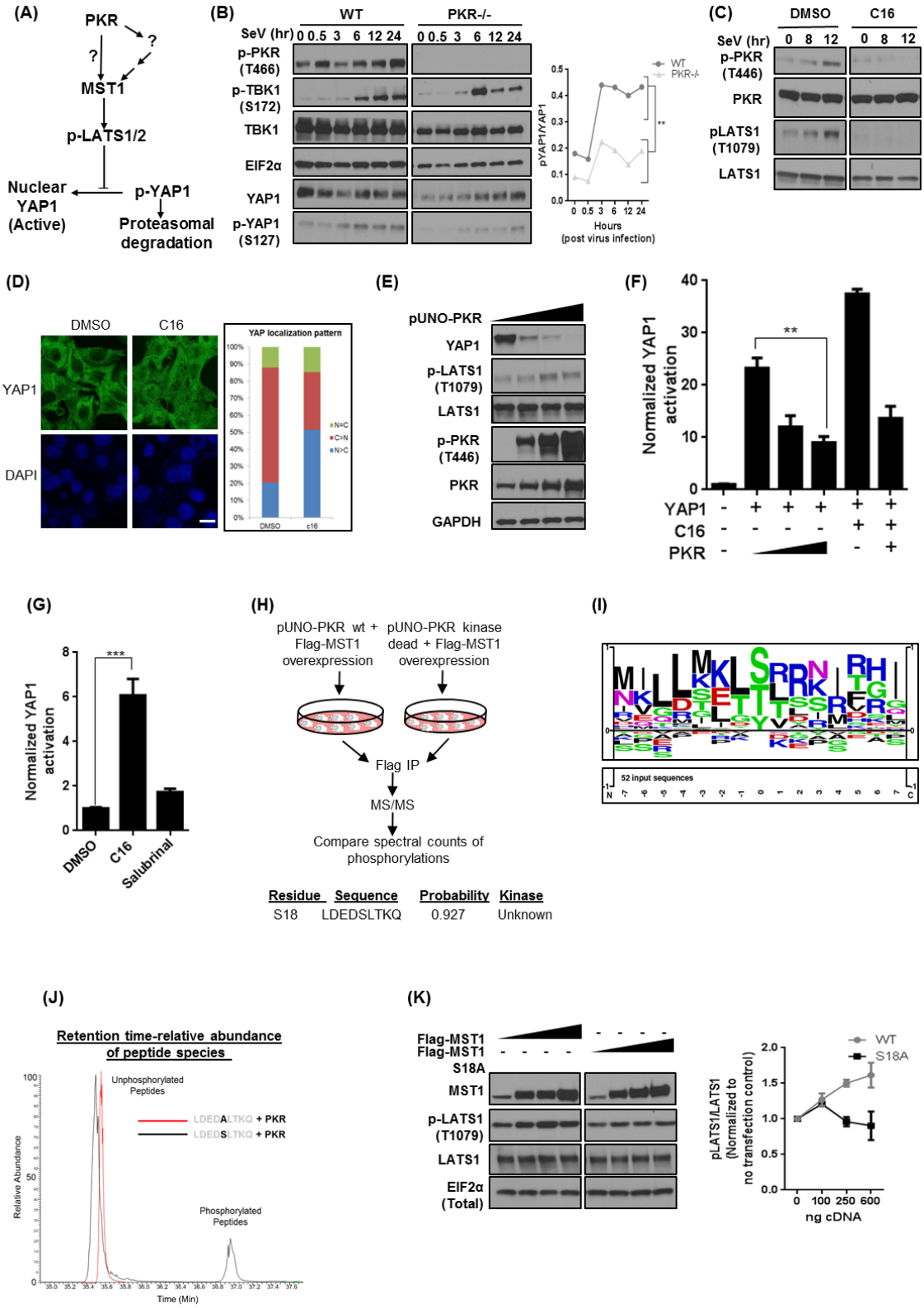
(A)
PKR
?
?
MST1
p-LATS1/2
Nuclear YAP1 (Active)
p-YAP1
Proteasomal degradation
(B)
WT
PKR-/-
SeV (hr) 0 0.5 3 6 12 24
p-PKR (T466)
p-TBK1 (S172)
TBK1
EIF2α
YAP1
p-YAP1 (S127)
pYAP1/YAP1
Hours (post virus infection)
(C)
DMSO
C16
SeV (hr) 0 8 12 0 8 12
p-PKR (T446)
PKR
pLATS1 (T1079)
LATS1
(D)
DMSO
C16
YAP1
DAPI
YAP localization pattern
N=C
C>N
N>C
(E)
pUNO-PKR
YAP1
p-LATS1 (T1079)
LATS1
p-PKR (T446)
PKR
GAPDH
(F)
Normalized YAP1 activation
YAP1
C16
PKR
(G)
Normalized YAP1 activation
DMSO
C16
Salubrinal
(H)
pUNO-PKR wt + Flag-MST1 overexpression
pUNO-PKR kinase dead + Flag-MST1 overexpression
Flag IP
MS/MS
Compare spectral counts of phosphorylations
Residue Sequence Probability Kinase
S18 LDEDSLTKQ 0.927 Unknown
(I)
52 input sequences
(J)
Retention time-relative abundance of peptide species
Unphosphorylated Peptides
LDEDALTKQ + PKR
LDEDSLTKQ + PKR
Phosphorylated Peptides
Relative Abundance
Time (Min)
(K)
Flag-MST1
Flag-MST1
S18A
MST1
p-LATS1 (T1079)
LATS1
EIF2α (Total)
WT
S18A
pLATS1/LATS1 (Normalized to no transfection control)
ng cDNA

Figure 2.8: PKR regulates Hippo signaling through MST1

(A) Schematic diagram outlines the Hippo signaling and potential direct or indirect regulation by PKR

(B and C) PKR is required for maximal activation of Hippo signaling under immune challenge. (B) (Left) Non confluent PKR null MEFs and WT MEFs were incubated with SeV for indicated hours and analyzed for indicated proteins using SDS-PAGE. (Right) p-YAP1/YAP1 ratio for each time point was calculated by measuring individual band intensity. Data was represented as line plot as a function of SeV incubation time. Statistical significance for the data-points in each cohort were calculated using paired t-test **(C)** HEK293T cells either pre-treated with DMSO or 0.2μM C16 for 14 hours. Confluent cells were treated with Sendai virus for indicated hours and collected for analyzing level of the indicated proteins using SDS-PAGE.

(D) PKR inhibition cause nuclear localization of YAP1. HepG2 cells were grown to confluence and treated with DMSO or C16 for 10 hours. Cells were fixed and stained for YAP1 level using monoclonal antibody against endogenous protein. Scale bar represents 10μm.

(E) PKR is sufficient to induce Hippo signaling. Titrating amount of PKR cDNA was expressed in non-confluent HEK293T cells and cell lysates were analyzed using SDS-PAGE for indicated proteins.

(F) PKR negatively regulates YAP1 transcription and rescues C16 mediated Hippo activation. HEK293T cells ectopically expressing 8XGTIIC-luc luciferase regulating firefly luciferase with a renilla luciferase control reporter and plasmids expressing indicated cDNA or empty vector were grown for 24 hours and normalized Hippo induction were measured using standard dual luciferase assay. **(D)** Additionally, Cells were treated with 0.1 μM C16 for 6 hour in the indicated sample in the presence or absence of PKR cDNA.

(G) PKR inhibition mediated Hippo pathway downregulation is EIF2α independent. HEK293T cells transiently dual transfected with 8XGTIIC-luc luciferase regulating firefly luciferase and CMV promoter regulated renilla luciferase reporter were treated 6 hr with ED50

dose of C16 and Salubrinal (EIF2αi) or vehicle control (DMSO). The reporter activity was measured by specific/control luminescence signal ratio. Data was normalized to vehicle treatment. Statistical comparison between treatment cohorts were measured using Student's t test where p value < 0.001

(H) PKR activity is associated with MST1 phosphorylation on S18. MST1 was immunoprecipitated separately from HEK293T cells transiently expressing Flag-MST1 and either pUNO-PKR wt or pUNO-PKR dominant negative kinase dead mutant forms and run on SDS-PAGE. Colloidal coomassie stained gel was cut spanning a region of 55-95 kDa to accommodate the molecular weight corresponding to MST1 (69 KDa). In-gel digested proteins were analyzed using LC-MS/MS and probed for MST1 post translational modifications, enriched specifically on PKR WT over in PKR kinase dead overexpressing sample. Identified peptide sequence around MST1 S18 phosphorylation were searched for de-novo kinase phosphorylation probability in NetPhos3.1 server. The results from the server are summarized in the table.

(I) PKR recognition motif. The sequence recognition motif for PKR is represented as a logo based on 52 input sequences from PhosphoSitePlus database.

(J) *In vitro* phosphorylation of MST1 peptide by purified PKR. Homologous peptide sequence ±4 residue around MST1 S18 region was synthesized artificially keeping the Serine in the middle or replaced with an unphosphorylable Alanine. Peptides were incubated with purified active PKR protein for 2 hours. Purified peptides from the reaction mixture was analyzed using LC-MS/MS and the abundance of the peptide species phosphorylated or unphosphorylated were recorded along the retention time duration.

(K) Characterization of MST1-S18A mutant: HEK293T cells were transfected with titrating amount of MST1 WT or MST1 S18A mutant cDNA expressing plasmids for 48 hours and grown up to 90% confluency. Cell lysates were collected and probed for indicated proteins using SDS-PAGE.

TBK1 supports mTOR signaling and regulates YAP1 through kinase independent cytosolic sequestration

We have shown that virus exposure favors Sec5/8-TBK1-mTOR complex formation (Figure 2,5 F,G,H). Since TBK1 and mTOR have kinase activity, we recognized the likelihood of kinase-substrate relationship between them. However, TBK1 is a sentinel kinase for sensing and responding to viral nucleic acid (Tanaka and Chen 2012). Therefore, we hypothesized that if there is such a relationship, TBK1 might function as a kinase for mTOR. Additionally, the TBK1 interactome also revealed YAP1 as an interacting partner. These observations were consistent with recent studies that have suggested that TBK1 is a regulator of core Hippo pathway molecule YAP1 and immediate mTOR substrate S6K (Cooper, Ou et al. 2017, Wang, Xie et al. 2017, Zhang, Meng et al. 2017). Interestingly, TBK1 showed reciprocal interaction kinetics with YAP1 and mTOR when exposed to SeV (Figure 2.9 A). Since virus exposure also activated TBK1, we hypothesized that TBK1 bound to the Sec5 subcomplex is in an active form and TBK1 bound to YAP1 is inactive. If true, this would be consistent with a model that the impact of virus exposure could result in disassembly of an inactive TBK1-YAP1 complex and subsequent assembly of a Sec5/8-TBK1-mTOR complex.

To test whether YAP1 itself is inhibitory for TBK1, we tested whether ectopic overexpression of YAP1 inhibited TBK1. As shown, increasing amount of YAP1 encoding cDNA reduced TBK1 phosphorylation and IFN-β activity (Figure 2.9 B and C). Interestingly, this IFN-β inactivation could be overcome by ectopic overexpression of LATS1 (Figure 2.9 C). Although consistent with recently published work (Zhang, Meng et al. 2017), this observation did not reveal if TBK1 affects YAP1 activity or stability. We have already shown that virus exposure reduced YAP1 stability and activity through PKR (Figure 2.8 B). Since PKR and TBK1 are major anti-viral immune kinases, we reasoned that TBK1-mediated YAP1 regulation might be an additional axis of Hippo regulation.

To test whether TBK1 regulates YAP1 activity and stability, we used TBK1-deficient MEFs (Cooper, Ou et al. 2017). Interestingly, spontaneously immortalized MEFs deficient in TBK1, stimulated Hippo induction when infected with SeV (Figure 2.9 D). Because, LATS is the major regulator of YAP1 stability, these data suggested that TBK1-YAP1 interaction is competitive to LATS-YAP1 interaction. To test this hypothesis, we measured the effect of YAP1-LATS1 interaction in the presence of ectopic overexpression of TBK1 or control, by probing for the amount of LATS1 that co-immunoprecipitated with YAP1. We found that TBK1 over expression did not affect YAP1 or LATS1 protein stability, but eliminated LATS1-YAP1 interaction suggesting a competitive binding between TBK1 and LATS1 for YAP1 (Figure 2.9 E).

Because TBK1 has kinase dependent and independent functions, we then examined whether TBK1 kinase activity was required for YAP1 activation. We found that, under steady state, when TBK1 is bound to YAP1 (Figure 2.9 A), TBK1 kinase function inhibition (Cmpd II and BX795), did not affect YAP1 transcriptional activity (Figure 2.9 G). These results suggest that TBK1 kinase activity is dispensable for YAP1 regulation.

Surprisingly, we found that TBK1 over expression also resulted in a down regulation of YAP1 activity indicating an intriguingly opposite effect of TBK1 on YAP1 stability and activity. (Figure 2.9 E). Although, this observation was consistent with previous reports (Wang, Xie et al. 2017), these data placed TBK1 as a positive regulator of YAP1 stability but a negative regulator of YAP1 activity. Interestingly, ectopic overexpression of kinase defective TBK1 also inactivated YAP1 transcriptional activity, indicating inhibition of YAP1 activity by TBK1 in a kinase-independent manner (Figure 2.9 E). From these combined observations, we concluded that TBK1 sequesters YAP1 from both its degradation and activation.

Next we examined the functional relevance of TBK1-mTOR interaction. TBK1 and IKKε (TBK1 homolog) double knockout MEFs and TBK1-dficient MEFs, when compared to WT MEFs,

showed attenuated activation of mTOR signaling after viral infection (Figure 2.10 A and Figure 2.10 B). However, the effect was more significant in double knock out MEFs than TBK1-deficient MEFs suggesting that virus-induced mTOR activation might be regulated by TBK1 and IKKε and therefore the Sec5/8-TBK1 complex likely only regulates a subset of mTOR activity.

A growing body of literature suggests that TBK1 might regulate mTOR signaling in multiple regulatory steps. However, previous works from us along with others have shown direct regulation of mTOR substrate S6K activity by TBK1 (Kim, Welsh et al. 2013, Cooper, Ou et al. 2017). Consistent with this, the TBK1 inhibitor CmpdII ablated S6K phosphorylation on T421/S424 (Figure 2.10 C). Moreover, loss of TBK1 and TBK1 interactor Sec8 attenuated S6K phosphorylation after viral infection (Figure 2.10 D). Accordingly, loss of Sec8 was associated with selective disruption of Sec5-mTOR-TBK1 complex and not Exo84-RALB complex (Figure 2.10 E).

Therefore, these combined observations suggest that TBK1 supports mTOR signaling in a kinase-dependent manner and antagonizes degradation and activation of YAP1 by kinase-independent cytosolic sequestration (Figure 2.10 F).

Figure 2.9

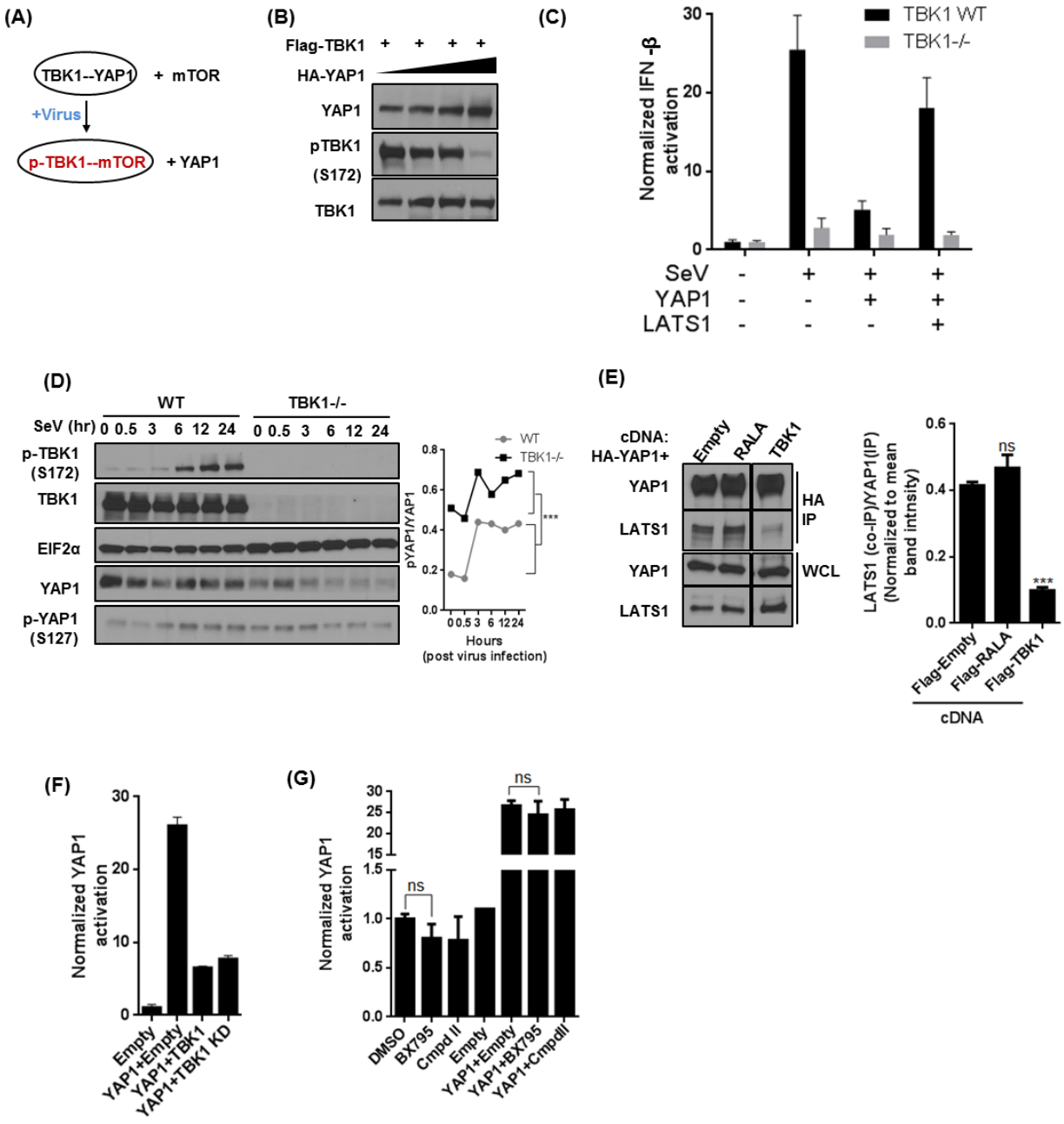
(A)
TBK1--YAP1
+ mTOR
+Virus
p-TBK1--mTOR
+ YAP1
(B)
Flag-TBK1 + + + +
HA-YAP1
YAP1
pTBK1 (S172)
TBK1
(C)
TBK1 WT
TBK1-/-
Normalized IFN-β activation
SeV - + + +
YAP1 - - + +
LATS1 - - - +
(D)
WT
TBK1-/-
SeV (hr) 0 0.5 3 6 12 24 0 0.5 3 6 12 24
p-TBK1 (S172)
TBK1
EIF2α
YAP1
p-YAP1 (S127)
pYAP1/YAP1
Hours (post virus infection)
(E)
cDNA: HA-YAP1+
Empty
RALA
TBK1
YAP1
LATS1
HA IP
YAP1
LATS1
WCL
LATS1 (co-IP)/YAP1(IP) (Normalized to mean band intnsity)
ns
Flag-Empty
Flag-RALA
Flag-TBK1
cDNA
(F)
Normalized YAP1 activation
Empty
YAP1+Empty
YAP1+TBK1
YAP1+TBK1 KD
(G)
Normalized YAP1 activation
ns
DMSO
BX795
Cmpd II
Empty
YAP1+Empty
YAP1+BX795
YAP1+Cmpdll

Figure 2.9: TBK1 is a negative regulator of YAP1 stability and LATS1 mediated turn over through kinase independent mechanism

(A) Schematic diagram illustrating partner swapping event for TBK1 stable complex. Stable complexes are marked as ellipses. TBK1 switches from YAP1 to mTOR when exposed to virus.

(B) YAP1 inhibits TBK1 activity. HEK293T cells transiently expressing Flag-TBK1 or indicated increasing amount of HA-YAP1 were grown to confluence and collected for analyzing levels of indicated proteins.

(C) YAP1 inhibits IFN-β response. HEK293T cells were transiently transfected with IFN-β promoter regulated firefly luciferase, CMV promoter regulated renilla luciferase reporters along with indicated cDNAs treated with or without 6 hour with 50 HA/ml dose of SeV. IFN-β activation was measured using a standard dual luciferase assay.

(D) TBK1 is protective for YAP1. (Left) Non confluent TBK1 null MEFs and WT MEFs were incubated with SeV for indicated hours and analyzed for indicated proteins using SDS-PAGE. (Right) p-YAP1/YAP1 ratio for each time point was calculated by measuring individual band intensity of the proteins. Data was represented as line plot as a function of SeV incubation time. Statistical significance for the data-points in each cohort were calculated using paired t-test where p-value<0.01

(E) TBK1 competes with LATS1/2 for binding with YAP1. Cells transiently expressing HA-YAP1 with or without plasmids expressing indicated cDNAs were grown to confluence and YAP1 was affinity purified using an antibody against HA tag and was analyzed for levels of indicated proteins run using SDS-PAGE on the same gel. Intensities of the bands were quantified and represented as mean ± SEM in the bar graph.

(F) TBK1 inhibits YAP1 activity. YAP transcriptional activity was assayed from HEK293T cells transiently transfected with 8XGTIIC-luc luciferase regulating firefly luciferase, CMV promoter regulated renilla luciferase reporter and empty vector or cDNAs indicated. Normalized Hippo

activation fold change is represented as histograms representing mean ± SEM. Statistical comparison between treatment cohorts were measured using Student's unpaired t test where p value < 0.001

(G) TBK1 mediated regulation of YAP1 is kinase independent. HEK293T cells were transiently transfected with 8XGTIIC-luc firefly luciferase, renilla luciferase reporters along with indicated cDNAs and/or treated 6 hr with ED50 dose of TBK1 inhibitors BX795 and Cmpd II or vehicle control (DMSO). YAP1 activation was measured using a standard dual luciferase assay

Figure 2.10

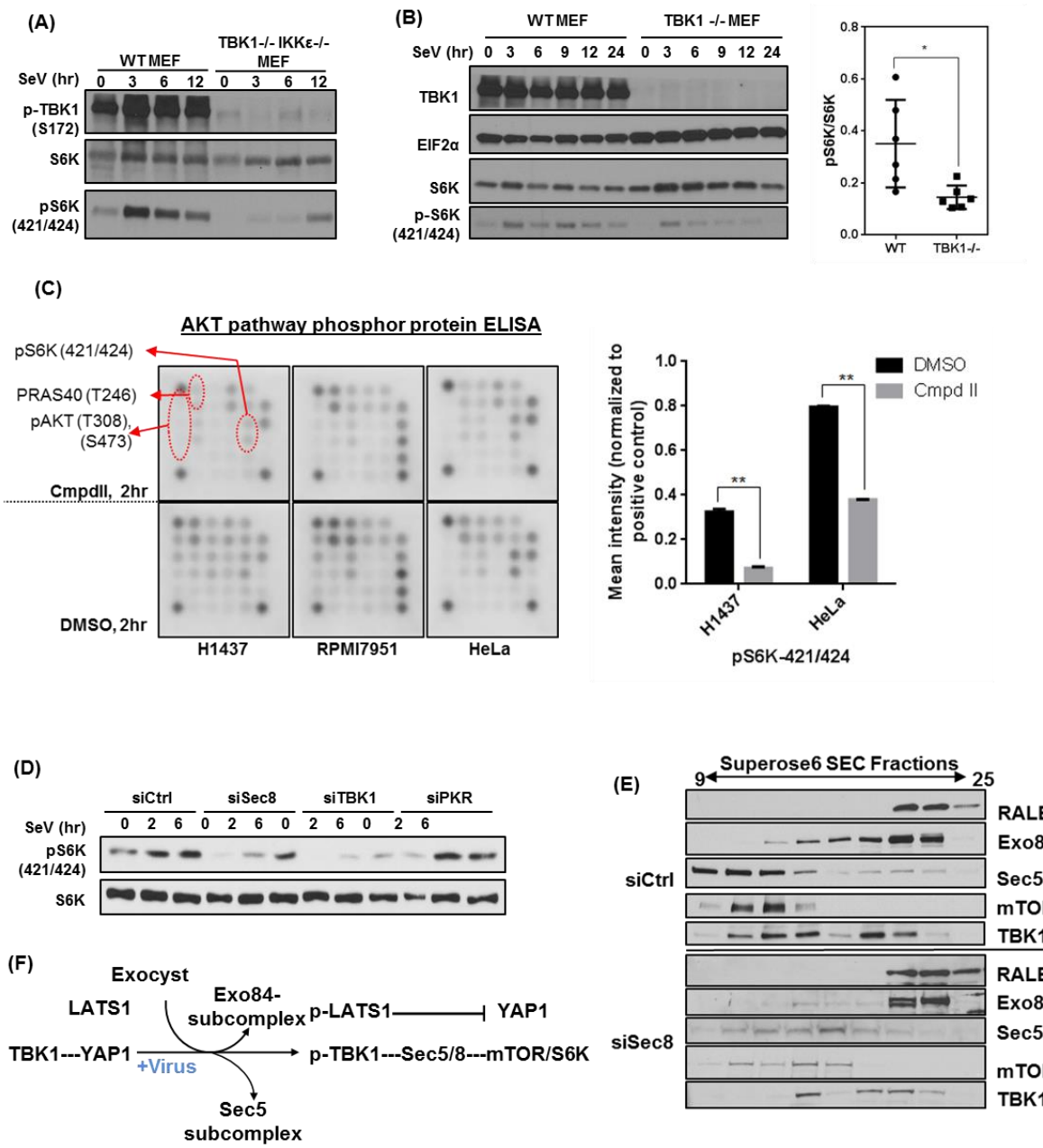
(A)
WT MEF
TBK1-/- IKKε-/- MEF
SeV (hr) 0 3 6 12 0 3 6 12
p-TBK1 (S172)
S6K
pS6K (421/424)
(B)
WT MEF
TBK1 -/- MEF
SeV (hr) 0 3 6 9 12 24 0 3 6 9 12 24
TBK1
EIF2α
S6K
p-S6K (421/424)
pS6K/S6K
WT
TBK1-/-
(C)
AKT pathway phosphor protein ELISA
pS6K (421/424)
PRAS40 (T246)
pAKT (T308), (S473)
Cmpdll, 2hr
DMSO, 2hr
H1437
RPMI7951
HeLa
Mean intensity (normalized to positive control)
DMSO
Cmpd II
pS6K-421/424
(D)
siCtrl
siSec8
siTBK1
siPKR
SeV (hr) 0 2 6 0 2 6 0 2 6 0 2 6
pS6K (421/424)
S6K
(E)
Superose6 SEC Fractions
9
25
RALB
Exo84
siCtrl
Sec5
mTOR
TBK1
siSec8
(F)
Exocyst
LATS1
Exo84-subcomplex
p-LATS1
YAP1
TBK1---YAP1
+Virus
p-TBK1---Sec5/8---mTOR/S6K
Sec5 subcomplex

Figure 2.10: TBK1 is a positive regulator for mTOR activity

(A and B) TBK1 regulates virus infection induced S6K phosphorylation. Near confluent culture of TBK1 WT and TBK1 and IKKε double null MEFs **(A)** and TBK1 null MEFs **(B)** were incubated with 50 HA/ml Sendai virus for indicated hours. Lysates were collected and analyzed for indicated proteins using SDS-PAGE.

(C) CompoundII, a specific TBK1 inhibitor, inhibits S6K phosphorylation on 421/424 site. Confluent culture from 8 cell lines from melanoma and lung cancer origin were treated either with DMSO or CmpdII (TBK1i) for 30 minutes and cells harvested were analyzed for phospho-protein level of 16 AKT pathway proteins by using phospho-ELISA array. Quantification of the phosphorylations of p70S6K in DMSO versus CmpdII treated H1437 and HeLa cell lines samples in Supplementary Figure 4E are represented as bar graph, data are represented as mean ± SEM. Statistical significance was calculated using unpaired student's t test where p value <0.01

(D) The exocyst and TBK1 supports virus challenge induced S6K phosphorylation. HEK293T cells reverse transfected with indicated siRNAs were grown to confluence and incubated with Sendai virus for indicated hours. Cell lysates were analyzed for S6K phosphorylation using SDS-PAGE.

(E) Sec8 knock down disrupts Sec5-mTOR-TBK1 complex. HEK293T cells reverse transfected with indicated siRNAs were grown to confluence and high molecular weight complexes were isolated and were analyzed for partition profile of the indicated proteins using supersoe6 size exclusion chromatography.

(F) Summary of the virus infection stimulus specific regulatory interaction from TBK1's orientation.

Functional requirement of RAL-exocyst for activation of TBK1, PKR and Hippo signaling

Having established context specific exocyst interactomes, we next examined whether the exocyst was required for activity of PKR, TBK1 and MST1. Because, we found that Sec8 ablation attenuated TBK1 mediated mTOR activation and TBK1 is activated through autophosphorylation (Figure 2.10 D and E), we hypothesized that Sec8-TBK1 interaction might be directly necessary for TBK1 activity. To examine this, we induced TBK1 activation using pI:C and SeV and measured the effect of partial loss of Sec8 by siRNA-mediated knock down in human epithelial cell lines. Our data suggested that siRNA-mediated ablation of Sec8 delayed phospho TBK1 accumulation under immunogenic signals suggesting requirement of Sec8 for TBK1 activation (Figure 2.11 A). These observations indicated that a pool of TBK1 might be activated on Sec5/8 subcomplex after immune stimulation. Because TBK1 regulates antiviral IFN-β signaling, we reasoned that TBK1-mediated mTOR induction might also be necessary for proper induction of IFN-β signaling. Consistent with this, in osteosarcoma cells, we found that the TBK1 inhibitor CmpoundII and mTOR inhibitor Rapamycin attenuated IFN-β signaling induced by ectopic expression of TBK1 (Figure 2.11E).

Next we examined whether Exo84-PKR interaction was necessary for PKR activity. For this, we induced PKR activity by SeV infection and found loss of Exo84 to be mostly innocuous (Figure 2.11 B). However, Exo84 was required for SeV-induced LATS1 activation, suggesting that active PKR mediated phosphorylation of MST1 required Exo84 (Figure 2.11 C). These suggested that Exo84 is a negative regulator of YAP1 activity. Consistent with this overexpression of Exo84, but not Sec5, attenuated YAP1 transcriptional activity (Figure 2.11 D). Taken together, these data established Sec8 and Exo84 as essential for virus induced TBK1 and Hippo induction, respectively.

Mobilization of the exocyst is a major occupation of the RALB (Moskalenko, Henry et al. 2002, Chien, Kim et al. 2006, Ishikawa and Barber 2008). RALB was also activated by immunogenic signals as indicated by accumulation of the GTP-bound-RALB conformation (Figure 2.12 A). Hence, we hypothesized that the bifurcation of Hippo and mTOR induction after immune stimulation is mediated by the exocyst through RALB activation. In accordance with this, ectopic expression of a constitutively active RALB23V was sufficient to induce robust TBK1 and modest LATS1 phosphorylation (Figure 2.12 C). Additionally, ectopic expression of RALB23V was sufficient to induce IFN-β promoter activation and lowered YAP1 transcriptional activity in osteosarcoma cells and embryonic kidney cells, respectively (Figure 2.12 D). These data, along with previous reports (Chien, Kim et al. 2006), establish RALB activation as a potent surrogate for signaling induced by viral infection.

RALB has previously been reported to be required for TBK1 mediated IFN-β signaling (Chien, Kim et al. 2006). Consistent with this, expression of a dominant RAL-effector interaction interfering protein RLIP-RBD, reduced SeV induced IFN-β response (Figure 2.12 E). To test whether this was also true for induction of Hippo signaling, we examined broad-scale functional similarities between RAL-exocyst components and Hippo core components by taking advantage of the FUSION database (Potts, Kim et al. 2013). We parsed pairwise p-values for functional interactions of a biased set of genes; which included exocyst subunits, RALA/B, Hippo core components, KIBRA, mTOR, RPTOR, PKR and TBK1. This resulted in a diagonally asymmetric square matrix as knock down effect of gene X on Y was not equal to gene Y's effect on X (see methods for details). A two-way clustering of the resulting matrix revealed that RALA/B clustered with LATS1 and MST1 indicating broad-scale functional similarities between knock down of RALA/B and LATS1, MST1 (Figure 2.12 B).

Consistent with viral infection-mediated temporal activation of Hippo signaling, SeV infection also inhibited YAP1 activity and RLIP-RBD was sufficient to rescue this (Figure 2.12 E). These

observations indicate that RALB is required and sufficient for IFN-β and Hippo signaling induction after viral challenge.

Figure 2.11

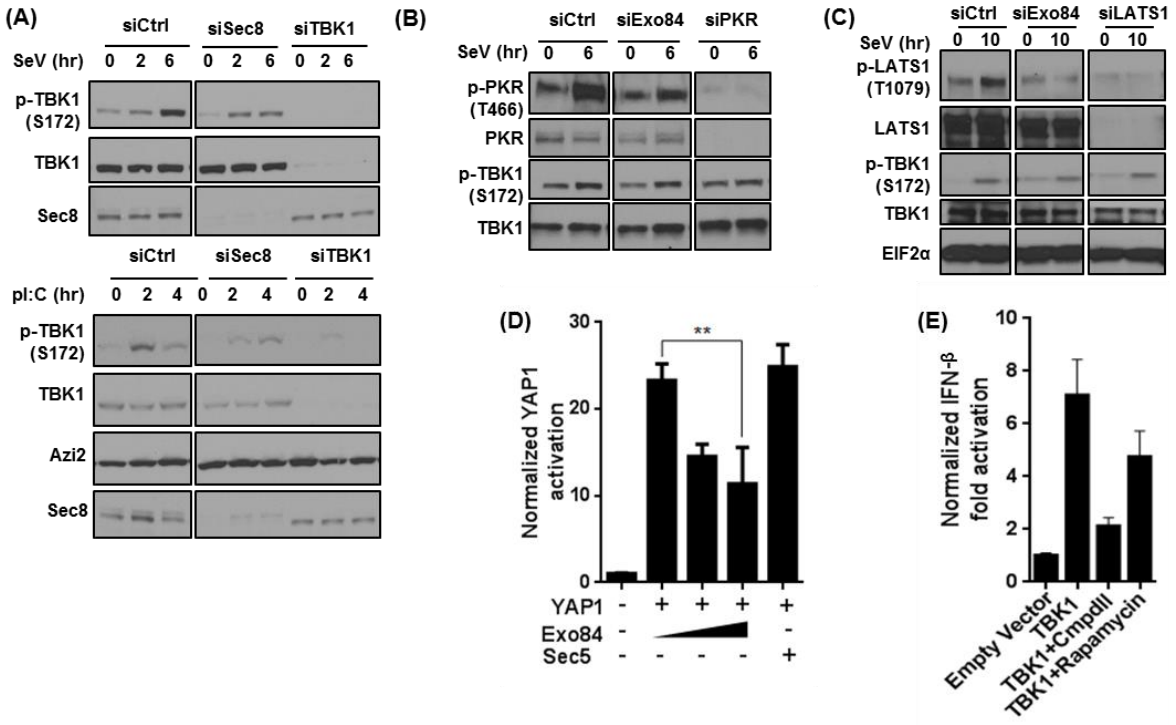

Figure 2.11: Functional requirement and sufficiency of exocyst for TBK1, PKR and Hippo signaling.

(A) Sec8 supports virus infection dependent TBK1 activation. HEK293T cells were reverse transfected with indicated short interfering RNAs and were incubated with Sendai virus or pI:C for indicated time periods. Cell lysates were analyzed for indicated proteins using SDS-PAGE.

(B and C) Exo84 is required for virus challenge dependent LATS1 phosphorylation. HEK293T cells were reverse transfected with indicated short interfering RNAs and were

incubated with growth media in presence of Sendai virus (50 HA/ml) for indicated time periods. Cell lysates were collected and analyzed for indicated proteins using SDS-PAGE.

(D) Exo84 overexpression inactivates YAP transcriptional activity. YAP transcriptional activity was assayed from HEK293T cells transiently transfected with 8XGTIIC-luc luciferase reporter expressing firefly luciferase, CMV promoter regulated renilla luciferase and empty vector or cDNAs indicated. A titrating amount of Exo84 cDNA was expressed and indicated by the black triangle. Normalized Hippo activation fold change is represented as histograms representing mean ± SEM. Statistical comparison between treatment cohorts were measured using Student's unpaired t test where p value < 0.01

(E) mTOR activation is necessary for maximal IFN-β promoter activation. U2OS cells ectopically expressing IFN-β reporter expressing firefly luciferase with a renilla luciferase control and plasmids expressing indicated cDNA or empty vector were grown for 24 hours and normalized IFN-β promoter induction was measured using standard dual luciferase assay. Data is represented as a histogram representing mean ± SEM.

Figure 2.12

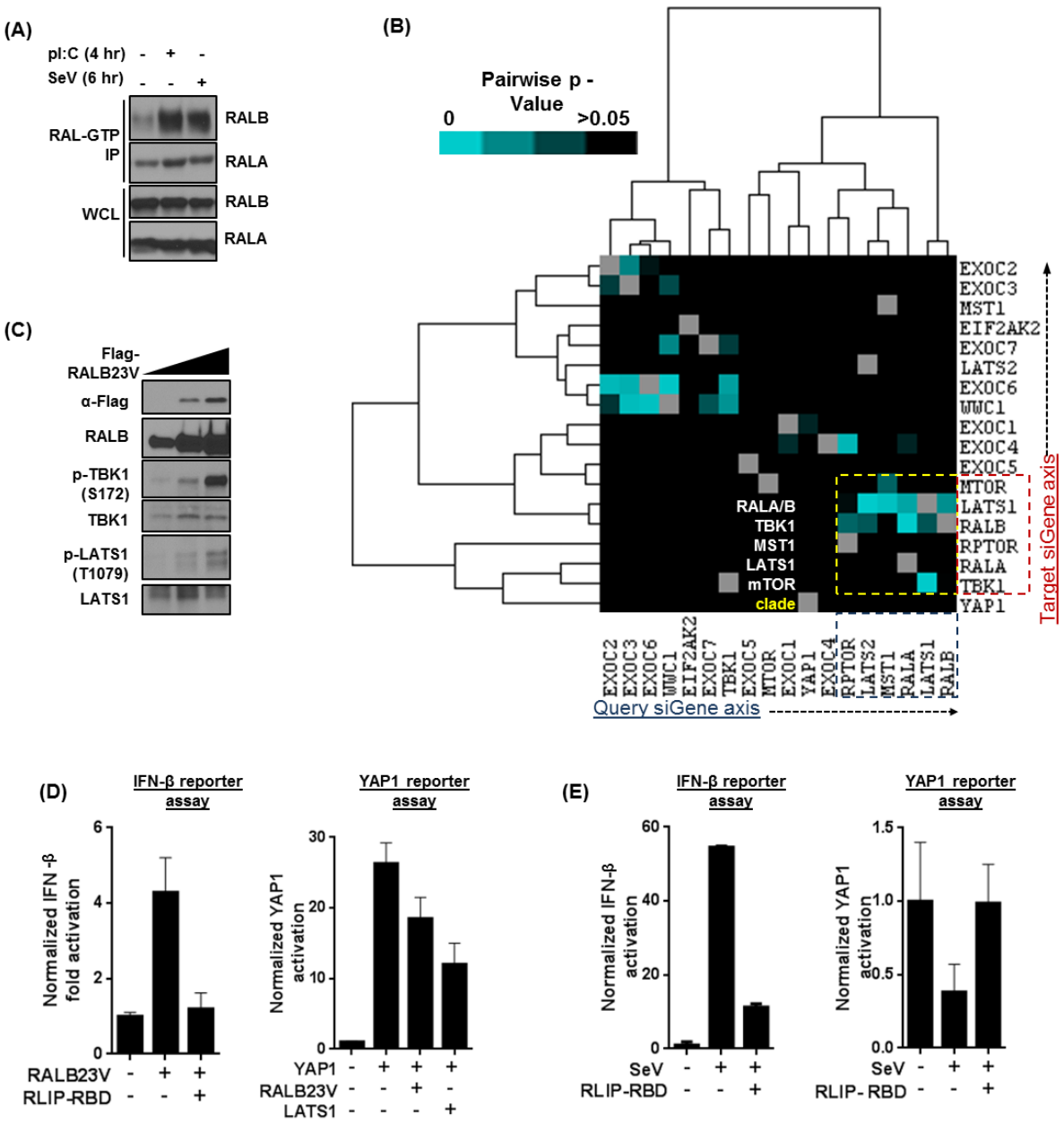

Figure 2.12: Functional requirement and sufficiency of RALB for TBK1, PKR and Hippo signaling.

(A) Host defense stimulus activates RALB. HEK293T cells were incubated in growth media with pI:C (2µg/ml) for 4 hour or SeV (50 HA/ml) for 6 hour and active RAL-GTP was pulled down

using GST-RBD under each conditions. Active RAL IPs and total proteins were analyzed for RALA and RALB.

(B) Functional relationship between RAL-exocyst and Hippo signaling using FUSION data. Functional association between exocyst subunits, core Hippo pathway proteins and mTOR related hits were calculated from FUSION1.5 dataset by measuring similarity between their gene knock down effects expressed as a 6 gene reporter feature as described in Potts *et. al.* 2013. For a query gene knock down pair-wise p value for each of the rest of the 'target genes' in the list were exported from the database and henceforth an asymmetric square matrix (where query to target≠ target to query) was generated. p-value was capped as insignificant for any value above at 0.05. Generated matrix was 2 way-clustered to find genes behaving most similarly within the biased list of proteins.

(C) Active RALB is sufficient to induce PKR and LATS1/2 phosphorylation. U2OS cells overexpressing varying amount of active RALB cDNA were collected and analyzed for indicated proteins using SDS-PAGE.

(D) RALB is sufficient to induce IFN-β promoter activation and inhibit YAP1 activity. U2OS cells overexpressing IFN-β or HEK293T cells overexpressing 8XGTIIC-luc promoter regulating firefly luciferase, CMV promoter regulated renilla luciferase along with indicated cDNAs were subjected to a standard reporter dual luciferase assay. Normalized Hippo or IFN-β activation fold changes are represented as histograms representing mean ± SEM.

(E) RALB is required to induce IFN-β promoter activation and inhibit YAP1 activity required. HEK293T cells overexpressing IFN-β overexpressing 8XGTIIC-luc promoter regulating firefly luciferase, CMV promoter regulated renilla luciferase along with indicated cDNAs were subjected to a standard reporter dual luciferase assay. Normalized Hippo or IFN-β activation fold changes are represented as histograms representing mean ± SEM.

RALB drives MST1-PKR-Exo84 and TBK1-mTOR-Sec5 interactions

Given that Exo84 and Sec5 are major RALB effectors and RALB activation is a potent proxy for immunogenic regulatory inputs, we hypothesized that the majority of host defense stimulus dependent partners of the exocyst might also be RALB driven. Hence, using spectral count based semi quantitative MS/MS methods we generated a de-novo endogenous RALB interactome (Figure 2. 14 A and B) and Exo84 or Sec5 interactome on the backdrop of ectopic RALBV23 expression. Datasets were compared for identifying candidates with known gene function in Hippo and mTOR pathways. These cherry-picked hits were further validated using immunoblot (Figure 2.14 B, D and E).

We hypothesized that RALB activation would have two consequences on the exocyst. Firstly, an engagement of exocyst holocomplex and secondly, reorganization of exocyst subcomplexes for RALB driven subcomplex specific functions. When compared, RALB and RALB-dependent Sec5 and Exo84 interactome, Ragulator subunits LAMTOR1 and LAMTOR3 were identified as common partners (Figure 2.13 A, B and C). Interestingly, RALB and LAMTOR3 have recently been reported to be in the same endogenous complexes in a high throughput fractionation based screen (Havugimana, Hart et al. 2012). Because Ragulator subunits interacted with both exocyst subunits, we hypothesized that Ragulator-RALB-exocyst interaction happens in the octameric holocomplex. Since Sec8 is a core component of the exocyst holocomplex, we hypothesized that we should recover Ragulator components in anti-Sec8 immunoprecipitation. As expected, under ectopic expression of active RALB variant, LAMTOR1 and LAMTOR3 co-immunoprecipitated with Sec8 (Figure 2.14 F). Finally, pair-wise interactions between RALB, Sec5 or Exo84 and LAMTOR3 were validated by immunoprecipitating the first and probing for co-immunoprecipitation of the latter (Figure 2.14 B, D and E) and vice versa (Figure 2.14 G).

Additionally, LAMTOR3 and RPTOR IP-MS data identified exocyst subunits Sec5 and Sec8 as candidates (Figure 2.15 A). Ragulator subunits were also present in RPTOR interactome, recapitulating LAMTOR's reported physical proximity to the mTOR complex (Figure 2.15 A). RPTOR inetarctome also identified exocyst core components Sec8 and EXOC3 as partners indicating proximity of the exocyst with mTOR (Figure 2.15 A)

Conversely, our RALB dependent Sec5 and Exo84 interactome identified mTOR and RPTOR respectively suggesting a RALB-dependent association of both subunits with mTOR components (Figure 2.14 C). However, previously we have shown that, under virus exposure, the kinetics of mTOR-Sec5 and mTOR-Exo84 interactions were reciprocal (Figure 2.5 C and F). Since, Ragulator is a known endosomal scaffold for mTOR (Sancak, Bar-Peled et al. 2010) we hypothesized that Ragulator-RAL-exocyst interactions might demonstrate similar interaction kinetics when exposed to virus.

Interestingly, virus exposure favored dissociation of LAMTOR3 from Exo84 and assembly on Sec5 (Figure 2.15 B). Based on these data we concluded that virus infection favors Ragulator assembly with holocomplex and Sec5 subcomplex but not with Exo84 subcomplex. These interaction kinetics were consistent with that of Sec5-mTOR and Exo84-mTOR. Because mTOR assembles onto the Ragulator complex when induced by appropriate stimuli (Sancak, Bar-Peled et al. 2010), these data indicated that, in the absence of viral infection the exocyst holocomplex and Sec5 subcomplex forms a stable complex with Ragulator, which upon virus infection leads to holocomplex decomposition and engagement of mTOR onto Sec5-Ragulator complex.

Moreover, as active RALB mimics virus infection, we reasoned that active RALB overexpression would favor Ragulator-mTOR interaction with RALB-holocomplex and RALB-Sec5 subcomplex but not with RALB-Exo84 subcomplex. To examine this, we needed to distinguish between two pools of Exo84 subunits- Exo84 present in holocomplex and Exo84 present in Exo84

subcomplex. To do so, we took advantage of constitutively active RALB variant F39L and partial loss of function RALB variants that discriminate between Exo84 and Sec5 as effectors. For example, RALB23V48W (48W in short) has 40-fold higher affinity for Sec5 and RALB23V38R (38R in short) has 100-fold higher affinity for Exo84. As shown, ectopic overexpression of F39L and 48W, but not 38R, was considerably more effective at promoting Sec5-LAMTOR3 interactions indicating LAMTOR3-Sec5 or LAMTOR3-Exo84 interaction is mediated by active RALB. On the other hand, LAMTOR3-Exo84 interaction is not favored by ectopic expression of Exo84 specific variant 38R but is favored in the presence of a Sec5 specific variant 48W and constitutively active RALB variant F39L (Figure 2.15 C). These combined observations indicated that LAMTOR3 preferentially associates with the exocyst holocomplex and the Sec5 subcomplex but not with the Exo84 subcomplex.

Next we compared RALB, RALB-dependent Exo84 and PKR interactome and found MST1 to be at the intersection, suggesting that PKR-MST1-Exo84 interaction might be favored in the context of RALB activation (Figure 2.13 A, Figure 2.14 D). On the other hand, comparing RALB, RALB-dependent Sec5 and TBK1 interactome identifies RPTOR as a common partner of Sec5 and TBK1 and mTOR as a common partner of RALB and Sec5 (Figure 2.13 B, Figure 2.13 E). However, because RPTOR is an integral adapter for mTOR and mTOR was established as a bona fide interactor for active TBK1 (Figure 2.5 C and Figure 2.5 F), we hypothesized that RALB activation might favor TBK1-mTOR-Sec5/8 complex formation.

Additionally, ectopic overexpression of active RALB variant altered regular diffused MST1 partition profile to a more concentrated one, where it co-eluted with the majority of endogenous Exo84 and PKR at a molecular weight of around ~500 KDa (Figure 2.13 C and D). Active RALB overexpression also caused a significant portion of Sec8 and Sec5 to co-purify at higher molecular weight complexes where they co-eluted with mTOR (Figure 2.13 C). Hence, ectopic expression of active RALB was sufficient to mobilize MST1 onto a lower and Sec5/8 onto a

higher molecular weight complex. Active RALB-dependent molecular rearrangements were also associated with an increased accumulation of Exo84-MST1 (Figure 2.13 E), Sec5-mTOR (Figure 2.13 F), PKR-MST1 (Figure 2.13 G and H) and mTOR-TBK1 (Figure 2.13 I) complexes in the human epithelial cells. These observations position RALB as a sufficient instructive signal for formation of signaling complexes during virus infection.

Previously, under viral infection, we have established Exo84 interaction with MST1 and mTOR to be reciprocal (Figure 2.5 E). Since RALB caused Exo84 interaction with both mTOR and MST1 (Figure 2.14 D), we hypothesized that these interactions happen in two distinct Exo84 entities- a full octameric complex and Exo84 subcomplex. To test whether mTOR and MST1 reciprocal interaction with Exo84 was also competitive, we immunoprecipitated Exo84 under ectopic overexpression of MST1 or mTOR and probed for their interaction strengths with Exo84. Our data suggests that ectopic expression of MST1 eliminated mTOR Exo84 interaction, whereas expression of mTOR eliminated MST1 Exo84 interaction (Figure 2.15 D). These data indicated that MST1 and mTOR might compete for same binding surface on Exo84.

Importantly, co-expression of active RALB and Exo84, but not RALB and Sec5, decreased YAP1 transcriptional activity significantly. This indicated a distinct contribution of the RALB-Exo84 subcomplex, and not the RALB-Sec5 subcomplex, for exocyst-mediated Hippo induction (Figure 2.13 J). On the other hand RALB Sec5 co-expression, but not RALB Exo84 coexpression, was associated with an alteration in TBK1 partition profile (Figure 2.15 E) and resulted in IFN-β promoter activation (Figure 2.15 K). These combined observations suggest that RALB mediates dynamic reorganization of the steady state population of exocyst holocomplex and Exo84 or Sec5 subcomplex interaction with effectors. Consequently, distinct RAL-exocyst subcomplexes assist concomitant engagement of mTOR and Hippo pathway (Figure 2.13 L).

Figure 2.13

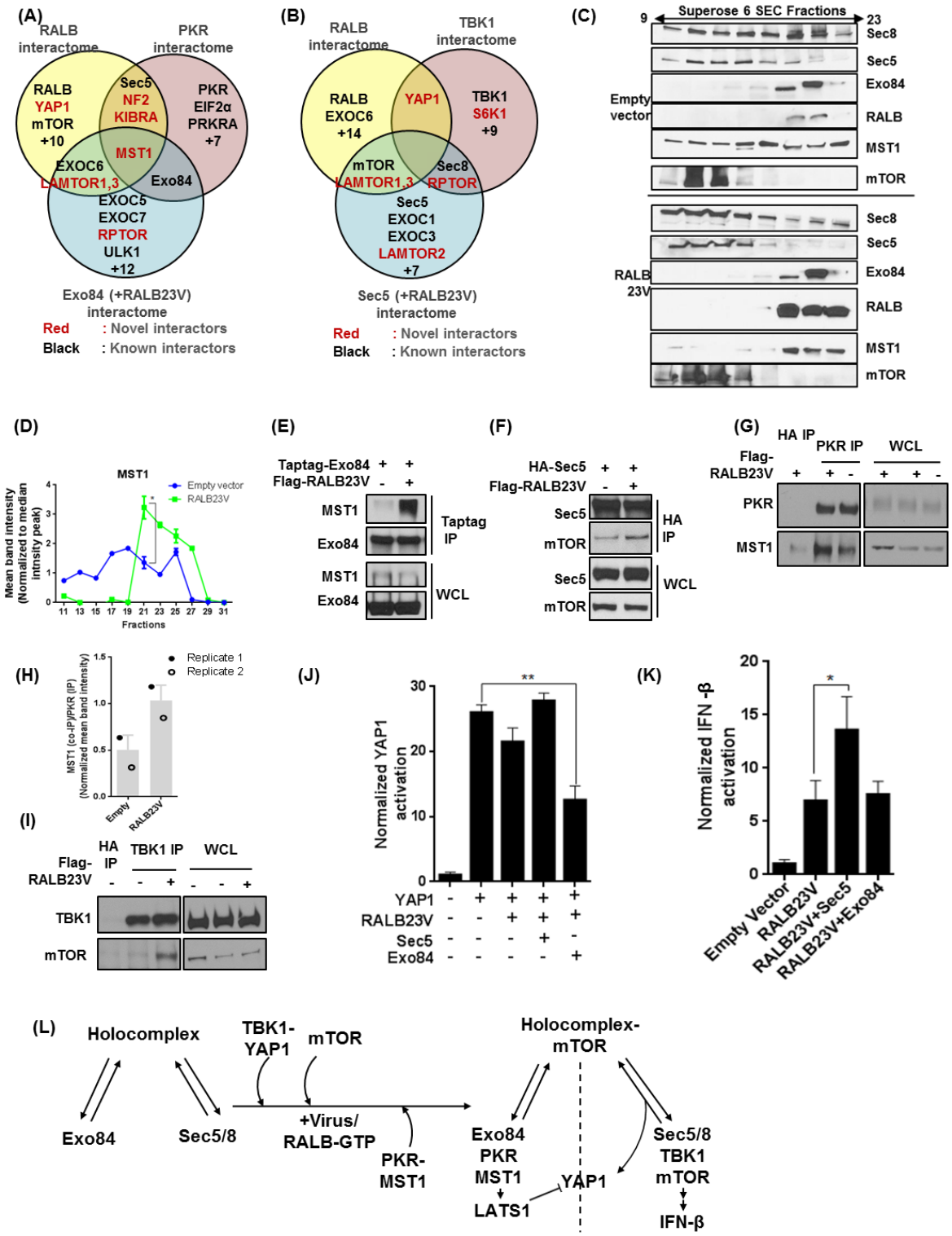
(A)
RALB interactome
PKR interactome
RALB YAP1 mTOR +10
Sec5 NF2 KIBRA
PKR EIF2α PRKRA +7
MST1
EXOC6 LAMTOR1,3
Exo84
EXOC5 EXOC7 RPTOR ULK1 +12
Exo84 (+RALB23V) interactome
Red : Novel interactors
Black : Known interactors
(B)
RALB interactome
TBK1 interactome
RALB EXOC6 +14
YAP1
TBK1 S6K1 +9
mTOR LAMTOR1,3
Sec8 RPTOR
Sec5 EXOC1 EXOC3 LAMTOR2 +7
Sec5 (+RALB23V) interactome
Red : Novel interactors
Black : Known interactors
(C)
Superose 6 SEC Fractions
9
23
Empty vector
RALB 23V
Sec8
Sec5
Exo84
RALB
MST1
mTOR
(D)
MST1
Empty vector
RALB23V
Mean band intensity (Normalized to median intnsity peak)
Fractions
(E)
Taptag-Exo84
Flag-RALB23V
MST1
Exo84
Taptag IP
WCL
(F)
HA-Sec5
Flag-RALB23V
Sec5
mTOR
HA IP
WCL
(G)
HA IP
PKR IP
WCL
Flag-RALB23V
PKR
MST1
(H)
Replicate 1
Replicate 2
MST1 (co-IP)/PKR (IP) (Normalized mean band intensity)
Empty
RALB23V
(I)
HA IP
TBK1 IP
WCL
Flag-RALB23V
TBK1
mTOR
(J)
Normalized YAP1 activation
YAP1
RALB23V
Sec5
Exo84
(K)
Normalized IFN-β activation
Empty Vector
RALB23V
RALB23V+Sec5
RALB23V+Exo84
(L)
Holocomplex
Exo84
Sec5/8
TBK1-YAP1
mTOR
+Virus/ RALB-GTP
PKR-MST1
Holocomplex-mTOR
Exo84 PKR MST1
LATS1
YAP1
Sec5/8 TBK1 mTOR
IFN-β

Figure 2.13: RALB drives formation of Ex084-PKR-MST1 and Sec5-TBK1-mTOR complexes.

(A and B) Euler plot representation for identifying RALB dependent exocyst interactors. Endogenous RALB, PKR, overexpressed TBK1 and overexpressed Exo84 or Sec5 in presence or absence of RALB23V, from HEK293T cells were analyzed for coimmunoprecipitation of proteins using mass spectrometry. Euler diagram shows comparison amongst PKR (described before), RALB driven Exo84 and RALB interactome **(A)** and TBK1 (described before), RALB driven Sec5 and RALB interactome **(B)**.

(C and D) RALB23V expression is sufficient to change endogenous high molecular weight complexes of MST1 and Sec5/8 subunits. (C) Size exclusion column chromatography fractions of high molecular weight complexes in HEK29T cells were analyzed for partition profile of indicated proteins using SDS-PAGE in presence or absence of transient expression of RALB23V cDNA. **(D)** Band intensity of the MST1 partition profile was quantified and represented as a line graph. Statistical comparison between the cohorts were measured using Student's unpaired t test where p value < 0.01

(E) Active RALB causes Exo84-MST1 interaction. Exo84 was immunoprecipitated from HEK293T cells transiently expressing Myc-Exo84 with or without Flag-RALB and analyzed for coimmunoprecipitation of MST1.

(F) Active RALB causes Sec5-mTOR interaction. Sec5 was immunoprecipitated from HEK293T cells transiently expressing HA-Sec5 with or without Flag-RALB and analyzed for coimmunoprecipitation of mTOR.

(G and H) RALB is sufficient to increase PKR-MST1 interaction. HEK293T cells transfected with indicated cDNAs were grown to confluence and endogenous PKR was immunoprecipitated and analyzed for coimmunoprecipitation of indicated proteins. **(H)** Quantification of two replicates of representative data demonstrated in **(G).** Normalized mean band intensity for MST1 co-IP on PKR IP was represented as a bar graph. Error bar indicates SEM.

(I) RALB is sufficient to increase TBK1-mTOR interaction. HEK293T cells transfected with indicated cDNAs were grown to confluence and endogenous TBK1 was immunoprecipitated and analyzed for coimmunoprecipitation of indicated proteins.

(J) RALB23V-Exo84 overexpression was sufficient to inactivate YAP1 transcriptional activity. HEK293T cells ectopically expressing 8XGTIIC-luc luciferase reporter expressing firefly luciferase with a renilla luciferase control and plasmids expressing indicated cDNA or empty vector were grown for 24 hours and normalized Hippo induction were measured using standard dual luciferase assay. Data is represented as a histogram representing mean ± SEM. Statistical comparison between the cohorts were measured using Student's unpaired t test where p value < 0.01

(K) RALB23V and Sec5 coexpression activates IFN-β activity. HEK293T cells ectopically expressing 8XGTIIC-luc luciferase reporter expressing firefly luciferase with a renilla luciferase control and plasmids expressing indicated cDNA or empty vector were grown for 24 hours and normalized Hippo induction were measured using standard dual luciferase assay. Data is represented as a histogram representing mean ± SEM.

(L) Summary of the virus or RALB driven partnership of exocyst entities and their functional significance

Figure 2.14

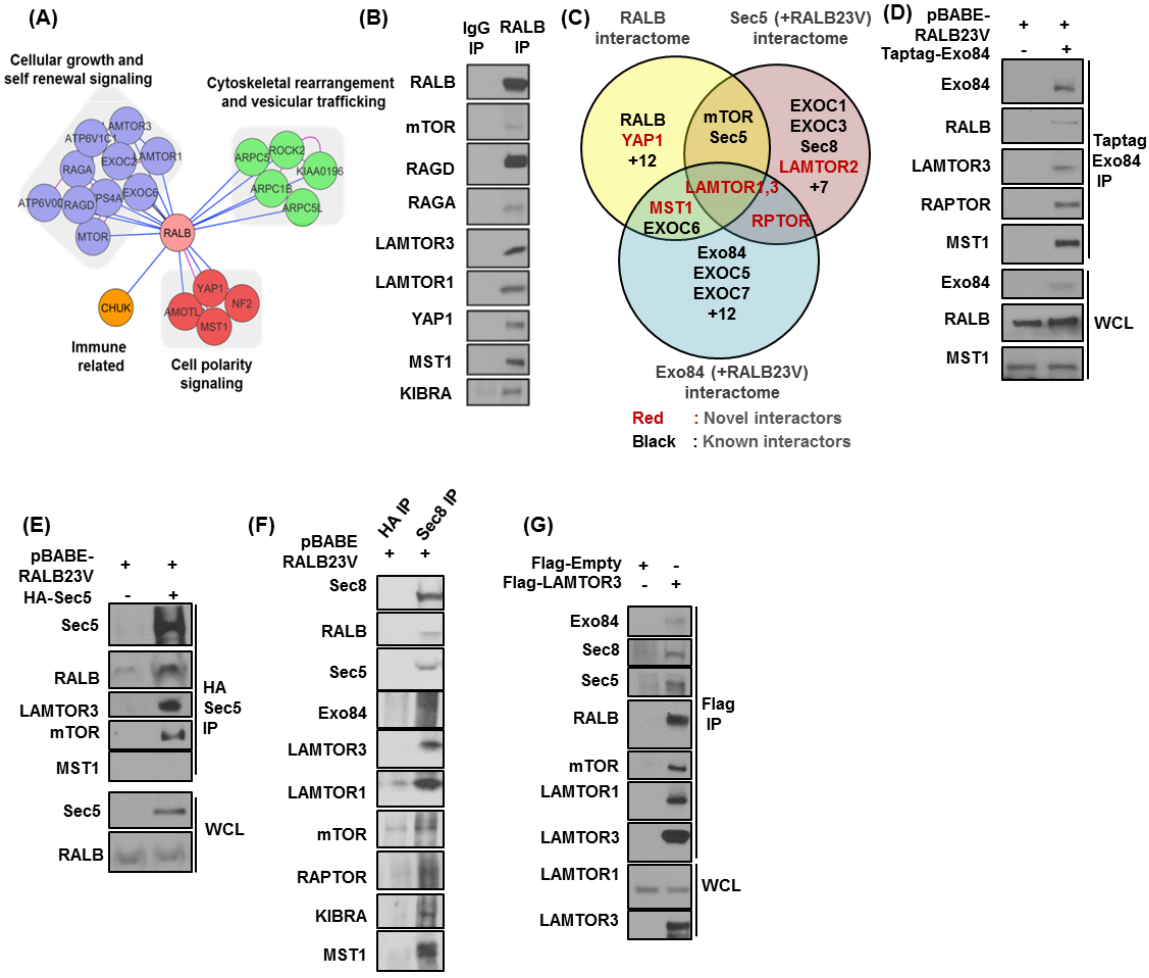

Figure 2.14: Validation of RALB and RALB dependent exocyst interactomes.

(A and B) RALB core complex identifies MST1 and LAMTORs as novel interactors. (A) Using antibodies specific for RALB, a de-novo RALB interactome was generated using the AP-MS pipeline. The blue edges emanating from RAL represent experimental interaction; pink edges between other nodes represent interaction reported in the BIOGRID database. The nodes were manually classified into different functional groups as indicated by the grey box. **(B)** Western blot validation of the cherry-picked hits from (**A)**.

(C) Active RALB driven exocyst interactome. (Left) Transiently overexpressed Taptag-Exo84 and HA-Sec5 were immunoprecipitated from HEK293T cells stably overexpressing RALB23V. IP was analyzed for coimmunoprecipitation of proteins using LC-MS/MS. RALB driven Exo84 and Sec5 interactome was superimposed on de-novo RAL interactome to generate comparisons represented as an euler plot.

(D, E, F) Western blot validation of active RALB driven Exo84 and Sec5 interactome. Endogenous Sec8, Taptag-Exo84, HA-Sec5 or was immunoprecipitated from HEK293T cells in the presence of stable expression of only RALB23V **(F)** or RALB23V and Exo84 **(D)** or RALB23V and Sec5 **(E)** respectively. **(D and E)** Exo84 and Sec5 was immunoprecipitated with antibodies directed to the specified tags. **(F)** Endogenous Sec8 was immunoiprecipitated using anti-Sec8 antibody. Immunoprecipitates were analyzed for coimmunoprecipitation of the indicated proteins.

(G) LAMTOR3 and mTOR interacts with RALB and exocyst holocomplex subunits. HEK293T transiently overexpressing Flag-LAMTOR3 was used to immunoprecipitate LAMTOR3 and indicated proteins were analyzed for coimmunoprecipitation.

Figure 2.15

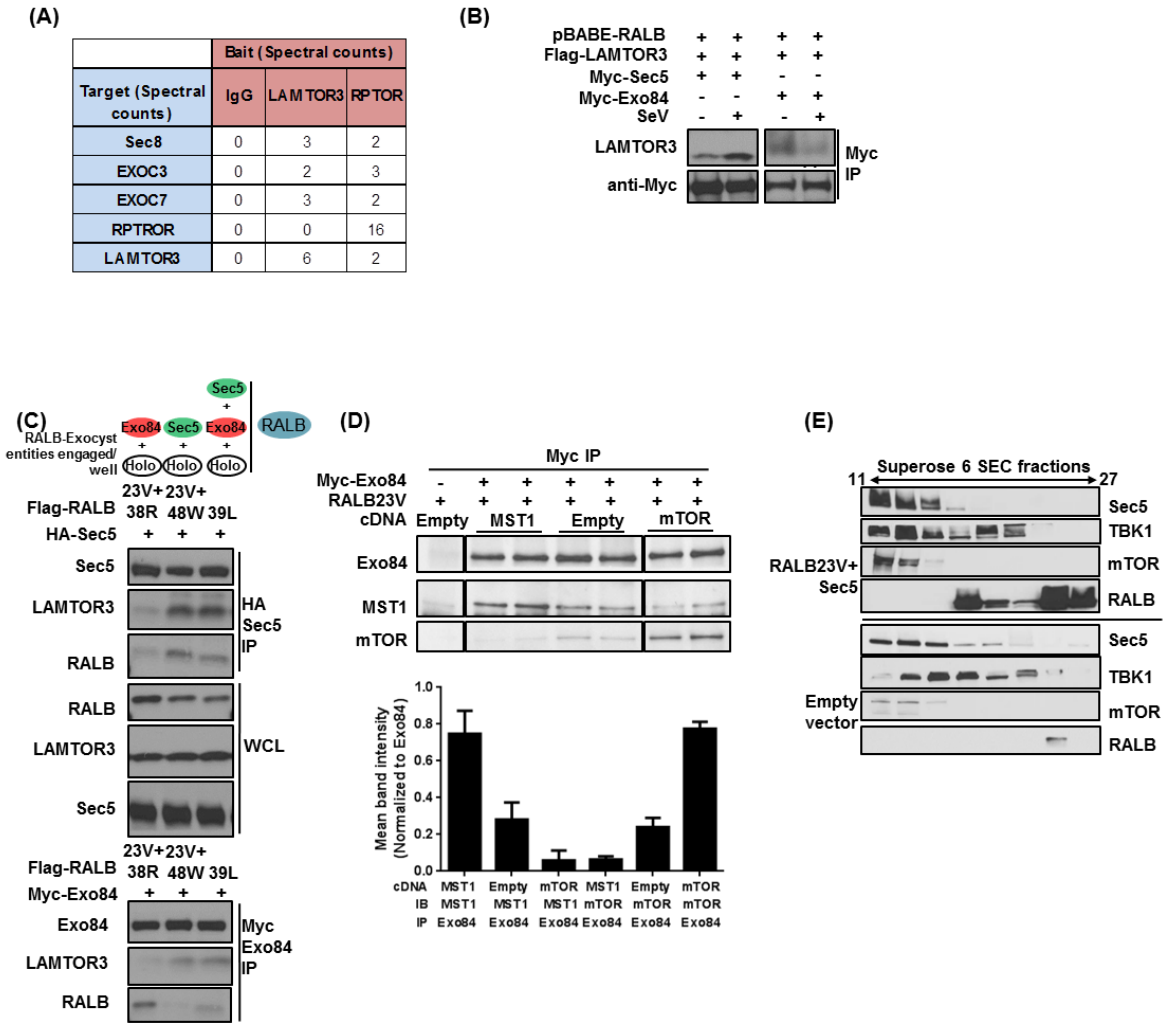

	Bait (Spectral counts)		
Target (Spectral counts)	IgG	LAMTOR3	RPTOR
Sec8	0	3	2
EXOC3	0	2	3
EXOC7	0	3	2
RPTROR	0	0	16
LAMTOR3	0	6	2

Figure 2.15: LAMTOR3 is a holocomplex, mTOR is a Sec5 subcomplex and MST1 is an Exo84 subcomplex partner

(A) LAMTOR complex components are a common interactor for exocyst and RPTOR. Table illustrates MS/MS spectral count values of exocyst subunits, LAMTOR3 and RPTOR identified in LAMTOR3 and RPTOR interactome.

(B) LAMTOR3 exocyst interaction is stimulus specific. HEK293T cells transiently expressing the indicated cDNA were grown to confluence and treated with SeV for indicated hours. Exo84

or Sec5 was immunoprecipitated using anti-Myc antibody and was analyzed for indicated proteins for coimmunoprecipitation using SDS-PAGE.

(C) MST1 and mTOR can competitively dissociate each other from Exo84. Myc-Exo84 and RALB23V expressing HEK293T cell line were transfected with either MST1 or empty vector or mTOR overexpression cDNA constructs and grown to confluence and Exo84 was immunoprecipitated using anti-Myc antibody and analyzed for coimmunoprecipitation of the indicated proteins using SDS-PAGE. Band intensities were quantified and statistical significance for co-IP/IP level among each cohort was measured using unpaired student's t-test.

(D) RALB drives LAMTOR3 interaction with exocyst holocomplex and Sec5 subcomplex. Point mutations in RALB23V that that has differential association of RALB with either Exo84 or Sec5 were overexpressed in stably fusion tagged Sec5 HEK293T cells. Sec5 were immunoprecipitated and indicated proteins were analyzed using SDS-PAGE. Cartoons on top of the immunoblots indicate schema indicating RALB-exocyst entities engaged in each sample.

(E) Active RALB and Sec5 coexpression results in distinct high molecular weight complex partition profile for TBK1 and mTOR. HEK293T cells transiently expressing indicated cDNAs were grown to confluence on and cells were collected in gel filtration buffer. Filtered lysates were injected on a supersoe6 column at 0.2ml/min rate and forty 0.5ml fractions were collected and fractions 13^{th} till 29^{th} were analyzed on SDS-PAGE for indicated proteins.

PKR and TBK1 mediated Hippo and mTOR activation is pro-survival

We next tested if exocyst-driven Hippo and mTOR signaling was dependent on each other. To test this we utilized LATS1/2 knock out HEK293A cells generated by RNA editing technology (Moroishi, Hayashi et al. 2016). When we compared the signaling output of mTOR signaling in these cell lines, we observed a dramatic increase in baseline mTOR signaling as measured by activating phosphorylation on S6 (Figure 2.16 A). This mTOR upregulation correlated with higher activating phosphorylation on TBK1 (Figure 2.16 A). If this adaptive compensation was conserved between the two pathways then one would expect PKR and TBK1 to be compensatory as well. Indeed, PKR-deficient MEFs had higher baseline TBK1 activity (Figure 2.16 B). From these observations, we reasoned that immune signaling where concomitant induction of TBK1-mTOR and PKR-Hippo occur, are two distinct host anti-viral responses that facilitate cell survival after viral challenge. However, YAP1 knock out cells had higher TBK1 responsiveness to SeV infection probably through loss of inhibitory TBK1-YAP1 interaction (Figure 2.16 C). These results suggest that YAP1, but not LATS1 genetic status defines TBK1 responsiveness.

Next, we tested the biological significance of PKR and TBK1-mediated Hippo and mTOR activation. YAP deficiency has recently been shown to be sufficient to potentiate antiviral response in mammalian cells *in vivo* (Wang, Xie et al. 2017). Therefore, we tested the ability of YAP1 deleted mouse myoblast cells to cope with HSV1-mediated toxicity (Figure 2.16 D) in 2D cell culture model. Our data indicates that YAP1 deficiency imparted survival benefits for cells to tolerate viral load. Additionally, stable overexpression of RALB was immune protective and loss of PKR and TBK1 accelerated virus-mediated toxicity (Figure 2.17 A). These results put RALB, TBK1, PKR and YAP1 as antiviral pro-survival molecules. Moreover, cells treated with Rapamycin were more sensitive to HSV1 cytopathic effect indicating mTOR also functions as a pro-survival signal (Figure 2.16 E)

Innate immune signaling addiction has already been shown to be required for oncogenic transformation in multiple settings (Chien, Kim et al. 2006, Chien and White 2008, Barbie, Tamayo et al. 2009)(Blakely, Pazarentzos et al. 2015). We hypothesized that transformed cells can establish cell autonomous tumorigenic regulatory networks for survival by abusing TBK1 and PKR immune signaling, as a result, would have higher baseline activation of Hippo and mTOR signaling. We also reasoned that such cells might be more likely to be sensitive to combined TBK1 and PKR pharmacological ablation (Figure 2.18 B). Thus to identify such 'immune addicted' lines we generated ED_{50} values for TBK1i (Cmpd II) and PKRi (C16) in a cohort of lines from lung and melanoma lineages. As expected, our data suggests that cell lines that were sensitive to either or both of the compounds, had higher expression of genes that belonged to immune inflammatory pathways (Figure 2.18 A). From this sensitive cohort of lines, we identified A375, a melanoma and HCC44, a lung cancer cell line, which were sensitive to both compounds (Figure 2.18 C). We used LM38 and H1437, melanoma and lung cancer cell lines resistant to both compounds, as controls for subsequent pathway analysis in presence or absence of immune inductive stimuli.

As predicted, the data indicated that the 'immune addicted' TBK1i PKRi double sensitive lines had higher baseline mTOR and LATS1 activity (Figure 2.18 D). Moreover, selective toxicity of the sensitive lines to TBK1i and PKRi were not due to a selective effect of these compounds in sensitive cells; TBK1i and PKRi equally ablated S6K and LATS1 phosphorylation respectively in sensitive and resistant cell lines (Figure 2.18 E). These data suggest that, during tumorigenic transformation, intrinsic commandeering of Hippo and mTOR signaling renders a survival advantage to a cohort of cell lines and these dependencies can be chemically addressed as a vulnerability using immune kinase inhibitors.

Our genetic and biochemical assays firmly put RALB as a central regulatory signal for PKR and TBK1, thus we examined RALB activity in 'immune addicted' cell lines and found it to be higher

than resistant lines (Figure 2.18 E). Taken together, these data indicate RALB-mediated immune survival signaling can be exploited by tumor cells as a strategy to deflect cell-death.

Figure 2.16

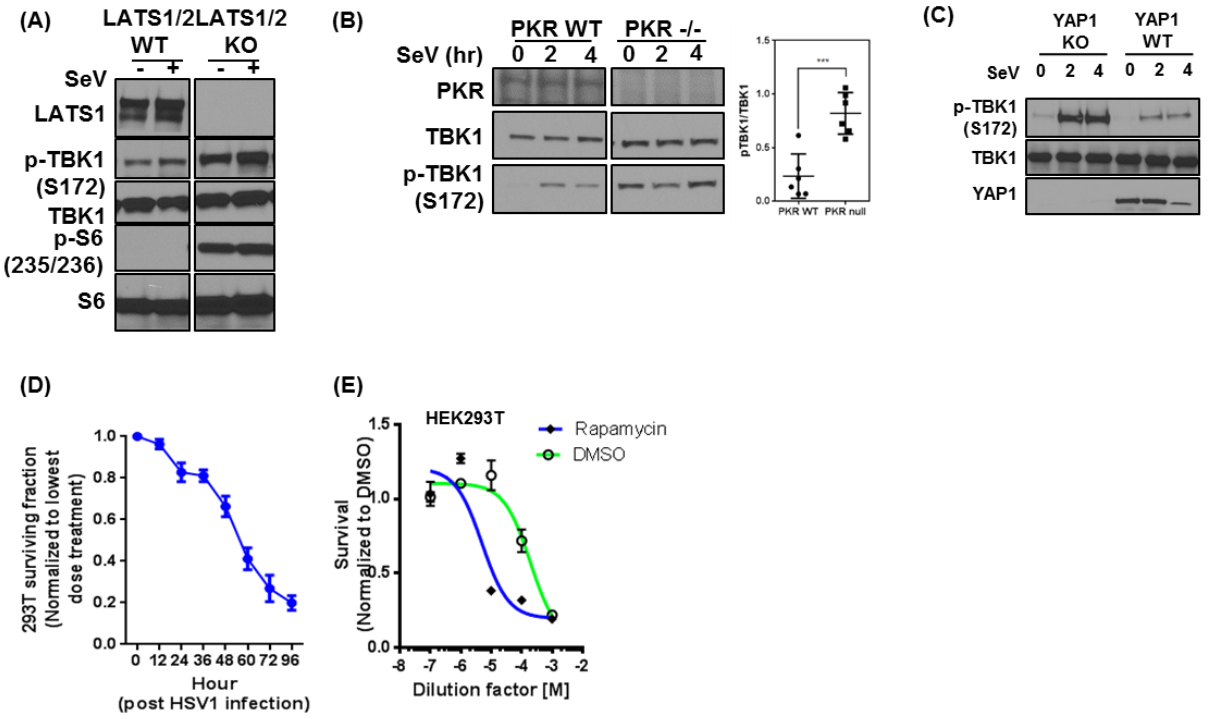

Figure 2.16: Nature of Hippo and mTOR signaling

(A) High baseline TBK1 and mTOR activity in LATS1/2 knock out cells. LATS1/2 WT and knock out 293A cells were grown to confluence and treated as indicated. Post treatment- cells were harvested and lysates were analyzed for indicated proteins using SDS-PAGE.

(B) High baseline TBK1 activity in PKR null MEFs. TBK1 and PKR wt and null MEFs were grown to confluence and treated as indicated. Post treatment- cells were harvested and lysates were analyzed for indicated proteins using SDS-PAGE.

(C) YAP1 loss causes higher responsiveness of TBK1 to immune challenge. WT or YAP KO C2C12 cells were grown to 90% confluency and treated with SeV for indicated time periods and analyzed for levels of indicated proteins using SDS-PAGE.

(D) HSV1 toxicity kinetics. HEK293T cells were incubated with 10^6 PFU HSV1 virus stock for indicated hours and their post infection normalized viability was measured.

(E) mTOR signaling is immune protective. HEK293T cells were pretreated with 0.2µM Rapamycin for 6 hour followed by indicated dilutions of 10^6 PFU HSV1 virus stock. 48 hours post infection relative cell viability was counted using cell titer glo.

Figure 2.17

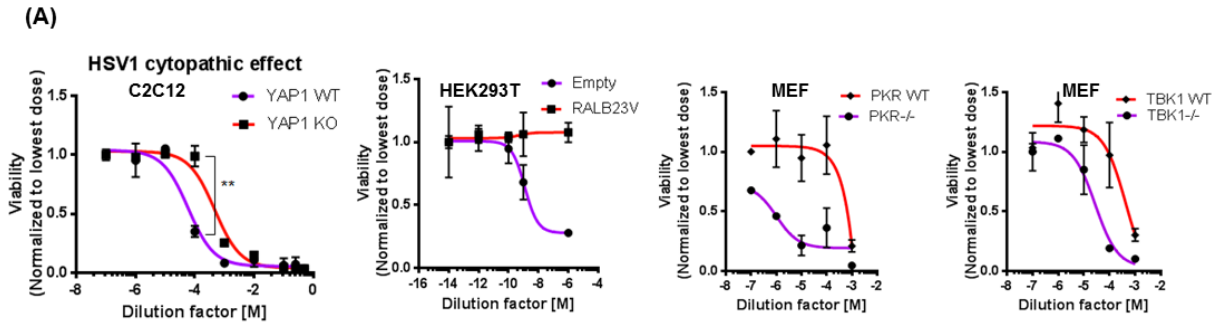

Figure 2.17: YAP1 degradation, RALB overexpression, PKR and TBK1 activation plays pro-survival role during viral infection

(A) Hippo induction, active RALB, TBK1 and PKR are immune protective. 10^9 PFU HSV1 virus stock were diluted as indicated and YAP1 wt or knock out C2C12 cell line, HEK293T cells stably expressing RALB23V or empty vector control and MEFs wt or null for TBK1 and PKR were infected with the virus for indicated hours. 96 hours post infection relative cell viability was counted cell titer glo.

Figure 2.18

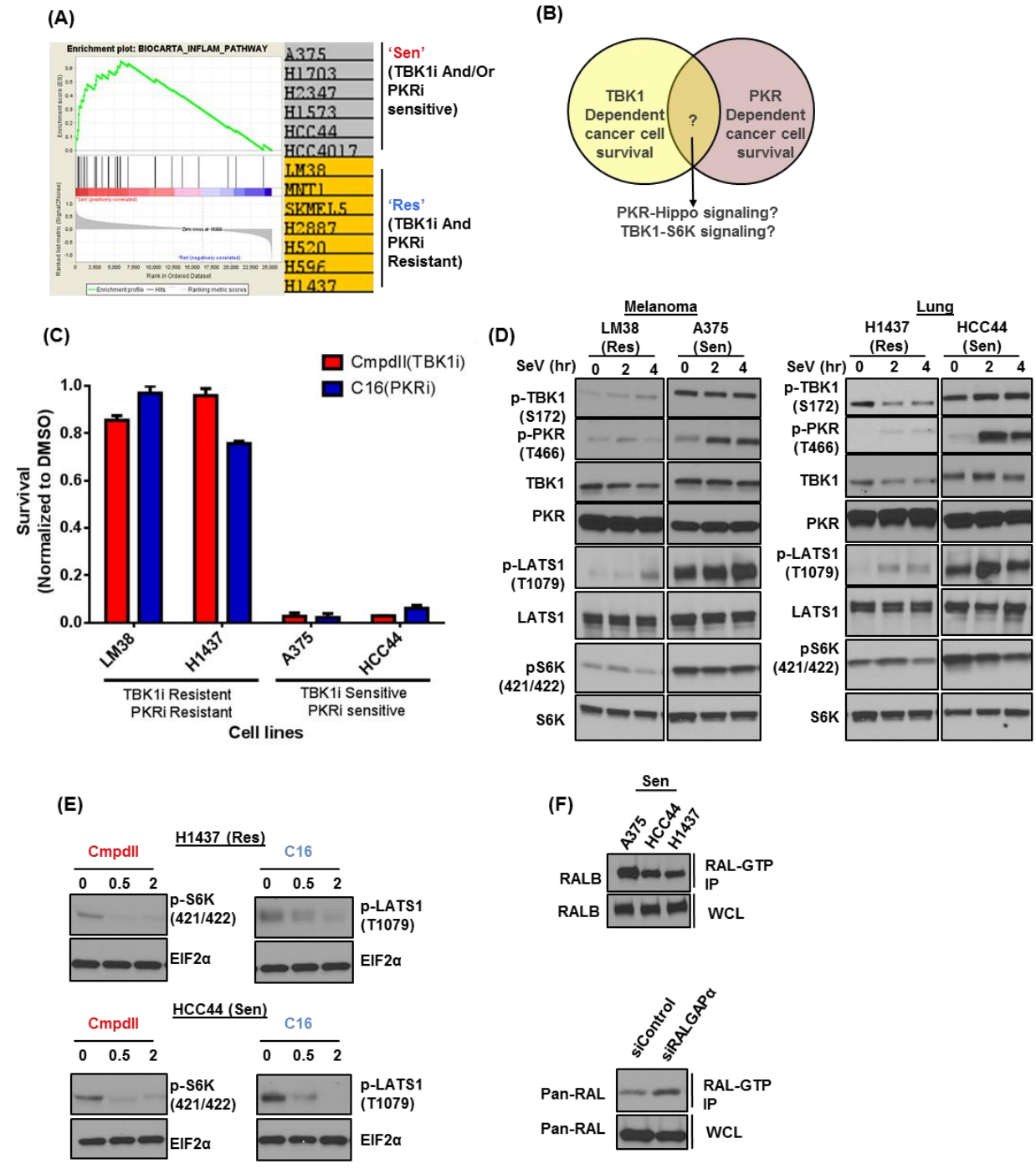
(A)
Enrichment plot: BIOCARTA_INFLAM_PATHWAY
A375
H1703
H2347
H1573
HCC44
HCC4017
LM38
MNT1
SKMEL5
H2887
H520
H596
H1437
'Sen' (TBK1i And/Or PKRi sensitive)
'Res' (TBK1i And PKRi Resistant)
(B)
TBK1 Dependent cancer cell survival
?
PKR Dependent cancer cell survival
PKR-Hippo signaling?
TBK1-S6K signaling?
(C)
CmpdII(TBK1i)
C16(PKRi)
Survival (Normalized to DMSO)
1.0
0.8
0.6
0.4
0.2
0.0
LM38
H1437
A375
HCC44
TBK1i Resistent
PKRi Resistant
TBK1i Sensitive
PKRi sensitive
Cell lines
(D)
Melanoma
LM38 (Res)
A375 (Sen)
Lung
H1437 (Res)
HCC44 (Sen)
SeV (hr) 0 2 4
p-TBK1 (S172)
p-PKR (T466)
TBK1
PKR
p-LATS1 (T1079)
LATS1
pS6K (421/422)
S6K
(E)
H1437 (Res)
CmpdII
C16
0 0.5 2
p-S6K (421/422)
p-LATS1 (T1079)
EIF2α
HCC44 (Sen)
(F)
Sen
A375
HCC44
H1437
RALB
RAL-GTP IP
WCL
siControl
siRALGAPα
Pan-RAL

Figure 2.18: Concomitant PKR and TBK1 activation favors survival against viral infection and oncogenic stress

(A) A subset of 'immune pathway' addicted cancer cells use PKR and TBK1 for survival. 17 lung cancer and 10 melanoma cell lines were treated with PKR inhibitor (C16) or TBK1 inhibitor (CmpdII) for 72 hours and cell viability was measured using cell titer glo. Measured ED50 values for each lineage were separately rank ordered and cell lines with values in the first and third quartile forTBK1i or PKRi were individually selected. GSEA was run for analyzing gene set enrichment analysis between cell lines that were TBK1i And/Or PKRi sensitive versus TBK1i And PKRi resistant cohort. GSEA analysis identifies gene set 'BIOCARTA-INFLAM-PATHWAY' as a gene set enriched with Normalized enrichment score (NES) of 0.65.

(B) Theoretical representation of strategy for identifying TBK1 and PKR mediated supports of tumor cell viability. Schematic Venn diagram outlining unknown overlapping between the PKR and TBK1 mediated cell viability. TBK1i (CmpdII) and PKRi (C16) ED50 values on 17 lung cancer and 10 melanoma cell lines were measured and were used for defining this cohort.

(C) Identifying PKR and TBK1 immune pathway 'addicted' melanoma and lung cancer cells lines. Indicated cells were treated with 2μM TBK1i (CmpdII) and PKRi (C16) for 72 hours and cell viability was measured by cell titer glo. Normalized viability is illustrated as a bar graph representing Mean ± SEM.

(D) 'Immune addicted' cancer cell lines with high PKR and TBK1 activity has high Hippo, S6K and RALB activity. (C) Indicated lung cancer and melanoma cell lines were incubated with SeV for indicated hours and levels of the indicated proteins were measured using SDS-PAGE.

(E) PKR ablation causes LATS1 downregulation whereas TBK1 ablation causes S6K downregulation in cancer cells. Indicated cell lines were treated with indicated compounds for hours indicated. Lysates were collected and were analyzed for indicated proteins.

(F) 'Immune addicted' cancer cell lines with high PKR and TBK1 activity has high RALB activity. Active RALB from indicated cell lines were immunoprecipitated using GST-RBD and analyzed for indicated proteins in immunopreciptates and whole cell lysate. As an assay control, active RALB from HEK293T cells reverse transfected with indicated siRNAs were immunoprecipitated using GST-Sec5-RBD and analyzed for indicated proteins in immunopreciptates and whole cell lysate.

RALB and Exo84 mediate PKR mediated xenophagy response.

Since PKR is also an important mediator for cellular xenophagy response (Talloczy, Virgin et al. 2006) and RALB and Exo84 has previously been shown to participate in autophagy (Bodemann, Orvedahl et al. 2011), we also tested whether RAL exocyst was required for PKR mediated xenophagy response. As shown in Figure 2.7 A and B, autophagy induction is not a conserved phenomenon upon SeV and HSV1 infection. Because, HSV1 infection caused LC3-II degradation and ULK1 activating phosphorylation along with PKR activation, we hypothesized that this might be due to initiation of a PKR mediated xenophagy response in the host cells. This LC3 modification was coupled with emergence of punctate LC3 immunofluorescence pattern (data not shown) as well as punctate LAMP1 staining suggesting lysosomal biogenesis (Figure 2.19 B).

To test whether RAL and exocyst subunits were required for this response, we knocked down genes of interest in cervical cancer cells and infected them with HSV1 to measure the effect of gene knock down on the phenotype. As indicated we found that RALB and Exo84 along with PKR knockdown had a profound attenuation of LC3 puncta accumulation (Figure 2.19 C and D).

Lack of LC3 puncta accumulation is indicative of either a block or a greater flux through the autophagy process. To test whether attenuation of LC3 puncta was due to the former, but not the latter, we used a small molecule agonist- STATIC that activates PKR mediated autophagy inducing EIF2α phosphorylation. As indicated, STATIC treatment robustly activated EIF2α and initiated autophagy response in osteosarcoma cells (Figure 2.19 A). More importantly, as demonstrated RALB, Exo84 and PKR gene knock down again greatly attenuated of the LC3 puncta accumulation (Figure 2.19 C and D). These results suggest that, RALB and Exo84 also participate in PKR mediated xenophagy response.

Figure 2.19

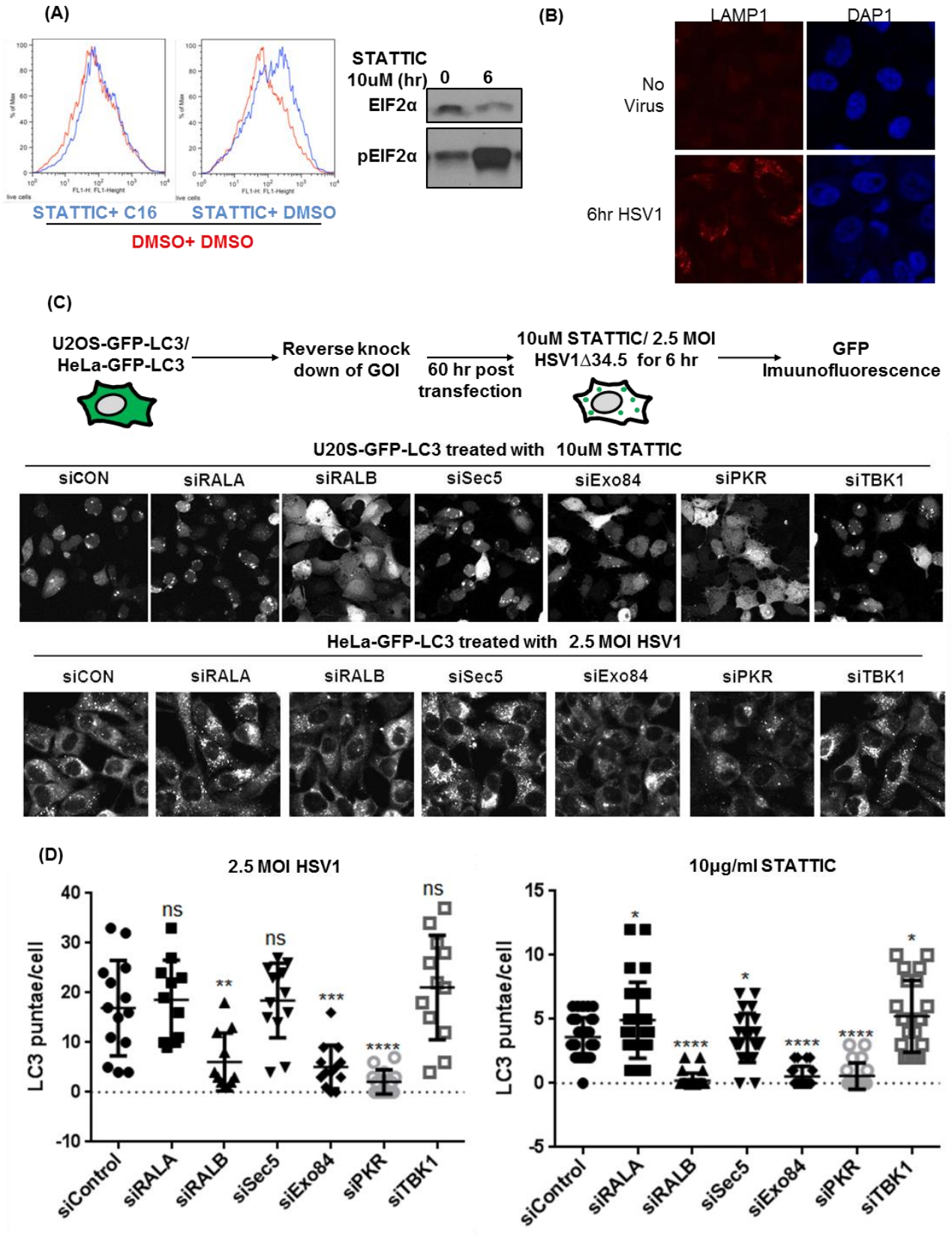
(A)
STATTIC+ C16
STATTIC+ DMSO
DMSO+ DMSO
STATTIC 10uM (hr) 0 6
EIF2α
pEIF2α
(B)
LAMP1
DAP1
No Virus
6hr HSV1
(C)
U2OS-GFP-LC3/ HeLa-GFP-LC3
Reverse knock down of GOI
60 hr post transfection
10uM STATTIC/ 2.5 MOI HSV1Δ34.5 for 6 hr
GFP Imuunofluorescence
U20S-GFP-LC3 treated with 10uM STATTIC
siCON
siRALA
siRALB
siSec5
siExo84
siPKR
siTBK1
HeLa-GFP-LC3 treated with 2.5 MOI HSV1
(D)
2.5 MOI HSV1
10μg/ml STATTIC
LC3 puntae/cell
siControl
siRALA
siRALB
siSec5
siExo84
siPKR
siTBK1

Figure 2.19: RALB and Exo84 mediate PKR mediated xenophagy response

(A) STATTIC induces PKR mediated autophagy. (Left) U2OS cells stably transfected with GFP tagged LC3 construct were grown to confluence and treated 10 hour with 2 μM of the indicated compounds. Cells were collected and Single-cell fluorescence intensity was measure for GFP positive cells. (Right) In a parallel experiment confluent HeLa cells were incubated with 10μM of the STATTIC and were analyzed for the proteins indicated using SDS-PAGE.

(B) HSV1 infection causes lysosome nucleation. HeLa cells were infected with or without HSV1 Δ34.5 for 6 hour. Fixed cells were analyzed for immunofluorescence for LAMP1- a lysosomal marker.

(C and D) Exo84 and RALB are required for PKR induced xenophagy. (C) U2OS-LC3-GFP cells were transiently transfected with indicated siRNAs and grown to confluence before treatment with 10μM of the STATTIC. Cell were fixed and analyzed for accumulation of GFP-LC3 punctae/cells. (Bottom) HeLa cells were reverse transfected with indicated short interfering RNAs and were incubated with growth media with or without HSVΔ34.5 mutant (MOI 2.5) for 6 hours. Cell were fixed and analyzed for accumulation of LC3 punctae/cells using endogenous LC3 antibody. **(D)** Statistical analysis for the punctae/cells were compared between each cohorts using unpaired student's t test ($p<0.01$)

CHAPTER THREE

Discussion and conclusion

High fidelity host defense response to pathogens requires mobilization, assembly and synchronized activation of adaptive signaling cascade components. Over the years, a confluence of observations has exposed the critical role of RAL-exocyst signaling as a proximal regulatory platform for kinase dependent innate immune signaling activation (Chien, Kim et al. 2006, Chien and White 2008, Ou, Torres et al. 2011). Although, some key partners of this regulatory circuit have previously been characterized, the precise signaling contribution of these partnerships along with dynamic state-switching of participating kinases have not been studied in a systematic fashion before this study. Through quantitative proteomics driven analysis of dynamic exocyst interactome together with focused biochemistry and cell biology, we have identified functional regulatory contribution of the exocyst complex during RALB dependent immunogenic signaling. Previous works have indicated that during induction dependent exocytosis, RAL GTPases mobilize both Exo84 and Sec5 subcomplexes to form a holocomplex that assist in vesicular targeting and tethering for secretory events (Moskalenko, Henry et al. 2002, Moskalenko, Tong et al. 2003). Our findings are also consistent with a dual subcomplex model, in which Exo84 and Sec5 subcomplexes define RAL pathway responses to virus infection. One RALB effectors, Exo84, accommodates catalytically active PKR and MST1 to activate Hippo signaling. In parallel, another RALB effector, Sec5, assists in potent activation of innate immune kinase TBK1 and TBK1 effector mTOR signaling for appropriate induction of interferon response. We also found that concomitant activation of these two distinct signaling arms is required for cells to antagonize viral challenge and can be corrupted by oncogenes to help deflect apoptotic checkpoint activation.

Loss of cell polarity and disruption of contact inhibition by tumorigenic viruses in epithelial cells have suggested a connection between host defense, Hippo and oncogenic signaling (Banks, Pim et al. 2012). Participation of the exocyst in these combinations of roles implied a possible central role of it in supporting signaling crosstalk between Hippo, host defense and RAL pathway (Moskalenko, Henry et al. 2002, Horikoshi, Suzuki et al. 2009, Bryant, Datta et al. 2010, Das, Fischer et al. 2016). Recently, albeit with limited understanding of the upstream and contextual regulation, direct interplay between host defense and Hippo signaling became substantiated (Liu, Zheng et al. 2016, Eskiocak, McMillan et al. 2017, Moroishi, Hansen et al. 2015, Zhang, Meng et al. 2017, Wang, Xie et al. 2017). Here, we have identified additional evidences for an exocyst dependent regulatory partnership between Hippo and host defense signaling. Following viral infection, consistent with previous models, our data indicate simultaneous activation of interferon response, Hippo signaling and consequent inactivation of YAP driven transcription program. Our work is also in accordance with a previous study, which demonstrated that YAP impede IFN-β response independent of its transcriptional activity and this inhibition can be relieved by Hippo activation (Zhang, Meng et al. 2017) (Supplementary Figure 4A). Although YAP is known to promote cell proliferation, it appears that YAP1 deficiency promotes resistance to viral cytotoxicity (Wang, Xie et al. 2017, Zhang, Meng et al. 2017) (Figure 2.17A). Given the general role of Hippo signaling in antagonizing cellular growth and favoring cell cycle arrest, infection mediated Hippo induction could be an adaptive cellular response for preventing propagation of infection while allowing a healing period for infected cells (Meng, Moroishi et al. 2015, Zhang, Meng et al. 2017).

In this study, we identify two immune kinases- PKR, through a kinase dependent indirect manner, and TBK1, through a kinase independent direct manner, as crucial regulator for YAP1 activity. In this two factor system, TBK1 sequesters YAP1 on inactive-state, which in result also competitively mask YAP1 from Hippo kinase cascade by substrate retention. Accordingly,

recent publications indicate that a direct physical association between the YAP translocation domain and TBK1 prevents formation of TBK1 signaling complex (Zhang, Meng et al. 2017, Eskiocak, McMillan et al. 2017, Couzens, Knight et al. 2013). Hence, mutually inhibitory TBK1-YAP1 complex appears to prevent aberrant triggering of TBK1 kinase or YAP transcription program in the absence of appropriate stimuli. In contrast, when activated during virally compromised environment, PKR and TBK1, on two distinct exocyst subcomplexes, support activation of Hippo and mTOR kinase cascades respectively. And these signaling contributions are independent of PKR and TBK1's canonical substrates EIF2α and IRF3. PKR mediated regulation of anti-viral immunity is thought to be mediated by direct regulation of protein translation through EIF2α and indirect regulation of xenophagy and apoptosis (Talloczy, Jiang et al. 2002, Asakura, Fujiwara et al. 2007). In this study, we demonstrate PKR as a host defense stimuli responsive Exo84 effector that directly phosphorylate MST1 on a novel site for induction of Hippo signaling. Although, in liver tumor settings, EIF2α dependent unfolded protein response has been linked to Hippo induction, our data identifies a direct and context relevant functional role of PKR on Hippo signaling (Wu, Wei et al. 2015). Resembling the established obligatory role of Sec5-TBK1 effector complex for TBK1 activation (Chien, Kim et al. 2006), these observations establish Exo84 as an additional physical platform for establishing precise substrate specificity for PKR upon pathogenic infection.

In addition, we find evidences for active RALB mediated instructive bifurcation of host defense signaling response. RALB activation is sufficient and required for PKR-MST1 complex mediated Hippo induction on Exo84 subcomplex as well as TBK1-mTOR complex mediated IFNβ induction on Sec5 subcomplex. However, coordination and crosstalk between the Exo84 and Sec5 subcomplex regulated signaling arms are not fully obvious. We found that both of these arms converge on YAP1: the Sec5 arm by releasing YAP from TBK1 and the Exo84 arm by activating LATS for YAP proteolysis. Hence, it appears that YAP may function as a 'rheostat' by

calibrating the fluxes across the arms. However, using both complete and partial loss-of-function epistasis experiments we do not find evidences of such redundancy between activation of Hippo and TBK1 signaling (Figure 2.11C and Figure 2.17A). Instead, complete loss of PKR-Hippo arm activated the TBK1-mTOR arm, which suggests a steady state compensatory nature of these exocyst regulated pathways (Figure 2.16A and B). This is line with the general perception where mTOR is considered a pro-growth anabolic and Hippo is considered an anti-growth catabolic signaling pathway (Zoncu, Efeyan et al. 2011, Hansen, Moroishi et al. 2015). Yet, in response to virus infection, both signaling pathways appear to be induced simultaneously (Figure 2C). And because we also find that both of these pathways are necessary for productive anti-viral host defense responses, it appears that virus infection function as an instructive signal for switching on two compensatory 'or' type into 'and' type pathways for survival. These observations are consistent with a model where chronic virus infection or constitutive RALB activation is able to alter the normal homeostasis to create an endpoint steady state that is significantly different from original signaling landscape. In accordance with that, in at least two cancer cell lines with immune-inflammatory gene signatures, concomitant activation of Hippo and mTOR signaling was identified due to chemically addressable addiction to PKR and TBK1 signaling. Although we have not yet determined the coordination between exocyst dependent and independent signaling contribution of these immune kinases, it is possible that during certain contexts, such as malignant tumorigenesis, exocyst may deflect PKR and TBK1 from their canonical substrates for hyper-induction of mTOR and Hippo signaling. Besides, because the tested 'immune addicted' cells also have higher level of RALB activation (Supplementary Figure 7I), expanding PKR and TBK1 addicted subset of cell line and defining their molecular correlates might enable us to classify RAL driven tumors. Thus it might also enable us to determine the overlapping between RAS and RAL driven tumors. These efforts might yield new biomarkers and novel synthetic lethal targets for RAS or RAL driven tumors. Notably, targeted therapy using direct intervention against KRAS has been refractory and in KRAS mutant lung cancers TBK1

addiction previously has been identified as a selective vulnerability (Barbie, Tamayo et al. 2009). Interestingly, a broad range EMT programs was shown to be a synthetic lethal partner for TBK1 inhibitors and this EMT addiction for TBK1i sensitive lines has been credited speculatively to RAL-exocyst and/or AKT/mTOR pathways (Cooper, Ou et al. 2017). These observations highlight an opportunistic usage of TBK1 by KRAS mutant tumors. It will be interesting to see if overlaying PKR inhibitor sensitivity dataset on the existing TBK1 inhibitor sensitivity information on lung cancer cell lines will allow us to fine-tune RAL or RAS dependent so called 'immune addicted' cell lines.

However, our study does not address the localization of these signaling complexes. RALB mediated host defense signaling might take place in spatially distinct compartments as previous work have suggested discrete cellular localization pattern of Exo84 and Sec5 (Bodemann, Orvedahl et al. 2011). In our experience, and other reported studies, sites of localization of total TBK1 in the cell includes mitochondria, lysosome and Golgi vesicles (Sun, Sun et al. 2006, Matsumoto, Shimogori et al. 2015, Pourcelot, Zemirli et al. 2016, Richter, Sliter et al. 2016). On the other hand, localization pattern of total PKR is usually diffused in the cytosol (data not shown). It will be of great interest to determine if the compartments accommodating Exo84 and Sec5 are also temporally occupied with activated PKR or TBK1 under virally challenged cells. Given exocyst's pivotal role in endosomal trafficking, compartmentalization of these immune kinases onto endosomes might explain a surveillance strategy evolutionarily adopted in higher metazoans. However, lack of specific antibodies that differentiate between different cellular pools of Exo84 or Sec5 and active or inactive forms of PKR or TBK1 have made determination of cellular localization of the complexes daunting. Recent publications indicated that epitope specific Sec6 antibodies were able to probe functional changes in the exocyst configurations. Although, in absence of active PKR or TBK1 specific antibodies, colocalization experiments

might not be possible, it would be interesting to annotate signaling pattern alterations of different exocyst pools in the presence or absence of the immunogenic stimuli.

To summarize, we have defined a mechanistic contribution of enzymatically inactive exocyst complex during host defense signaling through dynamic and precise engagement of innate immune kinases. During pathogenic invasion, the exocyst integrates pro-survival mTOR and anti-growth Hippo pathway in response to RAL GTPase activation. Concomitant induction of these otherwise exclusive pathways may represent an antiviral surveillance strategy adopted by cells for activation of focused cell survival programs in the backdrop of global inhibition of infection propagation. Of note, mTOR signaling is known to cause selective translation of specific interferons and accentuate secretion of danger signals from infected cells to alert neighbors (Clohessy, Reschke et al. 2012, Tang, Ioja et al. 2015). Loss of fidelity in these regulations might cause aberrant activation of chronic innate immune signaling, which is upregulated in multiple oncogene driven tumors as a strategy to deflect apoptotic checkpoint activation (Chien, Kim et al. 2006, Barbie, Tamayo et al. 2009, Blakely, Pazarentzos et al. 2015). Thus, the regulatory network established in our study reveal the exocyst as a physical scaffold for establishing accurate substrate specificity for PKR and TBK1 and hence both of these kinases may be conceptually ideal candidates for antineoplastic drug development against oncogene driven tumors.

CHAPTER FOUR

MATERIALS AND METHODS

Cell culture and transfection

HEK293T, HeLa, HEBC30, U2OS, TBK1+/+ and TBK1-/- MEFs, were cultured as previously described (Stojdl, Abraham et al. 2000, Chien, Kim et al. 2006). Following melanoma cell lines- A2058, LM20, RPMI7951, LOXIMVI, MNT1, SKMEL5, YUMAC, LM38, A375, PKR wt and PKR-/- MEFs cells, C2C12 wt and C2C12 YAP knock out cell lines were grown on DMEM supplemented with 10% fetal bovine serum (Atlanta Biologicals), 100 U/mL penicillin and 100 µg/mL streptomycin (Invitrogen). HepG2 cells were cultured on EMEM supplemented with 10% fetal bovine serum, 100 U/mL penicillin and 100 µg/mL streptomycin. C2C12 wt and C2C12 YAP knock out cell lines were kindly provided by Dr. Doujia Pan (University of Texas Southwestern Medical Center), PKR wt and PKR-/- MEFs were kindly provided by Dr. John Bell (Ottawa Hospital, University of Ottawa), TBK1 wt and TBK1-/- MEFs were generated from mouse fibroblasts were kindly provided by Dr. Rolf Brekken (University of Texas Southwestern Medical Center). Lung cancer cell lines H596, H1437, H1573, HCC2450, H2887, H2347, H3255, A427, H1705, HCC44, HCC4017, H1755, H596, H125, HCC2279, HCC4019 cells were cultured in RPMI supplemented with 5% fetal bovine serum (Atlanta Biologicals), 100 U/mL penicillin and 100 µg/mL streptomycin (Invitrogen). Cell lines were fingerprinted and mycoplasma tested every 12 months.

Plasmids, cloning and stable cell preparation

The mammalian expression plasmids pCDNA-FLAG-TBK1 (WT) and (K38M) were generously provided by Dr. James Chen (UT Southwestern Medical Center), and are cloned as described earlier (Seth et al., 2005). Exo84 was PCR amplified from Myc-Exo84 vector (Bodemann,

Orvedahl et al. 2011) using primers with an overhang 5' NOT1 and a 3' KPN1 site and cloned in N-terminal 3XFLAG pIRESpuro (Invitrogen) vector by dual restriction digestion of vector and insert with the aforementioned enzymes followed by ligation with T4 DNA ligase. pUNO-PKR and pUNO-PKR-DN (kinase dead) expressing cDNA were bought from invivogen. Flag-MST1 plasmid was generously provided by Doujia Pan (University of Texas Southwestern Medical Center). Myc-Sec8, HA-Sec5, Myc-Sec5 and Myc-exo84 expression constructs were amplified from previously generated constructs (Bodemann *et al.* 2013). pBABE-RALB-Hygro constructs were generated by restriction digestion of pBABE-RALB-puro construct with EcoRI and BamHI followed by relegation with pBABE-Hygro empty vector.

For stable RALB23V expressing cell lines, retroviral expression constructs were packaged by cotransfection of phoenix cells (ATCC CRL-3213) with pBABE-RALB-Hygro plasmid using Fugene6. 48 hour and 72 hour viral supernatants were collected. HEK293T cells were plated at a density of $2.5x10^6$ cells/10-cm dish. Two virus infections, one at 24 hour and another at 48 hours later, were carried out with retroviral particles and polybrene (10 µg/ml). On day 3 post-infection, cells were seeded onto multiple 6-well wells on 50% confluency. 24 hour post-seeding cells were subjected to antibiotic selection at a dose that kills the untransduced cells but not transduced cells. Five Single clone survivors were selected. Protein expression of gene of interest was validated using SDS-PAGE.

Antibodies and regents

Anti-Sec8, Sec5, EXOC3, Exo84 and RALB monoclonal antibodies were used as before (Bodemann, Orvedahl et al. 2011). Protein A/G Plus-Agarose beads (sc-2003) and anti-HA antibody (sc-7392 and sc-805) were purchased from Santa Cruz. Anti-FLAG antibody (F3165) (A2220 were purchased from Sigma. Additional antibodies were purchased from Sigma (anti-Actin, A1978), Santa Cruz Technology (anti-IRF3, YAP1 63.7, anti-ICP0), Cell Signaling

Technology (anti-PKR, 12297; S6K, 9202; p-S6K (T421/S424), 9204; S6, 2217; p-S6 (S235/236), 4858; TBK1, 3504; p-TBK1 5483S, YAP1 8418, p-YAP1 (S127), LATS1 9153, p-LATS1 (T1079) MST1 3682 p-MST1 (T183) 3681, EIF2α 5324, p-EIF2α 3398, ULK1 6439, LAMTOR3 8168 LAMTOR1 8175 LAMTOR2 8145, RAGA 4357, RAGD 4470, KIBRA 8774, GAPDH 5174, mTOR 2972, CDK7 2916), Abcam (p-PKR (T466) ab32036, Azi2 ab5242, WDR73 ab103864, PRPS1 ab137577, IVNS1ABP ab127566, anti-HNM), Fitzgerald (anti-ICP5) Bethyl laboratories (TP53BP1 A300-272A). pan-RAL antibodies were purchased from NewEast bioscience (#26913). GST-RBD was prepared as demonstrated before (Bodemann, Orvedahl et al. 2011)

Trophic and immunogenic stimulation

Cellular growth signaling was observed in HEK293T, HeLa or Human Bronchial Epithelial Cells (HBEC) cells grown on normal growth media enriched in growth nutrients (Gibco high glucose DMEM) or grown on nutrient depleted EBSS (Earle's basic saline solution) (Sigma# E2888). To mount a host defense response, HeLa cells were treated with DMEM (+10%FBS) with or without 2ug/ml or 50ug/ml pI:C or 200 HA/ml Sendai virus (Cantell strain), 2.5 MOI HSV1 (Orvedahl, Alexander et al. 2007) .

Western blot

Cells grown on appropriate scale were lysed with lysis buffer (40% Glycerol, 240mM Tris-HCl, pH 6.8, 8% SDS). Lysates' protein content was quantified using BCA kit (Thermo scientific). Equal content proteins were denatured by boiling at 95°C using 0.04% bromophenol blue, 5% β-marcapto ethanol. Samples were separated by 4-20% gradient gel and transferred onto PVDF membranes (BIO-RAD). Membranes were blocked with BSA for 1-2 hour before overnight primary antibody incubation followed by washes and 1-2 hour secondary antibody (peroxidase

conjugated antibody from Jackson lab fluorophore conjugated antibody from Licor) incubation. For enhanced chemiluminescence based method protein bands were detected using peroxidase substrate reagent (Pierce).

Immunoprecipitation

For endogenous IP, five 150 cm dishes of each HEK293T, HeLa or HBEC cells were grown to confluence per conditions and then were lysed with lysis buffer (20 mM Tris-HCl pH 7.4, 137mM NaCl, 1% Triton X-100, 0.5% sodium deoxycholate, 10mM MgCl2, 2mM EGTA, one tablet of each Roche EDTA-free cOmplete ULTRA protease inhibitor and PhosphoSTOP per 10 ml solution).

For overexpression based IP, $3X10^6$ HEK293T cells were seeded in four 10cm dishes grown each in 10 ml 10% FBS DMEM. Next day, cells were transfected with either 3μg of 3XFlag-TBK1 plasmid or 3XFlag-Empty using Fugene 6 at a ratio of 3:1 (mL Fugene 6 to μg DNA). 48 hours post transfection, the cells were lysed in immunoprecipitation lysis buffer (20 mM Tris-HCl pH 8.0, 100mM KCl, 0.1% NP-40, 0.5% sodium deoxycholate, 10mM MgCl2, 2mM EDTA) with protease and phosphatase inhibitors (Roche EDTA-free cOmplete ULTRA and PhosphoSTOP).

Cells were lysed for 1 hour and cleared at 16,000 X g for 10 min at 4°C. 2mg of lysate was brought to the concentration of 1.5mg/mL by diluting it with lysis buffer. The immunoprecipitation was carried out for 14 hours using 2.5mg of the antibodies: Sec8 2E12, 10C2, 5C3 epitope specific antibodies (Dr. Charles Yeamen); monoclonal anti-Flag M2 (Sigma Catalog#F1804) mouse anti-cMyc or mouse monoclonal anti-HA F-7 (Santa Cruz Biotechnology sc-7392). For endogenous and single tagged proteins this was followed by 2-18 hour precipitation of antibody-antigen complexes (depending on optimization protocol) using 90μl of Protein A/G-agarose beads (Santa Cruz Biotechnology, SC-2003). Subsequently, complexes were washed in lysis

buffer 4 times for 1 min at 4°C and finally was eluted with 90µl 2X SDS sample buffer (BIORAD Catalog#161-0737) followed by boiling at 95°C for 12 min.

For Taptagged proteins antibody-antigen complexes were isolated using 200ul of IgG-sepharose (GE healthcare) followed by a 10 hour protease digestion and subsequent second degree capture with 200ul of calmodulin-sepharose beads (GE healthcare) in calmodulin binding buffer (150mM Tris-HCl pH 8.0, 150mM NaCl, 1mM Mg-Acetate, 1mM Imidazole, 0.1% NP40, 2 mM $CaCl_2$). Complexes were washed in rinsing buffer (10mM Tris-HCl pH 8.0, 75mM NaCl, 1mM Mg-Acetate, 1mM Imidazole, 2 mM $CaCl_2$) 6 times for 1 min at 4°C and finally was eluted with 120µl 2X SDS sample buffer (BIORAD Catalog#161-0737) followed by boiling at 95°C for 12 min.

Mass spectrometry sample preparation

Following immunoprecipitation the sample were then run on a precast SDS-PAGE 4-20% gradient gel (Bio-Rad) and run until the dye front was approximately 15mm into the gel. The gel was washed with dH20 and stained with colloidal Coomassie stain Gel code Blue (Thermo Fisher Scientific, San Jose, CA)for 1 hour at RT to visualize and fix, followed by another 30 min dH20 wash. For each sample, fixed immunoprecipitated proteins separated on the gel were excised as a single fragment with sterile scalpel and homogenized in an Eppendorf tube with a sterile needle.

The gel pieces were distained with 50 mM triethylammonium bicarbonate (TEAB)/acetonitrile (1:1, v/v) by incubation at 37°C for 30 min. Gel pieces were dehydrated with acetonitrile at room temperature, followed by reduction/alkylation using DTT and iodoacetamide. Gel pieces were then rehydrated with trypsin solution (200ng/µl in 50mM TEAB). Trypsin digestion was carried out at 37°C overnight. Peptides were extracted after 30 min incubation at 37°C with extraction

buffer to a final concentration of 66.7% acetonitrile and 5% trifluoroacetic acid (TFA). All steps were carried out on a thermomixer shaker (Eppendorf, NJ) unless stated otherwise. Extracts were dried in vacuum centrifuge. Salts were removed using Oasis HLB µElution plate (Waters, MA) before LC-MS/MS analysis.

The samples were analyzed for mass spectrometry using Orbitrap Fusion Lumos^{TM} by the UTSW Proteomics core. MS/MS data were analyzed using PD2.1 for TMT based method (Proteome Discoverer 2.1 by Thermo-Fisher) and previously established CPFP pipeline (Trudgian, Thomas et al. 2010) for spectral count based method. To minimize batch variability, control and biological replicates were run consequently. To minimize antibody specific variability in endogenous IP, different epitope specific antibodies were used for Sec8. However, these antibodies have also shown to identify distinct pool of exocyst inside the cells (Inamdar, Hsu et al. 2016). Henceforth, these antibodies were useful for identifying both distinct and common pool of exocyst entities in cell steady state.

TMT labeling

Endogenous Sec8 was immunoprecipitated from HEK293T and HeLa cells. For each cell lines, a TMT-10plex and a 6-plex was generated. The 10-plex dataset contained a set of six Sec8 and four control immunoprecipitations whereas 6-plex dataset contained a set of four Sec8 and two control immunoprecipitations.

Six specific IPs in TMT 10-plex dataset were carried out using three epitope specific Sec8 antibodies each done upon cells incubated with either DMEM or ÉBSS. On the other hand, four specific IPs in TMT-6-plex dataset were carried out using two epitope specific Sec8 antibodies each done upon cells treated with DMEM or DMEM+pI:C. Henceforth, four quantitative datasets such as HEK293T-nutrient, HEK293T-immune, HeLa-nutrient, HeLa-immune were generated.

For TMT based MS/MS digested peptides samples were labeled with TMT reagents (Thermo Scientific). Each reagent was dissolved in 41 µl of acetonitrile to make a 20 ng/µl solution. 10 µL of TMT reagent stock solution was added to the peptides and incubated at room temperature for 2h. The reaction was quenched for 15 min by adding hydroxylamine to a final concentration of 0.5% (v/v). The TMT-labeled samples were mixed in equimolar ratio followed by clean up with C18 solid-phase extraction (SPE) cartridge (Sep-Pak, Waters). The TMT labeled mixed samples were lyophilized before fractionation.

labeled mixed digested peptides were reconstituted in 2% acetonitrile, 0.1% TFA prior to MS analysis using a Fusion Orbitrap Lumos (Thermo) mass spectrometer connected to a Dionex Ultimate 3000 UHPLC (Thermo). An Easy-Spray column (75 µm x 50 cm) packed with 2 µm C18 material was used for orthogonal peptide separation at low pH using a linear gradient from 100% mobile phase A (2% acetonitrile, 0.1% Formic acid) to 28% mobile phase B (80% acetonitrile, 0.1% Formic acid) in 90 min. Source voltage was set to 2.2 kv and capillary temperature at 275°C in the positive ion mode. The mass spectrometer was set to acquire data in data-dependent mode at MS1 level (full scan) ions within the m/z range of 400-1600 were scanned at the resolution of 120,000. In the second level of scanning (MS2), the top-10 previously selected ions were isolated and fragmented using collision-induced dissociation (CID) mode with collision energy of 35. At the MS3 level, a further fragmentation of the MS2 fragments was performed using high-energy collision-induced dissociation (HCD) mode to identify TMT labeled peptides. A multinotch MS3-based TMT method was used for analysis of the samples. Raw data acquired by the mass spectrometer was searched against a reviewed UniProt human database in Proteome Discoverer 2.2 (Thermo). Carbamidomethyl cysteine, TMT6 plex labeling at lysine and N terminus were set as static modifications and oxidation of methionine was used as dynamic modifications. False discovery rate was set to 1% and up to 3 missed cleavages were accepted. Reporter ion quantification method was used, top 3 peptides

were used for area calculation and results were normalized based on total peptide amount. In total ~9173 protein groups were identified of which 7801 protein groups were successfully labeled and quantified. Ingenuity Pathway analysis (IPA) was used to analysis the identified proteins.

Data analysis strategy for quantitative TMT based mass spectrometry

Data from the Orbitrap Fusion were processed using Proteome Discoverer Software (ver. 2.1.0.62). MS2 spectra were searched using Sequest HT and MS Amanda against UniProt database. Search parameters were specified as: trypsin enzyme, 3 missed cleavages allowed, minimum peptide length of 6, precursor mass tolerance of 10 ppm, and a fragment mass tolerance of 0.2 Daltons. Carbamidomethylation of cysteine residues (+57.021 Da) were set as static modifications, while oxidation of methionine residues (+15.995 Da), ubiquitination (+GG; +114.043 Da) and phosphorylation (+79.966 Da) was set as a dynamic modification. Peptide-spectral matches (PSMs) error rates were determined using the target-decoy strategy coupled to Percolator modeling of positive and false matches (Kall, Canterbury et al. 2007, Spivak, Weston et al. 2009).

Acquired quantitative reporter ion intensities were exported as a 10xN column matrix where N number of rows represented quantitative estimates of the candidate hits and column indicated sample IDs (Table 1). These columns were subjected to following adjustments- 1) columns were separated onto specific and control cohorts and a signal to noise ratio was measured between protein intensity profiles of the two cohorts to detect background noise; 2) proteins with negative S2N score were characterized as background and discarded from the dataset 3) noise-controlled matrix was row and column normalized and were clustered 1D along the protein intensity profile axis using Euclidian distance as a metric. This clustering method clustered the protein profiles based on their intensity across the specific and control samples as well as

variation within the intensity profiles within specific and control cohorts. From the generated clustered intensity profiles, a set of 50 protein profiles closest Euclidian rank to bait Sec8 was picked as a list of 'Top50' proteins from each of the four datasets.

Intersection of the four datasets was taken to define the Sec8 constitutive core interactome (Table 3.2-3.5). These core interactome was manually curated for functional annotation using STRING and GO databases and represented as 'hub and spoke network' here bait Sec8 is represented as a hub and rest of the hits as spoke surrounding it. Known interactions between the proteins were imported from BIORID database. Subsequently, the core Sec8 interactome partners were validated using western blot technique (Figure 2.4 G).

Furthermore, to define state sensitive interactors, control intensity profile values of the core interactors were subtracted and intensity profile values were further split into two cohorts- treated (DMEM/ -pI:C) and non-treated (EBSS/ +pI:C). Ratio was taken of the averages quantitative estimates of the two cohorts (+/-). Ratios were Log normalized to generate a linear scale ranging from +n to –n centered around 0. Candidate hits with positive value in this scale indicated hits that were enriched when exposed to stimuli. Statistical analysis was performed to measure the significance of the enrichment.

Data analysis strategy for semi-quantitative spectral count based mass spectrometry

For semi-quantitative spectral count based approach specific interactors/hits were characterized by quantitative enrichment of the protein in the sample over a negative control. For overexpression based IP-MS, this negative control represents IP enrichment value of the hit in an empty vector transfection sample. For endogenous IP, negative control represents IP enrichment value of the hit in a non-specific antibody control such as anti-HA or anti-IgG.

LC-MS/MS data was generated using the CPFP pipeline and quantified using spectral count-based, semi-quantitative label-free quantification. The finalized dataset for overexpression based IP was represented as a 2xN matrix where row indicates average intensity values of the potential hits and column indicates two cohorts: specific and controls. This dataset was further controlled for false positives using the “CRAPOME” database (www.crapome.org.) to exclude commonly identified non-specific interactors (Mellacheruvu, Wright et al. 2013). High stringency inclusion criteria cutoffs allowed proteins to pass if they were identified in less than 5% of the reports within the CRAPOME database, spectral count ≤1 in the negative control IP condition, and present in specific pull down with at least 2 spectral counts. Whenever a ratio was taken, empty cells in the generated matrix were replaced with a spectral count value of 0.5.

Following are the numbers of replicates for each interactome analysis: endogenous RALB endogenous interactome, n=4; Exo84/Sec5-pI:C, n=2; Exo84/Sec5-RALB23V, n=2; Exo84/Sec5+RALB23V, n=2; active TBK1/PKR and inactive TBK1/PKR n=2; TBK1/PKR-pI:C/SeV n=2; TBK1/PKR+pI:C/SeV n=2.

For RALB dependent Exo84 and Sec5 interactome, separately generated interactome was integrated and quantitative value for each proteins were represented as Log2 of the ratio of the intensity values in Exo84 (+RALB23V) and Sec5 (+RALB23V) datasets. Similarly for TBK1/PKR±pI:C/SeV quantitative value for each proteins were represented as Log2 of the ratio of the intensity values in TBK1/PKR-pI:C/SeV and TBK1/PKR+pI:C/SeV datasets (Table 3.6-3.11).

qPCR and RNAseq

500,000 HeLa cells were plated in 6-well cell culture dishes and the following day cells were then washed with PBS and then collected into PBS and pelleted via bench top centrifuge. Cell

pellets were lysed and RNA was collected via RNeasy Kit (Qiagen). mRNA was reverse transcribed into cDNA and relative transcript abundance was measured by Taqman-qPCR probe sets (Applied Bio- Science). RNAseq for the whole genome transcripts was performed using UTSW sequencing core facility (Table 3.1).

Immunofluorescence

Cells were seeded at optimized confluency at plastic-bottom 8-well chamber slides (Corning) were grown to 90% confluency in suitable growth medium with or without treatments or presence of small molecule dyes. Cells were fixed with 3.7% formaldehyde for 15 minutes, permeabilized with 0.5% Triton-X for 15 min. After optimized times of washing and rinsing, slides were stained with primary antibody for an hour followed by appropriate secondary antibody along with DAPI in the anti-fade mounting medium (VECTASHIELD ProLong Gold). Secondary antibodies: DyLight 488 donkey anti-Rabbit and DyLight 594 donkey anti-Mouse were purchased from Jackson ImmunoResearch Laboratories, inc. AlexaFluor 350 donkey anti-Mouse and Alexa Fluor 647 donkey anti-Mouse were purchased from Invitrogen. For blocking and washes, PBTA (PBS, 1% Tween 20, and 2% BSA) and PBS was used respectively.

HeLa LC3-GFP cells (Bodemann *et al.* 2013) were grown to 90% confluence and exposed to the mentioned stimuli. Cells were fixed with 3.7% PFA, quenched with NH4Cl, permeabilized with digitonin. Cell were mounted with the mounting media described above

Epifluorescence images (Figure 2.1I, 1L) were captured using appropriate excitation/emission filter sets(GFP, AlexaFluor 488) (Rhodamine,AlexaFluor 594) on a 40X objective on a Zeiss Axioplan 2E.

Superose 6 FPLC

HEK293T, HeLa and MDCK cells were grown to confluence on 15 cm dishes. Then followed by appropriate stimulation protocol, cells were washed 2X with PBS before lysis in DHE buffer (20mM HEPES, 150mM NaCl, 0.5% NP40, and the protease inhibitors Pefabloc, Antipain, Leupeptin, and Pepstatin A). Collected lysates were incubated on ice for 20 min, then cleared at 20,000Xg for 10 min at 4°C. The supernatant was filtered through 0.22um filter and 0.5 ml of filtered sample was injected into a Superose 6 column. The column was run at a flow rate of 0.2 ml/min and 0.5 ml fractions were collected. The collected samples were mixed with 100ml 6X Laemmli sample buffer and boiled.

siRNA sequences

Synthetic pool of four siRNAs targeting LONRF1 (control), Sec8, LATS1, TBK1 and PKR were obtained from Dharmacon. Sense sequences of these siRNAs are as follows

LONRF1#1: UCAGAGAGCUUCAUGAUUU; LONRF1#2: GACCAAGAAUGUUCCAAUA; LONRF1#3: UCACACAGCUGUUGGAAGA; LONRF1#4: GCACUGCCGACAUUGAAUA Sec8#1: GAAUUGAGCAUAAGCAUGU Sec8#2: UAACUGAGUACUUGGAUAU; Sec8#3: GCCGAGUUGUGCAGCGUAA; Sec8#4: ACUGAGUGACCUUCGACUA; LATS1#1: GAACCAAACUCUCAAACAA; LATS1#2: GCAAGUCACUCUGCUAAUU; LATS1#3: GAAAUCAAGUCGCUCAUGU; LATS1#4: GAUAAAGACACUAGGAAUA; TBK1#1: GAACGUAGAUUAGCUUAUA; TBK1#2: UGACAGAGAUUUACUAUCA; TBK1#3: UAAAGUACAUCCACGUUAU; TBK1#4: GGAUAUCGACAGCAGAUUA; PKR#1: CAAAUUAGCUGUUGAGAUA; PKR#2: GGAAAGACUUACGUUAUUA; PKR#3: GCAGAUACAUCAGAGAUAA; PKR#4: GAUCUUAAGCCAAGUAAUA

A pool of three siRNAs from Sigma was used for Exo84 and RALB knock down. Catalog numbers for them are: Exo84#1: SASI_Hs01_00215827; Exo84#2: SASI_Hs01_00215828

Exo84#3: SASI_Hs01_00215829; RALB#1: SASI_Hs02_00334659; RALB#2: SASI_Hs01_00242021; RALB#3: SASI_Hs01_00242022

Reporter assay

To measure gene-of-interest's effect on YAP1 transcriptional activity, cells were transiently transfected with 8XGTIIC-luc-TEAD (for YAP1) or IFN-β promoter luciferase reporter expressing firefly luciferase (~575nm), CMV promoter regulated renilla luciferase (~475nm) and empty vector or cDNAs of interest (Dupont, Morsut et al. 2011). Plates were read using standard dual luminescence protocol using PHERAstar plate reader (BMG Biotech). Firefly by renilla ratio was normalized to either a negative control transfection or a positive control transfection. Normalized Hippo activation fold change was represented as histograms representing mean ± SEM. Statistical comparison between treatment cohorts were measured using Student's unpaired t test

Small Molecule Cell Viability Assays

For dose response analyses, cells were first plated in 96-well plates at a density of 1-5K/well. Twenty-four hours post seeding, compounds solubilized in vehicle or vehicle alone (equal volume) were added to achieve the final concentrations. Cell viability was measured by CellTiter-Glo (Promega), 72-96 hours post compound exposure. Data were normalized using vehicle control treated cells. Response curves were modeled using a nonlinear regression curve fit with a three-parameter dose response using GraphPad Prism 6. All data point was done in biological triplicate.

HSV1 cytotoxic assay

Cells were plated in 96-well plates at a density of 1-5K/well in 90µl growth media. Twenty-four hours post seeding 10^9 PFU HSV1 virus stock were serially diluted in eppendorf tubes using growth media. 10µl of the virus stock dilution was added each 96-well. 72-96 hours post virus exposure, Cell viability was measured by CellTiter-Glo (Promega). Data were normalized to the lowest non-toxic dose treated cells. Response curves were modeled using a nonlinear regression curve fit with a three-parameter dose response using GraphPad Prism 6. All data point was done in biological triplicate.

Peptide phosphorylation assay

Peptide purified protein mixture samples were diluted to 1 ug/uL in 2% acetonitrile (ACN), 0.1% formic acid, and analyzed by LC-MS/MS, using an Orbitrap Fusion Lumos mass spectrometer (Thermo Electron) coupled to an Ultimate 3000 RSLC-Nano liquid chromatography system (Dionex). Samples were injected onto a 75 µm, 50-cm long EasySpray column (Thermo), and eluted with a gradient from 1-28% buffer B over 60 min. Buffer A contained 2% (v/v) ACN and 0.1% formic acid in water, and buffer B contained 80% (v/v) ACN, 10% (v/v) trifluoroethanol, and 0.1% formic acid in water. The mass spectrometer operated in positive ion mode with a source voltage of 2.2 kV and an ion transfer tube temperature of 275 °C. MS scans were acquired at 120,000 resolution in the Orbitrap and up to 10 MS/MS spectra were obtained in the ion trap for each full spectrum acquired using higher-energy collisional dissociation (HCD) for ions with charges 2-7. Phosphorylated peptides of interest were observed by generating an extracted ion chromatogram corresponding to a 0.01 Da window around the theoretical m/z of the +3 charged monoisotopic mass of the singly phosphorylated peptide of interest.

TABLE 3.1: RNASeq data for differential transcript level enrichment of genes in presence or absence of immune stimuli

Gene name	0 hr	4 hr SeV	4 hr pI:C	Average 4 hr	Log2FoldChange(4hr/0 hr)
TNFRSF9	0.13	1.05	0.95	1.00	2.94
HIVEP3	16.96	70.03	69.39	69.71	2.04
IFI44	5.98	13.89	44.99	29.44	2.30
GBP3	11.18	56.99	53.11	55.05	2.30
GBP4	0.23	2.20	6.17	4.18	4.20
GBP5	0.36	1.41	1.86	1.64	2.19
NGF	0.19	4.34	2.87	3.60	4.21
GPR37L1	0.16	0.85	1.70	1.28	2.97
DISC1	1.66	10.02	10.57	10.29	2.63
DKK1	10.37	72.10	29.59	50.84	2.29
IFIT2	5.98	262.46	186.73	224.59	5.23
IFIT3	5.98	100.06	109.05	104.55	4.13
IFIT1	8.45	117.17	81.65	99.41	3.56
NFKB2	40.59	212.82	263.81	238.32	2.55
PTPRE	3.48	23.39	14.55	18.97	2.45
SAA2	0.06	1.25	1.86	1.55	4.58
SAA1	0.32	1.48	2.67	2.08	2.68
BIRC3	28.21	132.15	136.49	134.32	2.25
MMP12	0.55	2.04	2.74	2.39	2.11
UBASH3B	5.13	25.92	18.33	22.13	2.11
OLR1	5.33	17.90	32.49	25.20	2.24
IFLTD1	0.42	5.26	3.91	4.59	3.44
KRT75	0.94	6.31	4.80	5.55	2.56
DRAM1	54.40	208.55	252.23	230.39	2.08
OAS2	0.26	1.58	2.28	1.93	2.89
OASL	2.18	36.40	52.42	44.41	4.35
SAMD4A	16.74	66.68	94.60	80.64	2.27
ASB2	0.55	2.82	2.12	2.47	2.16
RASGRP1	0.65	3.02	3.56	3.29	2.34
CDH5	0.03	1.31	0.98	1.15	5.14
CCL5	0.13	9.89	9.49	9.69	6.22
DHX58	0.62	1.91	4.60	3.25	2.40
ICAM1	31.10	111.32	165.52	138.42	2.15
RELB	5.20	59.36	75.98	67.67	3.70
IL11	6.53	58.34	22.74	40.54	2.63
TCF7L1	0.71	3.28	2.71	3.00	2.07
IFIH1	1.98	14.42	23.42	18.92	3.25
MX1	3.51	14.22	32.78	23.50	2.74
APOL6	3.74	15.41	33.34	24.37	2.71
APOL1	0.52	2.73	6.17	4.45	3.10
IRAK2	7.18	33.21	30.80	32.00	2.16

PTX3	0.49	2.07	4.01	3.04	2.64
CLDN1	70.36	274.25	337.54	305.89	2.12
CXCL10	0.03	3.97	4.31	4.14	6.99
NFKB1	41.24	149.98	182.85	166.41	2.01
TNIP3	0.36	6.18	9.69	7.93	4.47
FGF2	139.06	556.28	702.35	629.31	2.18
IL7R	25.22	89.18	115.38	102.28	2.02
VCAN	0.32	2.63	1.47	2.05	2.66
FGF1	0.23	1.35	1.08	1.21	2.41
BACH2	1.36	6.01	6.85	6.43	2.24
STX11	4.16	14.29	19.67	16.98	2.03
C8orf46	0.23	0.76	1.21	0.98	2.11
DDX58	5.13	72.50	181.05	126.77	4.63
TNC	19.43	87.67	85.27	86.47	2.15
TRAF1	0.97	5.95	6.88	6.41	2.72
BTG2	74.32	14.75	12.62	13.69	-2.44
ATF3	159.79	33.24	32.43	32.83	-2.28
FAM13C	11.24	1.51	1.60	1.55	-2.85
EGR2	34.58	1.71	0.55	1.13	-4.93
DUSP5	204.57	31.90	31.19	31.54	-2.70
NR4A1	1393.44	142.79	126.70	134.75	-3.37
BMF	60.22	6.14	4.08	5.11	-3.56
SEMA6D	7.25	1.05	1.50	1.28	-2.51
WSCD1	1.43	0.36	0.33	0.34	-2.06
PER1	94.67	15.11	15.79	15.45	-2.62
FOSB	203.08	8.97	2.15	5.56	-5.19
DBP	3.93	0.53	0.72	0.62	-2.66
FAM84A	0.91	0.10	0.29	0.20	-2.21
STON1-GTF2A1L	2.63	0.49	0.55	0.52	-2.33
STON1	6.08	1.02	1.30	1.16	-2.39
EGR4	3.90	0.00	0.03	0.02	-7.90
NR4A2	244.12	15.47	14.45	14.96	-4.03
SRGAP3	1.79	0.23	0.36	0.29	-2.60
KIT	1.88	0.36	0.52	0.44	-2.09
RASGEF1B	2.50	0.53	0.69	0.61	-2.05
CXXC4	4.81	1.05	1.24	1.15	-2.07
GALNTL6	1.10	0.23	0.16	0.20	-2.49
PLCXD3	10.46	2.07	2.38	2.23	-2.23
ST8SIA4	2.37	0.36	0.52	0.44	-2.43
EGR3	54.76	0.33	0.23	0.28	-7.62
ARC	14.72	1.38	0.78	1.08	-3.77
NR4A3	494.52	31.17	52.42	41.80	-3.56

TABLE 3.2: Sec8 IP-MS (TMT) on HeLa cells incubated with or without pI:C

Protein	# PSMs	MW [kDa]	Control1 - pI:C	Ab1 - pI:C	Ab2 - pI:C	Control 1 +pI:C	Ab1 +pI:C	Ab2+pI:C
AZI2	3	44.907	7.9	335.2	384.3	47.4	360.4	343
CCNH	17	37.619	263.7	2868	3469.4	229.4	3199.7	3421.4
CDK7	19	39.014	72.1	2415	3041.5	324.3	2827.9	3695.6
EXOC1	22	101.917	66	2856	2858.6	321.6	3313.6	3200.1
EXOC2	27	104	208.1	4235	4335.4	578.2	5555.1	4700.9
EXOC3	23	86.79	512.3	4453	4304.1	357.4	5685.1	5144.5
EXOC4	47	110.429	281.9	7589	7491.1	621.3	10203	8757.7
IVNS1ABP	16	71.683	105.2	1801	2048.4	204.3	1849.4	2470.9
MNAT1	15	35.8	99.9	3430	4176.9	259.6	4435.6	5166.9
PRPS1	19	34.812	64.6	3778	4164.3	206.3	4673.1	4987.4
PRPS2	20	35.032	138.1	4242	4609.1	699.6	5722.8	4720
PRPSAP1	23	42.44	279.2	4914	5409.8	1191.9	6160.2	6780.7
TBK1	5	83.589	20.3	403.3	428.6	77.1	1991.8	1869.2
TP53BP1	50	213.985	349.4	4896	6405.5	467.2	6169.1	7737.1
WDR73	7	41.659	61.3	1403	1207.9	82.4	1672.1	1623.3

TABLE 3.3: Sec8 IP-MS (TMT) on HEK293T cells incubated with or without pI:C

Protein	# PSMs	MW [kDa]	Control1 -pI:C	Ab1 - pI:C	Ab2- pI:C	Control 1 +pI:C	Ab1 +pI:C	Ab2+pI :C
AZI2	6	44.91	146.1	319.3	606	182.2	435.9	750.2
CCNH	13	37.62	133.1	1193.4	2738.2	183.4	1033.6	2152.5
CDK7	9	39.01	99.4	491.2	1004.5	140.4	482	951.4
EXOC1	28	101.9	638.6	4920.2	7143.7	752.5	4118	6534.9
EXOC2	18	104	478.7	2567.3	3889.4	835.2	2066.5	2989.4
EXOC3	26	86.79	438.4	3843.4	5836.9	578.9	3883.5	6016.2
EXOC4	41	110.4	599.9	5770	9941.4	735.3	4671.8	9015.8
IVNS1ABP	7	71.68	87.8	610.2	1368.2	138	514	1157.9
MNAT1	11	35.8	176.9	821.4	1668.1	221.2	908.6	1817
PRPS1	30	34.81	1188	5015.8	8908.8	1723.3	4904	9337.5
PRPS2	24	34.75	368.3	1327.8	2839.7	535	1617.5	3357.8
PRPSAP1	19	42.44	494	1806.6	3644	677.9	2131.3	4162.1
TBK1	4	83.59	106.3	298.3	407.3	123.2	789.9	880.8
TP53BP1	24	214	382.4	695.6	3614.3	446.4	767.4	2955.5
WDR73	11	41.66	415.7	1232.6	1621.5	494.2	1184.7	1477.9

TABLE 3.4: Sec8 IP-MS (TMT) on HEK293T cells incubated with DMEM or EBSS

Protein	# PSMs	MW [kDa]	Control1 DMEM	Ab1 DMEM	Ab2 DMEM	Ab3 DMEM	Control 2 DMEM	Control1 EBSS	Ab1 EBSS	Ab2 EBSS	Ab3 EBSS	Control2 EBSS
AZI2	5	44.907	31.9	152.5	178.6	401.5	47	71.6	256.6	360.6	574.2	47.1
CCNH	17	37.619	139.4	1009.2	1625.8	2036	147.8	264	972.9	1927.4	2776.5	133.3
CDK7	11	39.014	100.3	684	974	1656	136.8	188.9	626.6	1324.5	2168.3	115.3
EXOC1	30	101.917	588.5	2498.4	2034.4	5343	356.1	720.6	3047.2	3272.9	7641.4	437.5
EXOC2	25	104	469.5	2101.7	2064.8	4423	428.5	686.2	3145.7	3866.4	6794.6	351.4
EXOC3	26	85.513	516.3	2958.5	2285.1	6327	401.7	775.5	4185.1	4379.7	8834.6	408.3
EXOC4	47	110.429	1151.1	5590.8	3962.7	9254	1086.7	1485	5519.8	6139.3	13978	1013.2
IVNS1ABP	7	71.683	70	658.7	714.5	1025	53.3	106.8	744.1	1019.5	1475.4	52.7
MNAT1	14	35.8	116.8	842.1	1315.9	2138	193.8	297	997.5	2107.1	2380.2	222.7
PRPS1	25	34.812	595.3	2724.5	2944.6	7578	427.4	1011.1	4183.1	4704.8	7379.1	654.3
PRPS2	22	34.747	146.8	1132.9	860.3	2012	271.8	262	1246.2	1322.2	1843.4	299.1
PRPSAP1	22	42.44	654.8	2327.4	2383.7	3443	719.7	1062.9	3129.3	3487	3571.5	540.4
TBK1	3	83.589	148.8	427.5	394.6	571.6	114.3	162.2	252.5	367.4	712.2	67.4
TP53BP1	20	213.985	221.4	574.5	781.2	2049	244.1	244.2	424.3	738.4	2434.9	164.2
WDR73	9	41.659	335.6	1840	1223.1	5191	24.2	517.5	2128.3	1556	6528.4	160.4

TABLE 3.5: Sec8 IP-MS (TMT) on HeLa cells incubated with DMEM or EBSS

Protein	# PSMs	MW [kDa]	Control 1 DMEM	Ab1 DMEM	Ab2 DMEM	Ab3 DMEM	Control 2 DMEM	Control 1 EBSS	Ab1 EBSS	Ab2 EBSS	Ab3 EBSS	Control 2 EBSS
AZI2	2	44.91	12.4	74.1	68.3	44.7	12.3	14	57.9	69.8	49.9	14.4
CCNH	10	37.62	99.1	819.9	1637.9	354.8	192.5	170.3	1094	1004.9	597.2	138.5
CDK7	7	39.01	75.3	888.3	1392.2	373.7	127.7	130.1	927.7	1314.8	666.3	120.8
EXOC1	25	101.9	289	3688.8	4156.4	1542.2	491.9	411.4	3437	3437.2	1322.1	380.7
EXOC2	18	104	235.7	2141.9	3497.3	830.9	507.5	391.2	2446	2025.3	969.9	354.3
EXOC3	20	85.51	307.2	3178.9	3318.1	1664.8	446.2	388.7	2661	2828.3	1332.3	394.6
EXOC4	36	110.4	619.9	6426.4	7964.3	1870.8	1160.6	861.9	6521	5205.7	2086.1	789.4
IVNS1ABP	5	71.68	13.6	256.2	527.5	65.1	41	28.1	348.7	314	116.6	23.3
MNAT1	14	35.8	193.3	1247.2	1849.7	1851	348.9	315.6	1312	2059.9	2102.5	290
PRPS1	36	34.81	632.7	3029.9	5485.6	1660.9	925.8	863.5	3624	5362.2	2133.5	775
PRPS2	32	34.75	1031.6	4815.8	6570.7	2597.8	1184.1	1300.4	4971	7775.3	3111.1	1175.2
PRPSAP1	26	42.44	649.9	2639.3	4055.2	2053.1	966.1	1439.8	2901	3628.2	2462.6	1016.9
TBK1	2	83.59	9.3	55.5	61.1	37.5	9.2	14	47.9	63.5	45.1	14.2
TP53BP1	4	214	27.4	93.5	205	112.4	96.7	53.3	132.5	142	110	43.1
WDR73	14	41.66	362.4	4639.2	5759.8	1822	866.8	589.2	4871	3612.5	2076.1	474.9

TABLE 3.6: Myc-Exo84 IP-MS (Label free) on HEK293T cells incubated with or without pI:C

Proteins	Average -pI:C	Average +pI:C
Exo84	21.5	23
EXOC7	4.5	4.5
EXOC6	3	3.5
EXOC5	3	3
Sec8	14	3
EIF2AK2	0.5	7.5
NKRF	2.5	5.5
EIF23E	6	0.5

TABLE 3.7: HA-Sec5 IP-MS (Label free) on HEK293T cells incubated with or without pI:C

Proteins	Average - pI:C	Average +pI:C
Sec5	28	26
EXOC1	3.5	4.5
EXOC3	2.5	3.5
Sec8	4.5	6

TABLE 3.8: Endogenous RALB IP-MS (Label free) on HEK293T cells

Proteins	Run 1	Run2	Run3	Run4	IgG control
AMOTL1	2.0	2.0	5.0	1.0	0.00
ARPC1B	18.0	13.0	13.0	14.0	0.00
ARPC5	7.0	4.0	7.0	6.0	0.00
ARPC5L	4.0	3.0	4.0	4.0	0.00
ATP6V0D1	5.0	7.0	9.0	8.0	0.00
ATP6V1C1	3.0	2.0	3.0	2.0	0.00
CHUK	2.0	2.0	2.0	2.0	0.00
EXOC2	3.0	3.0	3.0	3.0	0.00
EXOC6	2.0	2.0	2.0	2.0	0.00
KIAA0196	2.0	3.0	4.0	3.0	0.00
LAMTOR1	6.0	5.0	6.0	7.0	0.00
LAMTOR3	2.0	2.0	3.0	1.0	0.00
MTOR	4.0	6.0	3.0	4.0	0.00
NF2	2.0	2.0	8.9	2.0	0.00
RAGA	2.0	2.0	2.0	2.0	0.00
RAGD	2.0	2.0	2.0	2.0	0.00
RALB	15.0	13.0	11.0	18.0	0.00
ROCK2	2.0	4.0	3.0	1.0	0.00
STK4	2.0	2.0	2.0	2.0	0.00
VPS4A	2.5	2.0	3.5	2.5	0.00
YAP1	2.0	2.0	9.0	2.0	0.00

TABLE 3.9: Myc-Ex084 and HA-Sec5 IP-MS (Label free) from RALB overexpressing HEK293T cells

Protein name	Avg. SC Exo84	Avg. SC Sec5	Exo84/Sec5	Log2 (Exo84+RALB23V/ Sec5+RALB23V)
Exo84	44	1	44	5.46
RIOK1	6	0.5	12	3.58
PRPSAP1	9	1	9	3.17
MST1	8	1	8	3.00
EIF3X	3.5	0.5	7	2.81
EIF2AK2	6	1	6	2.58
DENR	3	0.5	6	2.58
AP3S1	3	0.5	6	2.58
VPS4B	3	0.5	6	2.58
ULK1	5	1	5	2.32
RPTOR	5	1	5	2.32
EXOC7	2.5	0.5	5	2.32
LAMTOR2	4	1	4	2.00
LAMTOR3	2	0.5	4	2.00
LAMTOR1	5	2	2.5	1.32
EXOC6	2.5	1	2.5	1.32
EXOC5	1.5	3	0.5	-1.00
EXOC1	1.5	3.5	0.43	-1.22
VAPA	5	15	0.33	-1.58
mTOR	0.5	2	0.25	-2.00
METAP2	1	4.93	0.2	-2.30
Sec5	1	5.99	0.17	-2.58
METAP1	0.5	3	0.17	-2.58
MAP2K1	1	8	0.13	-3.00
COPS2	0.5	4.5	0.11	-3.17
Sec8	1	9.97	0.1	-3.32
MRTO4	1.5	16	0.09	-3.42
GTF2EF2	1	12	0.08	-3.58
EXOC3	1	18	0.06	-4.17

TABLE 3.10: TBK1 interactome

Protein	Flag-Empty	Flag-TBK1	Flag-TBK1-KD	Log2 TBK1-endogenous (+pI:C/-pI:C)
CEP128	0	9.5		
IFIT1	0	10.0		
IFITM2	0	4.5		
ISG15	0	3.0		
RPS6KB1	0	3.0		
RPTOR	0	4.5		
TBK1	0	26.0	16.5	0
ATR	0	4.0	2.5	0
DDRGK1				0
HERC2				-2.5
NUBP2				0
Sec5	0	2.0		2
Sec8	0	2.5		2.5
TOR1AIP1				-1
WASH6P				-0.5
BRE				-1
YAP1	0	2.0	2.5	
TGFBI	0	1.0	4.5	
YWHAE	0	0.0	2.5	

TABLE 3.11: Endogenous PKR interactome with or without pI:C stimuli

Protein	Log2 (+pI:C/-pI:C)
Exo84	6
WDR82	0.5
PTPN1	0
Sec5	0
EIF2A	0
KIBRA	0
MST1	0
CSNK2A2	0
PRKRA	0
NF2	0
PVR	0
NT5DC1	0
TBCD	0
ACOT9	0
PKR	-0.5
DDRGK1	-1

BIBLIOGRAPHY

Aragona, M., T. Panciera, A. Manfrin, S. Giulitti, F. Michielin, N. Elvassore, S. Dupont and S. Piccolo (2013). "A mechanical checkpoint controls multicellular growth through YAP/TAZ regulation by actin-processing factors." Cell **154**(5): 1047-1059.

Asakura, Y., Y. Fujiwara, N. Kato, Y. Sato and T. Komatsu (2007). "Serine/threonine kinase PKR: a sentinel kinase that discriminates a signaling pathway mediated by TLR4 from those mediated by TLR3 and TLR9." Am J Hematol **82**(7): 640-642.

Balakireva, M., C. Rosse, J. Langevin, Y. C. Chien, M. Gho, G. Gonzy-Treboul, S. Voegeling-Lemaire, S. Aresta, J. A. Lepesant, Y. Bellaiche, M. White and J. Camonis (2006). "The Ral/exocyst effector complex counters c-Jun N-terminal kinase-dependent apoptosis in Drosophila melanogaster." Mol Cell Biol **26**(23): 8953-8963.

Banks, L., D. Pim and M. Thomas (2012). "Human tumour viruses and the deregulation of cell polarity in cancer." Nat Rev Cancer **12**(12): 877-886.

Barbie, D. A., P. Tamayo, J. S. Boehm, S. Y. Kim, S. E. Moody, I. F. Dunn, A. C. Schinzel, P. Sandy, E. Meylan, C. Scholl, S. Frohling, E. M. Chan, M. L. Sos, K. Michel, C. Mermel, S. J. Silver, B. A. Weir, J. H. Reiling, Q. Sheng, P. B. Gupta, R. C. Wadlow, H. Le, S. Hoersch, B. S. Wittner, S. Ramaswamy, D. M. Livingston, D. M. Sabatini, M. Meyerson, R. K. Thomas, E. S. Lander, J. P. Mesirov, D. E. Root, D. G. Gilliland, T. Jacks and W. C. Hahn (2009). "Systematic RNA interference reveals that oncogenic KRAS-driven cancers require TBK1." Nature **462**(7269): 108-112.

Bhuvanakantham, R., J. Li, T. T. Tan and M. L. Ng (2010). "Human Sec3 protein is a novel transcriptional and translational repressor of flavivirus." Cell Microbiol **12**(4): 453-472.

Blakely, C. M., E. Pazarentzos, V. Olivas, S. Asthana, J. J. Yan, I. Tan, G. Hrustanovic, E. Chan, L. Lin, D. S. Neel, W. Newton, K. L. Bobb, T. R. Fouts, J. Meshulam, M. A. Gubens, D. M. Jablons, J. R. Johnson, S. Bandyopadhyay, N. J. Krogan and T. G. Bivona (2015). "NF-kappaB-activating complex engaged in response to EGFR oncogene inhibition drives tumor cell survival and residual disease in lung cancer." Cell Rep 11(1): 98-110.

Bodemann, B. O., A. Orvedahl, T. Cheng, R. R. Ram, Y. H. Ou, E. Formstecher, M. Maiti, C. C. Hazelett, E. M. Wauson, M. Balakireva, J. H. Camonis, C. Yeaman, B. Levine and M. A. White (2011). "RalB and the exocyst mediate the cellular starvation response by direct activation of autophagosome assembly." Cell **144**(2): 253-267.

Boldt, K., J. van Reeuwijk, Q. Lu, K. Koutroumpas, T. M. Nguyen, Y. Texier, S. E. van Beersum, N. Horn, J. R. Willer, D. A. Mans, G. Dougherty, I. J. Lamers, K. L. Coene, H. H. Arts, M. J. Betts, T. Beyer, E. Bolat, C. J. Gloeckner, K. Haidari, L. Hetterschijt, D. Iaconis, D. Jenkins, F. Klose, B. Knapp, B. Latour, S. J. Letteboer, C. L. Marcelis, D. Mitic, M. Morleo, M. M. Oud, M. Riemersma, S. Rix, P. A. Terhal, G. Toedt, T. J. van Dam, E. de Vrieze, Y. Wissinger, K. M. Wu, G. Apic, P. L. Beales, O. E. Blacque, T. J. Gibson, M. A. Huynen, N. Katsanis, H. Kremer, H. Omran, E. van Wijk, U. Wolfrum, F. Kepes, E. E. Davis, B. Franco, R. H. Giles, M. Ueffing, R. B. Russell, R. Roepman and U. K. R. D. Group (2016). "An organelle-specific protein landscape identifies novel diseases and molecular mechanisms." Nat Commun **7**: 11491.

Bryant, D. M., A. Datta, A. E. Rodriguez-Fraticelli, J. Peranen, F. Martin-Belmonte and K. E. Mostov (2010). "A molecular network for de novo generation of the apical surface and lumen." Nat Cell Biol **12**(11): 1035-1045.

Cepeda, E. B., T. Dediulia, J. Fernando, E. Bertran, G. Egea, E. Navarro and I. Fabregat (2015). "Mechanisms regulating cell membrane localization of the chemokine receptor CXCR4 in human hepatocarcinoma cells." Biochim Biophys Acta 1853(5): 1205-1218.

Chacon-Heszele, M. F., S. Y. Choi, X. Zuo, J. I. Baek, C. Ward and J. H. Lipschutz (2014). "The exocyst and regulatory GTPases in urinary exosomes." Physiol Rep 2(8).

Chien, Y., S. Kim, R. Bumeister, Y. M. Loo, S. W. Kwon, C. L. Johnson, M. G. Balakireva, Y. Romeo, L. Kopelovich, M. Gale, Jr., C. Yeaman, J. H. Camonis, Y. Zhao and M. A. White (2006). "RalB GTPase-mediated activation of the IkappaB family kinase TBK1 couples innate immune signaling to tumor cell survival." Cell **127**(1): 157-170.

Chien, Y. and M. A. White (2008). "Characterization of RalB-Sec5-TBK1 function in human oncogenesis." Methods Enzymol **438**: 321-329.

Chiu, Y. H., J. B. Macmillan and Z. J. Chen (2009). "RNA polymerase III detects cytosolic DNA and induces type I interferons through the RIG-I pathway." Cell **138**(3): 576-591.

Cooper, J. M., Y. H. Ou, E. McMillan, R. M. Vaden, A. Zaman, B. O. Bodemann, G. Makkar, B. A. Posner and M. White (2017). "TBK1 Provides Context-Selective Support of the Activated AKT/mTOR Pathway in Lung Cancer." Cancer Res.

Das, A., R. S. Fischer, D. Pan and C. M. Waterman (2016). "YAP Nuclear Localization in the Absence of Cell-Cell Contact Is Mediated by a Filamentous Actin-dependent, Myosin II- and Phospho-YAP-independent Pathway during Extracellular Matrix Mechanosensing." J Biol Chem **291**(12): 6096-6110.

David C. Trudgian, R. S., Matthew E. Cockman, Peter. J. Ratcliffe and Benedikt M. Kessler (2012). "ModLS: Post-Translational Modification Localization Scoring with Automatic Specificity Expansion." Journal of Proteomics & Bioinformatics **5**: 283-289.

Dupont, S., L. Morsut, M. Aragona, E. Enzo, S. Giulitti, M. Cordenonsi, F. Zanconato, J. Le Digabel, M. Forcato, S. Bicciato, N. Elvassore and S. Piccolo (2011). "Role of YAP/TAZ in mechanotransduction." Nature **474**(7350): 179-183.

Egan, D. F., D. B. Shackelford, M. M. Mihaylova, S. Gelino, R. A. Kohnz, W. Mair, D. S. Vasquez, A. Joshi, D. M. Gwinn, R. Taylor, J. M. Asara, J. Fitzpatrick, A. Dillin, B. Viollet, M. Kundu, M. Hansen and R. J. Shaw (2011). "Phosphorylation of ULK1 (hATG1) by AMP-activated protein kinase connects energy sensing to mitophagy." Science 331(6016): 456-461.

Everett, R. D. (2014). "HSV-1 biology and life cycle." Methods Mol Biol 1144: 1-17.

Feng, S., A. Knodler, J. Ren, J. Zhang, X. Zhang, Y. Hong, S. Huang, J. Peranen and W. Guo (2012). "A Rab8 guanine nucleotide exchange factor-effector interaction network regulates primary ciliogenesis." J Biol Chem 287(19): 15602-15609.

Fogelgren, B., X. Zuo, J. M. Buonato, A. Vasilyev, J. I. Baek, S. Y. Choi, M. F. Chacon-Heszele, A. Palmyre, N. Polgar, I. Drummond, K. M. Park, M. J. Lazzara and J. H. Lipschutz (2014). "Exocyst Sec10 protects renal tubule cells from injury by EGFR/MAPK activation and effects on endocytosis." Am J Physiol Renal Physiol 307(12): F1334-1341.

Fujisaki, K., Y. Abe, A. Ito, H. Saitoh, K. Yoshida, H. Kanzaki, E. Kanzaki, H. Utsushi, T. Yamashita, S. Kamoun and R. Terauchi (2015). "Rice Exo70 interacts with a fungal effector, AVR-Pii, and is required for AVR-Pii-triggered immunity." Plant J 83(5): 875-887.

Grindstaff, K. K., C. Yeaman, N. Anandasabapathy, S. C. Hsu, E. Rodriguez-Boulan, R. H. Scheller and W. J. Nelson (1998). "Sec6/8 complex is recruited to cell-cell contacts and specifies transport vesicle delivery to the basal-lateral membrane in epithelial cells." Cell **93**(5): 731-740.

Hansen, C. G., T. Moroishi and K. L. Guan (2015). "YAP and TAZ: a nexus for Hippo signaling and beyond." Trends Cell Biol **25**(9): 499-513.

Hasan, M., V. K. Gonugunta, N. Dobbs, A. Ali, G. Palchik, M. A. Calvaruso, R. J. DeBerardinis and N. Yan (2017). "Chronic innate immune activation of TBK1 suppresses mTORC1 activity and dysregulates cellular metabolism." Proc Natl Acad Sci U S A **114**(4): 746-751.

Heider, M. R., M. Gu, C. M. Duffy, A. M. Mirza, L. L. Marcotte, A. C. Walls, N. Farrall, Z. Hakhverdyan, M. C. Field, M. P. Rout, A. Frost and M. Munson (2016). "Subunit connectivity, assembly determinants and architecture of the yeast exocyst complex." Nat Struct Mol Biol 23(1): 59-66.

Havugimana, P. C., G. T. Hart, T. Nepusz, H. Yang, A. L. Turinsky, Z. Li, P. I. Wang, D. R. Boutz, V. Fong, S. Phanse, M. Babu, S. A. Craig, P. Hu, C. Wan, J. Vlasblom, V. U. Dar, A. Bezginov, G. W. Clark, G. C. Wu, S. J. Wodak, E. R. Tillier, A. Paccanaro, E. M. Marcotte and A. Emili (2012). "A census of human soluble protein complexes." Cell **150**(5): 1068-1081.

Horikoshi, Y., A. Suzuki, T. Yamanaka, K. Sasaki, K. Mizuno, H. Sawada, S. Yonemura and S. Ohno (2009). "Interaction between PAR-3 and the aPKC-PAR-6 complex is indispensable for apical domain development of epithelial cells." J Cell Sci **122**(Pt 10): 1595-1606.

Hyun, Y., J. Kim, S. W. Cho, Y. Choi, J. S. Kim and G. Coupland (2015). "Site-directed mutagenesis in Arabidopsis thaliana using dividing tissue-targeted RGEN of the CRISPR/Cas system to generate heritable null alleles." Planta 241(1): 271-284.

Inamdar, S. M., S. C. Hsu and C. Yeaman (2016). "Probing Functional Changes in Exocyst Configuration with Monoclonal Antibodies." Front Cell Dev Biol **4**: 51.

Ingrand, S., L. Barrier, C. Lafay-Chebassier, B. Fauconneau, G. Page and J. Hugon (2007). "The oxindole/imidazole derivative C16 reduces *in vivo* brain PKR activation." FEBS Lett **581**(23): 4473-4478.

Ishikawa, H. and G. N. Barber (2008). "STING is an endoplasmic reticulum adaptor that facilitates innate immune signalling." Nature **455**(7213): 674-678.

Kall, L., J. D. Canterbury, J. Weston, W. S. Noble and M. J. MacCoss (2007). "Semi-supervised learning for peptide identification from shotgun proteomics s." Nat Methods **4**(11): 923-925.

Kawai, T. and S. Akira (2010). "The role of pattern-recognition receptors in innate immunity: update on Toll-like receptors." Nat Immunol **11**(5): 373-384.

Kim, J. Y., E. A. Welsh, U. Oguz, B. Fang, Y. Bai, F. Kinose, C. Bronk, L. L. Remsing Rix, A. A. Beg, U. Rix, S. A. Eschrich, J. M. Koomen and E. B. Haura (2013). "Dissection of TBK1 signaling via phosphoproteomics in lung cancer cells." Proc Natl Acad Sci U S A **110**(30): 12414-12419.

Kim, J., M. Kundu, B. Viollet and K. L. Guan (2011). "AMPK and mTOR regulate autophagy through direct phosphorylation of Ulk1." Nat Cell Biol 13(2): 132-141.

Laplante, M. and D. M. Sabatini (2012). "mTOR signaling in growth control and disease." Cell **149**(2): 274-293.

Levine, B. and G. Kroemer (2008). "Autophagy in the pathogenesis of disease." Cell **132**(1): 27-42.

Liu, B., Y. Zheng, F. Yin, J. Yu, N. Silverman and D. Pan (2016). "Toll Receptor-Mediated Hippo Signaling Controls Innate Immunity in Drosophila." Cell **164**(3): 406-419.

Ma, X. M. and J. Blenis (2009). "Molecular mechanisms of mTOR-mediated translational control." Nat Rev Mol Cell Biol **10**(5): 307-318.

Martin, T. D., X. W. Chen, R. E. Kaplan, A. R. Saltiel, C. L. Walker, D. J. Reiner and C. J. Der (2014). "Ral and Rheb GTPase activating proteins integrate mTOR and GTPase signaling in aging, autophagy, and tumor cell invasion." Mol Cell **53**(2): 209-220.

Matern, H.T., Yeaman C, Nelson WJ, Scheller RH. The Sec6/8 complex in mammalian cells: characterization of mammalian Sec3, subunit interactions, and expression of subunits in polarized cells. Proc Natl Acad Sci U S A, 2001. 98(17): p. 9648-53.

Matsumoto, G., T. Shimogori, N. Hattori and N. Nukina (2015). "TBK1 controls autophagosomal engulfment of polyubiquitinated mitochondria through p62/SQSTM1 phosphorylation." Hum Mol Genet **24**(15): 4429-4442.

Mellacheruvu, D., Z. Wright, A. L. Couzens, J. P. Lambert, N. A. St-Denis, T. Li, Y. V. Miteva, S. Hauri, M. E. Sardiu, T. Y. Low, V. A. Halim, R. D. Bagshaw, N. C. Hubner, A. Al-Hakim, A. Bouchard, D. Faubert, D. Fermin, W. H. Dunham, M. Goudreault, Z. Y. Lin, B. G. Badillo, T. Pawson, D. Durocher, B. Coulombe, R. Aebersold, G. Superti-Furga, J. Colinge, A. J. Heck, H. Choi, M. Gstaiger, S. Mohammed, I. M. Cristea, K. L. Bennett, M. P. Washburn, B. Raught, R. M. Ewing, A. C. Gingras and A. I. Nesvizhskii (2013). "The CRAPome: a contaminant repository for affinity purification-mass spectrometry data." Nat Methods **10**(8): 730-736.

Meng, Z., T. Moroishi, V. Mottier-Pavie, S. W. Plouffe, C. G. Hansen, A. W. Hong, H. W. Park, J. S. Mo, W. Lu, S. Lu, F. Flores, F. X. Yu, G. Halder and K. L. Guan (2015). "MAP4K family kinases act in parallel to MST1/2 to activate LATS1/2 in the Hippo pathway." Nat Commun **6**: 8357.

Mizuno, S., K. Takami, Y. Daitoku, Y. Tanimoto, T. T. Dinh, S. Mizuno-Iijima, Y. Hasegawa, S. Takahashi, F. Sugiyama and K. Yagami (2015). "Peri-implantation lethality in mice carrying megabase-scale deletion on 5qc3.3 is caused by Exoc1 null mutation." Sci Rep 5: 13632.

Moroishi, T., C. G. Hansen and K. L. Guan (2015). "The emerging roles of YAP and TAZ in cancer." Nat Rev Cancer **15**(2): 73-79.

Moroishi, T., T. Hayashi, W. W. Pan, Y. Fujita, M. V. Holt, J. Qin, D. A. Carson and K. L. Guan (2016). "The Hippo Pathway Kinases LATS1/2 Suppress Cancer Immunity." Cell **167**(6): 1525-1539 e1517.

Moskalenko, S., D. O. Henry, C. Rosse, G. Mirey, J. H. Camonis and M. A. White (2002). "The exocyst is a Ral effector complex." Nat Cell Biol **4**(1): 66-72.

Moskalenko, S., C. Tong, C. Rosse, G. Mirey, E. Formstecher, L. Daviet, J. Camonis and M. A. White (2003). "Ral GTPases regulate exocyst assembly through dual subunit interactions." J Biol Chem **278**(51): 51743-51748.

Orvedahl, A., D. Alexander, Z. Talloczy, Q. Sun, Y. Wei, W. Zhang, D. Burns, D. A. Leib and B. Levine (2007). "HSV-1 ICP34.5 confers neurovirulence by targeting the Beclin 1 autophagy protein." Cell Host Microbe **1**(1): 23-35.

Ou, Y. H., M. Torres, R. Ram, E. Formstecher, C. Roland, T. Cheng, R. Brekken, R. Wurz, A. Tasker, T. Polverino, S. L. Tan and M. A. White (2011). "TBK1 directly engages Akt/PKB survival signaling to support oncogenic transformation." Mol Cell **41**(4): 458-470.

Perera, R. M., S. Stoykova, B. N. Nicolay, K. N. Ross, J. Fitamant, M. Boukhali, J. Lengrand, V. Deshpande, M. K. Selig, C. R. Ferrone, J. Settleman, G. Stephanopoulos, N. J. Dyson, R. Zoncu, S. Ramaswamy, W. Haas and N. Bardeesy (2015). "Transcriptional control of autophagy-lysosome function drives pancreatic cancer metabolism." Nature 524(7565): 361-365.

Potts, M. B., H. S. Kim, K. W. Fisher, Y. Hu, Y. P. Carrasco, G. B. Bulut, Y. H. Ou, M. L. Herrera-Herrera, F. Cubillos, S. Mendiratta, G. Xiao, M. Hofree, T. Ideker, Y. Xie, L. J. Huang, R. E. Lewis, J. B. MacMillan and M. A. White (2013). "Using functional signature ontology (FUSION) to identify mechanisms of action for natural products." Sci Signal **6**(297): ra90.

Pourcelot, M., N. Zemirli, L. Silva Da Costa, R. Loyant, D. Garcin, D. Vitour, I. Munitic, A. Vazquez and D. Arnoult (2016). "The Golgi apparatus acts as a platform for TBK1 activation after viral RNA sensing." BMC Biol **14**: 69.

Rangarajan, A., S. J. Hong, A. Gifford and R. A. Weinberg (2004). "Species- and cell type-specific requirements for cellular transformation." Cancer Cell **6**(2): 171-183.

Richter, B., D. A. Sliter, L. Herhaus, A. Stolz, C. Wang, P. Beli, G. Zaffagnini, P. Wild, S. Martens, S. A. Wagner, R. J. Youle and I. Dikic (2016). "Phosphorylation of OPTN by TBK1 enhances its binding to Ub chains and promotes selective autophagy of damaged mitochondria." Proc Natl Acad Sci U S A **113**(15): 4039-4044.

Rosse, C., E. Formstecher, K. Boeckeler, Y. Zhao, J. Kremerskothen, M. D. White, J. H. Camonis and P. J. Parker (2009). "An aPKC-exocyst complex controls paxillin phosphorylation and migration through localised JNK1 activation." PLoS Biol **7**(11): e1000235.

Russell, R. C., Y. Tian, H. Yuan, H. W. Park, Y. Y. Chang, J. Kim, H. Kim, T. P. Neufeld, A. Dillin and K. L. Guan (2013). "ULK1 induces autophagy by phosphorylating Beclin-1 and activating VPS34 lipid kinase." Nat Cell Biol 15(7): 741-750.

Sancak, Y., L. Bar-Peled, R. Zoncu, A. L. Markhard, S. Nada and D. M. Sabatini (2010). "Ragulator-Rag complex targets mTORC1 to the lysosomal surface and is necessary for its activation by amino acids." Cell **141**(2): 290-303.

Seixas, C., S. Y. Choi, N. Polgar, N. L. Umberger, M. P. East, X. Zuo, H. Moreiras, R. Ghossoub, A. Benmerah, R. A. Kahn, B. Fogelgren, T. Caspary, J. H. Lipschutz and D. C. Barral (2016). "Arl13b and the exocyst interact synergistically in ciliogenesis." Mol Biol Cell 27(2): 308-320

Settembre, C., C. Di Malta, V. A. Polito, M. Garcia Arencibia, F. Vetrini, S. Erdin, S. U. Erdin, T. Huynh, D. Medina, P. Colella, M. Sardiello, D. C. Rubinsztein and A. Ballabio (2011). "TFEB links autophagy to lysosomal biogenesis." Science 332(6036): 1429-1433.

Shen, S., M. Niso-Santano, S. Adjemian, T. Takehara, S. A. Malik, H. Minoux, S. Souquere, G. Marino, S. Lachkar, L. Senovilla, L. Galluzzi, O. Kepp, G. Pierron, M. C. Maiuri, H. Hikita, R. Kroemer and G. Kroemer (2012). "Cytoplasmic STAT3 represses autophagy by inhibiting PKR activity." Mol Cell **48**(5): 667-680.

Simicek, M., S. Lievens, M. Laga, D. Guzenko, V. N. Aushev, P. Kalev, M. F. Baietti, S. V. Strelkov, K. Gevaert, J. Tavernier and A. A. Sablina (2013). "The deubiquitylase USP33 discriminates between RALB functions in autophagy and innate immune response." Nat Cell Biol **15**(10): 1220-1230.

Spivak, M., J. Weston, L. Bottou, L. Kall and W. S. Noble (2009). "Improvements to the percolator algorithm for Peptide identification from shotgun proteomics data sets." J Proteome Res **8**(7): 3737-3745.

Stojdl, D. F., N. Abraham, S. Knowles, R. Marius, A. Brasey, B. D. Lichty, E. G. Brown, N. Sonenberg and J. C. Bell (2000). "The murine double-stranded RNA-dependent protein kinase PKR is required for resistance to vesicular stomatitis virus." J Virol **74**(20): 9580-9585.

Sun, Q., L. Sun, H. H. Liu, X. Chen, R. B. Seth, J. Forman and Z. J. Chen (2006). "The specific and essential role of MAVS in antiviral innate immune responses." Immunity **24**(5): 633-642.

Talloczy, Z., W. Jiang, H. W. t. Virgin, D. A. Leib, D. Scheuner, R. J. Kaufman, E. L. Eskelinen and B. Levine (2002). "Regulation of starvation- and virus-induced autophagy by the eIF2alpha kinase signaling pathway." Proc Natl Acad Sci U S A **99**(1): 190-195.

Talloczy, Z., H. W. t. Virgin and B. Levine (2006). "PKR-dependent autophagic degradation of herpes simplex virus type 1." Autophagy **2**(1): 24-29.

Tanaka, Y. and Z. J. Chen (2012). "STING specifies IRF3 phosphorylation by TBK1 in the cytosolic DNA signaling pathway." Sci Signal **5**(214): ra20.

Taylor, S. S., N. M. Haste and G. Ghosh (2005). "PKR and eIF2alpha: integration of kinase dimerization, activation, and substrate docking." Cell **122**(6): 823-825.

Tracy, K., P. D. Velentzas and E. H. Baehrecke (2016). "Ral GTPase and the exocyst regulate autophagy in a tissue-specific manner." EMBO Rep **17**(1): 110-121.

Tronel, C., G. Page, S. Bodard, S. Chalon and D. Antier (2014). "The specific PKR inhibitor C16 prevents apoptosis and IL-1beta production in an acute excitotoxic rat model with a neuroinflammatory component." Neurochem Int **64**: 73-83.

Trudgian, D. C., B. Thomas, S. J. McGowan, B. M. Kessler, M. Salek and O. Acuto (2010). "CPFP: a central proteomics facilities pipeline." Bioinformatics **26**(8): 1131-1132.

Uhm, M., M. Bazuine, P. Zhao, S. H. Chiang, T. Xiong, S. Karunanithi, L. Chang and A. R. Saltiel (2017). "Phosphorylation of the exocyst protein Exo84 by TBK1 promotes insulin-stimulated GLUT4 trafficking." Sci Signal **10**(471).

Vainionpaa, R. and T. Hyypia (1994). "Biology of parainfluenza viruses." Clin Microbiol Rev 7(2): 265-275.

Varelas, X., P. Samavarchi-Tehrani, M. Narimatsu, A. Weiss, K. Cockburn, B. G. Larsen, J. Rossant and J. L. Wrana (2010). "The Crumbs complex couples cell density sensing to Hippo-dependent control of the TGF-beta-SMAD pathway." Dev Cell **19**(6): 831-844.

Vega, I.E. and S.C. Hsu, The exocyst complex associates with microtubules to mediate vesicle targeting and neurite outgrowth. J Neurosci, 2001. 21(11): p.3839-48.

Wang, S., F. Xie, F. Chu, Z. Zhang, B. Yang, T. Dai, L. Gao, L. Wang, L. Ling, J. Jia, H. van Dam, J. Jin, L. Zhang and F. Zhou (2017). "YAP antagonizes innate antiviral immunity and is targeted for lysosomal degradation through IKKvarepsilon-mediated phosphorylation." Nat Immunol **18**(7): 733-743.

Williams, B. R. (1999). "PKR; a sentinel kinase for cellular stress." Oncogene **18**(45): 6112-6120.

Xiao, J., Y. Tan, Y. Li and Y. Luo (2016). "The Specific Protein Kinase R (PKR) Inhibitor C16 Protects Neonatal Hypoxia-Ischemia Brain Damages by Inhibiting Neuroinflammation in a Neonatal Rat Model." Med Sci Monit **22**: 5074-5081.

Yoshihama, Y., K. Sasaki, Y. Horikoshi, A. Suzuki, T. Ohtsuka, F. Hakuno, S. Takahashi, S. Ohno and K. Chida (2011). "KIBRA suppresses apical exocytosis through inhibition of aPKC kinase activity in epithelial cells." Curr Biol **21**(8): 705-711.

Yu, F. X., B. Zhao and K. L. Guan (2015). "Hippo Pathway in Organ Size Control, Tissue Homeostasis, and Cancer." Cell **163**(4): 811-828.

Yu, F. X., B. Zhao, N. Panupinthu, J. L. Jewell, I. Lian, L. H. Wang, J. Zhao, H. Yuan, K. Tumaneng, H. Li, X. D. Fu, G. B. Mills and K. L. Guan (2012). "Regulation of the Hippo-YAP pathway by G-protein-coupled receptor signaling." Cell **150**(4): 780-791.

Zhang, Q., F. Meng, S. Chen, S. W. Plouffe, S. Wu, S. Liu, X. Li, R. Zhou, J. Wang, B. Zhao, J. Liu, J. Qin, J. Zou, X. H. Feng, K. L. Guan and P. Xu (2017). "Hippo signalling governs cytosolic nucleic acid sensing through YAP/TAZ-mediated TBK1 blockade." Nat Cell Biol **19**(4): 362-374.

Zhao, B., L. Li, Q. Lei and K. L. Guan (2010). "The Hippo-YAP pathway in organ size control and tumorigenesis: an updated version." Genes Dev **24**(9): 862-874.

Zhou, D., C. Conrad, F. Xia, J. S. Park, B. Payer, Y. Yin, G. Y. Lauwers, W. Thasler, J. T. Lee, J. Avruch and N. Bardeesy (2009). "Mst1 and Mst2 maintain hepatocyte quiescence and suppress hepatocellular carcinoma development through inactivation of the Yap1 oncogene." Cancer Cell **16**(5): 425-438.

Zoncu, R., A. Efeyan and D. M. Sabatini (2011). "mTOR: from growth signal integration to cancer, diabetes and ageing." Nat Rev Mol Cell Biol **12**(1): 21-35.